CALCIUM PHOSPHATE COATINGS ON CORONARY STENTS BY ELECTROCHEMICAL DEPOSITION

by

MANUS PUI-HUNG TSUI

B.A.Sc., Department of Metals and Materials Engineering, The University of British Columbia, Vancouver, B.C., Canada, 2004

A THESIS SUBMITTED IN PARTIAL FULFILLMENT OF
THE REQUIREMENT FOR THE DEGREE OF

MASTER OF APPLIED SCIENCE

in

THE FACULTY OF GRADUATE STUDIES

(Materials Engineering)

THE UNIVERSITY OF BRITISH COLUMBIA

October 2006

ABSTRACT

Calcium phosphate ceramic coatings, especially hydroxyapatite (HA), have attracted much attention in the orthopedics and dentistry due to their excellent biocompatibility and bioactivity. Among the different methods of calcium phosphate coatings processing, electrochemical deposition (ECD) is a relatively low cost and flexible process technology. In this study, electrochemical deposition was used to deposit uniform calcium phosphate coatings on 316L stainless steel coronary stents. The influence of the ECD process parameters (deposition time, current density, electrolyte temperature, pH, and Ca/P ratio) on the resulting deposition morphology was investigated. Scanning electron microscopy (SEM) and X-Ray diffractometry (XRD) were used to analyze the coatings. The results demonstrated that both dicalcium phosphate dihydrate ($CaHPO_4 \cdot 2H_2O$, DCPD) and hydroxyapatite ($Ca_{10}(PO_4)(OH)_2$, HA) were present in the uniform ~0.5 μm thick as-deposited coating. However, a post-treatment process, including a 0.1N $NaOH_{(aq)}$ phase conversion at 75°C and a 500°C heat treatment produced a pure phase HA coating. The final deposit revealed a highly porous surface morphology which could be useful for drug encapsulation. With the application of the substrate surface modification and the post-treatment processes, sufficient coating adhesion was achieved as demonstrated by the in-vitro stent deployment tests without visible damage to the coating. Commercial in-vitro 40 million cycles fatigue tests demonstrated that the coatings exhibit good adhesion to the stent substrate, with no coating cracking or delamination. It was confirmed that the ECD-HA coating process for coronary stents is reliable and reproducible.

TABLE OF CONTENTS

LIST OF TABLES

LIST OF FIGURES

ACKNOWLEDGMENTS

I wish to express my sincere gratitude to the many people who have kindly provided me with great contribution to the completion of this thesis. I owe particular thanks to my supervisor, Dr Tom Troczynski for his advice and guidance during this project. I like to extend my appreciation to my fellow graduate students, faculty, and staff in the Department of Materials Engineering for all their support. Also, I thank MIV Therapeutics who has supported me and this research project in many ways. Special thanks are owed to my family and friends, whose have supported and encouraged me throughout my years of education.

1 INTRODUCTION

Coronary artery disease (CAD) is the leading cause of death in North America. In 2004, approximately 54% of all cardiovascular deaths are due to coronary artery disease[1]. CAD occurs when fat (cholesterol) deposit blocks the arteries, reducing the oxygen supply to the heart muscle. Angioplasty is a technique of opening a narrowed blood vessel without having to resort to a major bypass surgery. Metallic stents have been used successfully by cardiologists to battle the ravages of CAD. A stent is a stainless steel or Co-Cr alloy wire mesh tube designed to keep arteries open after the angioplasty procedure. Before implantation, stent is put over a balloon catheter and collapsed into a smaller diameter, then positioned to the site of blockage. When the balloon is inflated, the stent expands, locks in place and forms a scaffold. Stent stays in the artery permanently, keeps it open, improves blood flow to the heart muscle and relieves symptoms such as chest pain.

Although metallic stent is an effective solution in providing structural support, it does not eliminate the recurrence of blockage (restenosis) in the artery in all cases. The bare metal stent may trigger a natural inflammatory response resulting in proliferation of smooth muscle cells[2], thus, narrowing or re-closing of the artery, which often requires a repeat operation within a year. Unlike restenosis, which is fairly common, stent thrombosis is a rare but much more dangerous complication after coronary stent placement. A thrombus is dangerous because it can block a blood vessel partially or entirely, cutting off blood flow to the area supplied by that vessel. A thrombus will produce different symptoms depending on where it forms. A coronary thrombus will

produce chest pain and may result in artery blockage leading to a heart attack . A thrombus in the brain will result in a temporary ischemic attack (TIA) or even a stroke.

Restenosis, thrombosis, and inflammation are the problems associated with metallic stent implantation in coronary arteries. Applying biocompatible coatings on the stents, in particular drug eluting coatings, has been taken as a new approach to solve these problems[3, 4]. The new generation of coated coronary stents should be less restenotic, thrombogenic, be more acceptable by body environment, and should be capable of locally deliver drug to the surrounding tissue.

1.1 Biomaterial Coatings for Stents

A biomaterial is any synthetic material used to replace part of a living system or to function in intimate contact with living tissues[6]. The ability of such material, device or system to perform without a clinically significant host response in a specific application is defined as biocompatibility. The performance of a biomedical device is greatly depended on the material properties, design of the device, surgical techniques, health of patient, and the surface properties. Because of the complex interface of biomaterial-biological medium, surface properties is often the key to determine success of the device.

The interfacial phenomena at the biomaterial-biological medium are complex and involve water adsorption, ion exchange, cell and bacterial adhesion, corrosion, and decomposition of the biomaterial. Nowadays, medical devices and implants manufacturing commonly involves a biomaterial coating process and, as a result,

provides an opportunity to tailor the surface characteristics of the biomaterial to a specific application without detrimentally affecting its bulk properties. Ultimately, biomaterial coatings combine the advantages of bulk material and coating material to create the best desired biocompatible environment.

The state-of-the-art stents are coated with polymers carrying drugs. Unfortunately, there is accumulating evidence that after the drugs are leached from the coating, the polymer triggers a negative response from the surrounding tissue, referred to as "late restenosis"[5]. Consequently, there is a need for more biocompatible coatings on stents, which would not cause restenosis or thrombosis at any stage of post-implantation, and with or without drugs. It is hypothesized that calcium phosphate ceramic may constitute such coating, providing the motivation for the present work.

1.2 Calcium Phosphates and Hydroxyapatite

Calcium phosphates have been used since 1969 for manufacturing various forms of implants, as well as for solid or porous coating on other implants. Calcium phosphate can crystallize into various forms depending on the calcium to phosphorus ratio, presence of water, impurities, and temperature[6]. Calcium phosphate ceramics, particularly hydroxyapatite (HA), have received much attention and clinically applied in orthopedics and dental industries due to their excellent biocompatibility[7-9]. HA is recognized as osteoconductive and is able to accelerate bone ingrowth and attachment to the surface of implant during the early stages after implantation[8, 9]. In addition, it can induce tissue ingrowth and formation of chemical bonding to achieve better implant fixation. HA

interacts with the biological environment through a complex dissolution, precipitation, and ion exchange process[11, 12]. Following the introduction of HA to the biological environment, a partial dissolution of the surface is initiated causing the release of Ca^{2+}, HPO_4^{2-} and PO_4^{3-}, increasing the supersaturation of the micro-environment with respect to the stable (HA) phase. This saturation leads back to the precipitation hydroxyl-carbonate apatite (HCA) layer. The polycrystalline HCA phase is equivalent in composition and structure to the mineral phase of bone[10, 11]. HA coating can prevent the fibrous tissue encapsulation of implants and reduce the potentially harmful release of metallic ion from the implant into the biological environment[12]. Therefore, HA coatings on metallic substrate were applied to achieve better biocompatibility.

Hydroxyapatite $Ca_{10}(PO_4)(OH)_2$ is chemically similar to the mineral component of bones and hard tissues in mammals. Hydroxyapatite crystallizes into hexagonal crystal structure and has a unit cell dimension a = 9.432 Å and c = 6.881Å. The Ca/P ratio of HA is 10:6 and the density is 3.219 g/cm^3 [6]. The mechanical properties of synthetic calcium phosphate vary widely as a function of their crystallinity and porosity. Limitations of HA application relate to its brittleness (K_{IC} < 0.9 MPa·m$^{1/2}$) and low strength (generally, compressive strength <300 MPa, tensile < 50 MPa) [13]. Therefore, HA coatings on metallic implants were often combined to achieve high biocompatibility and high reliability. Although most data for HA performance comes from the field of orthopedics, there is accumulating evidence that HA performs equally well in blood circulation environment[14].

1.3 Electrochemical Deposition of HA Coatings

Different deposition technologies of HA have been investigated in the past including; plasma spray[15-17], sol-gel[18], pulse laser deposition[19], sputtering[20], electrophoretic deposition[21], and electrochemical deposition[22-24]. Electrochemical deposition (ECD) of calcium phosphate coatings at room (or near-room) temperature has been investigated since the 1990s. ECD is particularly attractive for coating internal surfaces of porous metallic substrates or highly complex surface. The resulting properties of HA can be controlled in ECD by regulating the electrochemical potential, current density, electrolyte concentration, and temperature of the process, as these conditions directly determine the deposition rate, morphology, and chemical composition of the HA coatings[25].

In the cathodic electrochemical deposition method, cathodic reactions are used to generate OH^- groups and increase pH at the electrode. Metal ions or complexes, which are stable in the bulk solution at low pH, are hydrolyzed by electrogenerated base at the electrode surface to form colloidal particles[23, 26].

All applications of HA coatings reported so far are related to solid implants which do not undergo any deformation during the implantation procedure. Coronary stents are very different in this respect as there is a significant strain of stent during expansion, as large as 15%[27]. Due to brittleness of ceramic, there exists a challenge for the ECD hydroxyapatite coating to survive under the stent expansion during the angioplasty procedure. While it is acceptable to micro-fracture the coating during stent expansion, it is not acceptable to separate the coating from stent during implantation. Debris of

separated coating have the potential to clog up blood supply causing fatal affect. Therefore, one of the crucial factors for ECD-HA film processing is the preparation of the metallic substrate such that the ECD coating can achieve high adhesion strength, sufficient to maintain coating/stent integrity during implantation of the stent.

Bio-resorption or dissolution is a major concern of in the biological environment. In terms of the HA coating, variables such as phase composition, crystallinity, Ca/P ratio, microstructure, thickness, porosity, and surface morphology are crucial. It is believed that amorphous coatings have a higher bio-resorption rate than crystalline coatings[28-30]. Thus, phase composition and crystallinity of ECD-HA coatings are important parameters for stability evaluation, and it is important to characterize these for the coatings on coronary artery stents.

1.4 Motivation and Focus of the Present Study

There is a need for a novel process for non-polymeric, biocompatible coatings for cardiovascular stents. Such ECD process is developed in the present work for deposition of calcium phosphate coatings on stents. The ECD parameters, such as deposition temperature, current density, heat treatment and different solvent systems, were investigated in the past to create thick film coatings (>10 μm). However, very few studies have applied these processes into implantable medical device or combine these finding to assess the mechanical behavior, and none was reported to concern HA coatings on cardiovascular stents. In the present study, we are exploring ECD process parameters, such as current density and time of deposition, to produce reliable thin film (<500nm)

calcium phosphate coatings at low temperatures (40-70°C) on cardiovascular stents. A substrate surface pre-treatment is employed prior to the electrochemical deposition to achieve high level of coating adhesion. The coatings phase composition and crystallinity are investigated and optimized through introduction of a post-deposition phase conversion process. Mechanical behavior of the coatings is characterized qualitatively through observation of the coatings behavior on expanded stents. HA was applied on coronary stents followed by a simulated stent implantation procedure to ensure high reliability of coating, i.e. no separation, delamination or visible damage. Finally, performance of the HA-ECD coated stents was evaluated in-vivo by the collaborating industry (MIV Therapeutics, Vancouver, B.C.) using porcine models.

2 LITERATURE REVIEW

2.1 Coronary Heart Disease (CHD)

Coronary heart disease (CHD), also called coronary artery disease (CAD), is the result of the atheromatous plaque accumulation, which composed of cholesterol, fatty compounds, and a blood-clotting material (fibrin), within the walls of the arteries that supply blood to the myocardium- the middle layer of the heart[31, 32]. Figure 2.1-1 illustrates accumulated atheromatous plaques on the inside of arteries. While the atheromatous plaques initially expand into the arteries walls, they will finally expand into the lumen of the vessel, affecting the blood flow through the arteries. When atheromatous plaques obstruct less than 70 percent of the diameter of the vessel, symptoms of obstructive CAD are rarely observed. However, as the plaques obstruct more than 70 percent of the diameter of the vessel, symptoms of obstructive CAD will starts to develop[33]. At this stage of the obstruction, the symptoms of ischemic heart disease are often first noted during increased workload of the heart. As the obstruction develops, there may be near complete blockage of the lumen of the coronary artery, restricting the flow of oxygen rich blood to the myocardium. Individuals with this degree of coronary heart disease will typically suffer from myocardial infarctions- heart attacks, and may have signs and symptoms of chronic coronary ischemia, including symptoms of angina at rest and flash pulmonary edema[1].

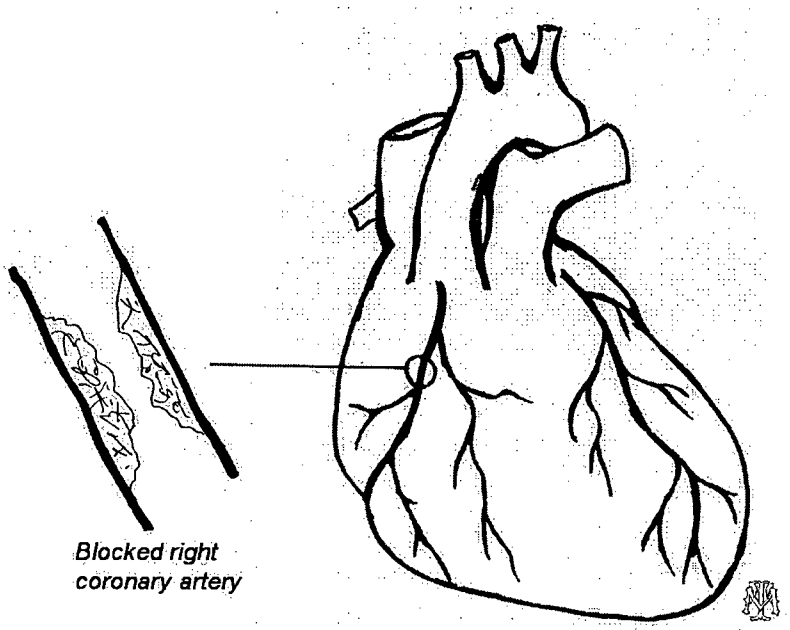

Figure 2.1-1. Fat and cholesterol accumulated on the inside of coronary arteries.

Coronary artery disease is the leading cause of death in North America. In 2004 approximately 54% of all cardiovascular deaths were due to coronary artery disease[1]. Due to the varying severity levels of CAD, treatments for the condition range from minor lifestyle alterations to major invasive surgery. There are three main objectives in treating CAD: (1) to prevent the development of symptoms or to reverse atherosclerosis; (2) to relieve symptoms; and (3) to lower an individual's risk of suffering from a heart attack and sudden death. CAD treatments are done in the following three stages:

(1) Initial Treatment: occurs immediately after an individual is diagnosed with CAD or is recognized as being at risk. This treatment stage is usually based on making key lifestyle changes, such as quitting smoking, eating healthier foods, and exercising.

(2) Ongoing Treatment: continue monitoring an individual following initial treatment, such as monitoring of blood pressure, weight, and cholesterol levels. This is used to

determine if the lifestyle changes have produced favorable results and to examine the patient's continued risk for developing CAD.

(3) Coronary Artery Bypass Surgery/Angioplasty Procedures: when an individual is determined to be at high risk for a heart attack, two revascularization procedures are available: coronary artery bypass graft (CABG), which is also called a "bypass", and Percutaneous Transluminal Coronary Angioplasty (PTCA). Since both therapies have established favorable results, the decisions are based primarily on several key factors, such as is the severity of the narrowing, number of arteries being affected, the location of the narrowing, and individuals' factors, such as age and general health.

Percutaneous transluminal coronary angioplasty is a technique of opening a narrowed or closed vessel without having to resort a major bypass surgery. PTCA has become an increasingly used and successful treatment by cardiologists to battle the ravages of CAD. Figure 2.1-2 demonstrates the PTCA technique with a balloon catheter. The balloon catheter is carefully positioned to the blockage site under fluoroscopy by the interventionist, and then it is inflated to compress the plaque against the artery wall. The use of a coronary artery stent together with balloon catheter in PTCA has been significantly increased during the past 10 years. Figure 2.1-3 illustrates the use of a coronary artery stent during and after PTCA to provide support for the artery wall. In 1996, stents were used in 50% of the 20,000 PTCA procedures in United Kingdom[34].

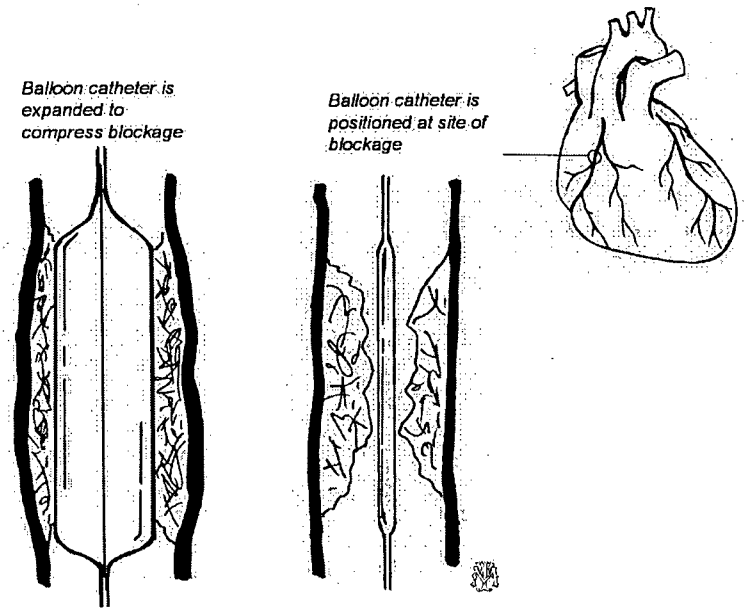

Figure 2.1-2. Schematic of percutaneous transluminal coronary angioplasty technique. A guide-wire is placed across the blocked section of the artery and a balloon is positioned beside the blockage. The balloon is then inflated compress the blockage against the artery wall.

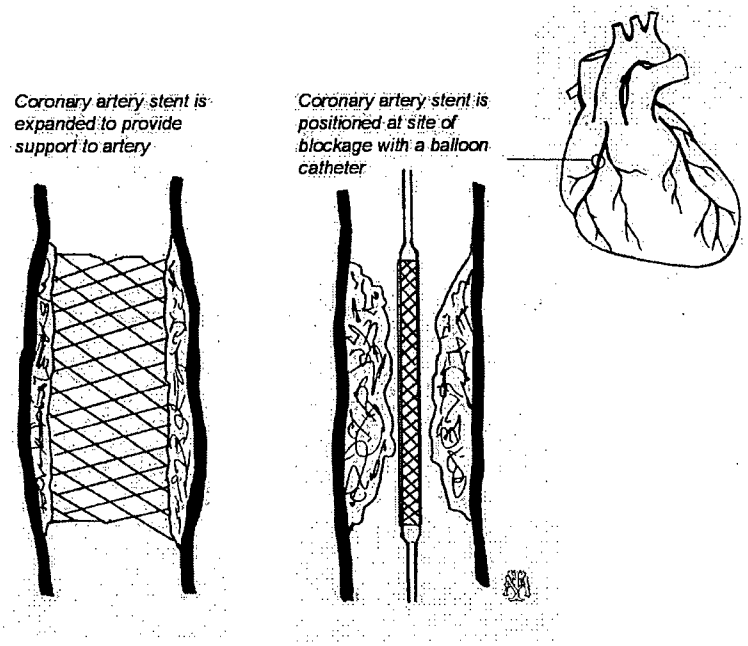

Figure 2.1-3. Schematic of percutaneous transluminal coronary angioplasty technique with the use of coronary artery stent. Coronary artery stent is used as mechanical scaffold to provide support to the vascular wall during and after the PTCA procedures.

2.2 Coronary Artery Stent

Coronary artery stents are metallic implantable tubular medical devices used as mechanical scaffolds to provide support to the vascular wall during and after the revascularization procedures of coronary arties. Stent is commonly mounted on a balloon catheter as a single unit, with the use of fluoroscopic screening and a radiopaque marker, the unit is carefully positioned across the site of lesion. Inflation of the balloon catheter results in expansion and deployment of the stent circumferentially to the surface of the coronary artery.

In 1964, Dotter et al were the first to describe a wire tubular implant as "stent" which was used in a non-surgical treatment for femoral arteries of animal[35]. In 1983, Dotter et al and Gragg et al implanted the first "stent-like device", a wire spring of nitinol, into the canine coronary arteries with a catheter[36]. In 1985, Palmaz et al reported the introduction of coronary artery stent together with a non-deployed balloon in the site of lesion[36]. Two years after, in 1987, Roussau et al tested a flexible, self expanding stainless steel stent. Forty-seven stents were implanted into 28 dogs, and 21 of these devices are implanted in the arteries. It was reported that 35% of the animals exhibited partial or total thrombotic occlusion[37]. It was in 1986 that the first implantation of coronary artery stent in human was performed and reported by Jacques Puel[36, 37]. In 1991, Schatz announced the results from a multicenter study of 229 successful deliveries of intracoronary stent placements in 230 lesions in 213 patients[37]. It was reported that the subacute thrombosis rate reached 14% and 40% of restenosis was determined in the following 6 months. The high level of thrombosis rate had convinced cardiologists that

stent, as a foreign object, when implanted will cause high thrombogenicity. In the early 1990s, the Belgian-Netherlands Stent study (BENESTENT-1)[38] and Stent Restenosis Study (STRESS)[39] were carried out to compare the conventional coronary balloon angioplasty with stent implantation. The results have shown beneficial effects of coronary stenting following balloon angioplasty, in comparison to angioplasty procedure alone. It was reported that among the 407 patients in the studies, the incidence of restenosis was significantly lower after stent implantation (BENESTENT 22%, STRESS 32%) when compared with after balloon angioplasty alone (BENESTENT 32%, STRESS 42%)[38, 39]. The beneficial effect of coronary stenting has been attributed to the larger acute lumen dimensions and to the prevention of constrictive remodeling[37]. It was until 1994, that the first FDA approval of stent device was issued to Palmaz-Schatz stent.

Many pioneer researches have underlined major problems with the use of stents. Subacute stent thrombosis is undoubtedly one of the problems despite the fact that very aggressive anticoagulation regiment was used in several studies. Restenosis, defined as the decrease of the vessel lumen diameter by at least 50% at the site of angioplasty procedure, is the other problem. Nevertheless, the combination of the technical advances and previous research data helped to define the ideal characters of today's stent as follows:[36, 37]

- Flexible
- Low unconstrained profile
- Radio-opaque
- Non-Thrombogenic

- Biocompatible
- Reliable
- High radial strength
- Circumferential coverage
- Low surface area

Alloys routinely used for the manufacture of stents include 316L stainless steel, nitinol, cobalt-chromium alloy, and tantalum. It is obvious that the mechanical properties of these alloy materials can dramatically influence the stent properties and stent design possibilities. In medical grade 316L stainless steel, L is used to indicate the low carbon content (0.03%). This alloy is composed of iron (60% to 65%), chromium (17% to 18%) and nickel (12% to 14%). Stainless steel provides good mechanical, chemical, and physical properties but its biocompatibility remains an issue. 316L stainless steel made stents often require plastic deformation by balloon catheter to deploy in the artery. Nitinol or NiTi alloy consists of ~55% Nickel and ~45% titanium. Nitinol is gaining popularity in the design of stent due to its shape memory capabilities. Under a mechanical load, nitinol can deform reversibly up to 10% of strain by the creation of a stress-induced phase transformation[37]. Once the applied load is removed, the stress-induced phase becomes unstable and the material recovers to the original shape. However, concerns regarding nickel release from Nitinol have limited its applications[36, 37]. Tantalum is another option for materials in stent manufacture, though questions have been raised because of its exaggerated radiopacity[37, 40]. Cobalt-chromium alloys based stents are under development by leading stent manufacturing companies such as: Guidant

and Medtronic. Cobalt-chromium alloys allow thinner strut design on stent without compromising radial strength and radiopacity[37, 40].

Although coronary artery stenting results in a larger acute lumen and prevents elastic retraction of vessel, the presence of a metallic stent stimulates the restenosis mechanisms more significantly than simple balloon angioplasty owing to intimal hyperplasia, i.e. the biological response of an injured vessel. The complex restenosis mechanism following the stent implantation is due to the following[38, 41]:

- The inner elastic membrane induced by injuries.
- The secretion of mitotic substances and growth factors.
- The prolonged and continuous stress created by the stent.
- The chronic irritation targeted by the presence of a foreign object.

In 2002, the worldwide market of coronary and peripheral intervention was about U.S. $5 billion dollars and growing 5% per annual. Of all percutaneous coronary intervention, 75% involve stent implantation and as much as 50% for peripheral intervention, approximately 1,000,000 stents are being implanted each year worldwide[1]. Nowadays, multidisciplinary studies are being conducted to enhance the overall stent performance. The current stenting technology includes: coated stents, biodegradable stents, radioactive stents, and drug-eluting stent that release pharmaceutical agents locally.

2.2.1 Coated Stents

Various coatings have been researched for coronary stents, including: diamond-like carbon[42, 43], hydrogen-rich amorphous silicon carbide[44, 45], amorphous titanium oxide[46], and gold[47]. Some of these inert or tissue friendly coatings do not cause platelet accumulation and inflammation. Comparing to uncoated stents, these coated stents demonstrated a lower thrombogenicity in the biological environment and improved overall biocompatibility. In an in-vitro study, Gutensohn et al have reported that diamond like carbon can not only reduce thrombogenicity but also reduces the release of metallic ions from the stainless steel to the surrounding tissue[43]. The inertness of gold was investigated by Kastrati et al with the expectation of increasing the stent biocompatibility and radiopacity. However, a randomized trial has suggested the gold coated stents exhibit an increased possibility of restenosis when compared with stainless steel stents[47]. It was further reported that the undesired result may be related to a coating defect rather than the gold itself. This demonstrates the importance of the coating processing along with biocompatible concerns, which together ultimately determines the outcome of the procedure.

Heparin coating on stent is another approach to reduce thrombogenicity. Heparin is a complex organic acid found in lung and liver tissue, having the ability to prevent blood clotting. Although heparin can not break down already formed clot, it allows the body to dissolve away the clot[48]. In animal model, heparin coatings have been proven to reduce thrombus formation, however, long term clinical data is still uncertain. One of the

commercialized heparin stents, BX Velocity by Johnson & Johnson, immobilizes heparin on the stent surface and remains free to inhibit thrombus formation[49].

2.2.2 Biodegradable Stents

One of the primary reasons to use coronary artery stents is for the scaffolding effect. While this is observed to be beneficial in the short term, the presence of a metallic stent may trigger chronic inflammation and in turn stimulate restenosis. To avoid the latter problem, a biodegradable stent has been proposed. A biodegradable stent exhibits similar mechanical functionality of a metallic stent but will then slowly degrade as the artery become stable. Stackle et al were the first to develop biodegradable stents with poly-L-lactase[50]. In 2000, Tamai et al have reported the results of the first 6-month clinical trial of biodegradable poly-l-lactic coronary stents in humans. In these results, no thrombosis or death was observed for the first 30 days, and an acceptable restenosis rate was reported to be 10.6%[51].

2.2.3 Radioactive Stents

It was demonstrated that a low dose of radiation can effectively inhibit or decelerate the proliferation of vegetative cells[37, 49, 52]. It is believed that this phenomenon can lead to a reduction of intimal hyperplasia and as a result decreases the chance of restenosis. Herlerin et al have reported the use of radioactive stent in an animal study[52]. The radioactive stents used are made of steel bombarded with Co, Mg, or Fe ions in a cyclotron, and thus emitted γ and β radiation. These stents can emit various radiations

doses between 15-23 μCurie. The animal study has shown that while both the low and high doses radiation reduces intimal hyperplasia, the intermediate dose caused an increase of hyperplasia[52]. This demonstrates the complexity between radiation and vessel response. While the therapeutic and toxic limits still have not been determined accurately, the rate of restenosis at the edges of radiated area remains a major problem[49]. In general, there still exist unsolved and unknown problem with the use of radiation in form of short therapy and radioactive stents.

2.2.4 Drug Eluting Stents

Drug eluting stents (DES) that can efficiently deliver biologically active agents locally to the vascular wall have been under intensive research in recent years. Early results with drug eluting stents were often unsatisfactory due to uncertain require dosage, uncertain delivery duration, poor drug efficacy, and proinflammatory polymeric coating[37]. More recent studies on DES with the use of anti-proliferation drugs have generated excellent results. Sirolimus and Paclitaxel are the two most commonly used anti-proliferation drugs. Sirolimus is a macrolide antibiotic that possesses immunosuppressant activity, it is also known to be an inhibitor of smooth muscle cells (SMC) proliferation and migration[53]. Paclitaxel is an approved drug used as cancer chemotherapeutic agents, it inhibits cell proliferation and migration by assembling the tubulin dimmers into the non-functional microtubules, causes alteration of the cell cytoskeleton structure[54]. Other anti-proliferation drugs under investigation includes: everolimus, tacrolimus, estradiol, dexamethasone, and angiopeptin.

Two of the commercialized polymer-based DES are CYPHER™ stent with sirolimus by Cordis® and EXPRESS™ stent with paclitaxel by Boston Scientific®. Both of these DES use polymer as a vehicle to carry the drug eluting into surrounding tissue through diffusion and convection[55]. While concerns have been raised with polymer coating, non-polymeric stents ACHIEVE™ coated with paclitaxel by Cook® is under investigation. However, clinical studies have been inconclusive. The question between the potential long term degradation and inflammatory effect of polymer coating and control release rate of non-polymeric coating are still in debate. Although there can be no doubt that the development and implementation of drug-eluting stent in past clinical studies has been a major milestone that will evolve the approach to the management of coronary artery disease, yet, it is also certain that more data are required to fully understand the scope of its benefits and to identify its limitations. In spite of the different drugs being investigated and their different therapeutic effects, the technique of coating, and drug delivery platform are still the key component leading to the success of the device.

2.3 Bioceramics

The American Society for Testing and Materials (ASTM) defines ceramics as "...essentially inorganic, nonmetallic substances..." [56]. Ceramic bonding is generally a hybrid of ionic and covalent bonds. The strong bonding forces of ceramic materials result in properties such as high elastic modulus and hardness, high melting points, low thermal expansion, and good chemical resistance[6]. However, the bonding nature and minimum number of slip system of ceramics make it difficult to shear or deform

plastically, therefore lowering the fracture toughness. Ceramic materials are hard and brittle. Unlike polymers and metals, ceramics are non-ductile and are very susceptible to notches or microcracks. It is not easy to process flawless ceramics, pores or micro-cracks often cause stress concentration to initiate cracks. Because of this, it is very difficult to precisely determine the tensile strength of ceramics, moreover, it is the reason why ceramics have low tensile strength compared to its high compressive strength. Modern advance techniques for ceramic processing have led them to become advance engineering materials.

More recently, the biocompatibility and bio-inertness of ceramics have been realized, and these "bioceramics" are being widely used in orthopedics and dental industries. Bioceramics can be manufactured in various forms such as: micro-spheres, thin film coatings, porous network blocks, composites with a polymer component, and well polished surfaces[57]. Bioceramics used within the body can be categorized into three classifications: bio-inert, bio-resorbable and bio-active[6]. Bio-inert ceramics are inert in the physiological processes, meaning that they maintain their physically and mechanical properties unchanged, and have almost no influence on the surrounding living tissue. Examples of bio-inert ceramics are alumina, zirconia, silicone nitride, and carbon. Most of these bioceramics are used in structural support devices such as: bone plates, bone spacers, bone screws, and femoral heads[57]. Alumina has been used in orthopedics and dental surgery for almost 20 years, it properties include high hardness, inertness, low coefficient of friction and wear resistance[58]. These have made alumina as the ideal candidate for joint replacement. Medical grade zirconia has been developed for use in

total joint prostheses because of its high fracture toughness and tensile strength. Such improved properties of zirconia have enable manufacture of femoral head into smaller diameter than present generation of alumina. Pyrolytic carbon is commonly used in coating of artificial heart valves for the last 30 years[59]. Properties that make this material suitable for this application include good strength, wear resistance, durability, and most importantly, thromboresistance.

Bio-resorbable ceramics, as its name implies, will dissolve or degrade upon implantation into the body. The degradation rate of bio-resorbable ceramics varies among different materials. Most of the bio-resorbable ceramics are in forms of calcium phosphate. Due to the resorbable nature of most calcium phosphate, they have been often used as potential bone defect fillers. In such application, the calcium phosphate filler would fill the void and gradually dissolve away, being replaced by host tissues. Two critical issues with the development of bio-resorbable ceramics are: maintenance of stability and strength during the degradation period, and matching resorption rate to the natural repair rates of the body tissues. Tricalcium phosphate is one example; it has been used as temporary bone substitute[60], where it has to maintain sufficient strength at first to allow bone ingrowth, then eventually degrade and be replaced by endogenous bone. Other uses of bio-resorbable ceramics include drug deliver devices and ocular implants. Tricalcium phosphate cysteine composites loaded with erythromycin or penicillin were developed by Morris et al. for the treatment of bone infection. It was reported that TCP/cysteine composite releases the antibiotics over a period of 3 weeks at the site of

infection. The authors suggested that antibiotics released from TCP amino acid composites effectively utilized in the treatment of bone infection[61].

Bio-active ceramics are surface reactive and bond to adjacent tissue some time after implantation[12]. In many cases, the interfacial bond strength is equivalent to or greater than the cohesive strength of the implant material. Bioactive glass and hydroxyapatite are examples of bio-active ceramics. Unlike the other bio-resorbable calcium phosphates, hydroxyapatite does not break down in physiological conditions. Hydroxyapatite is thermodynamically stable at physiological pH and actively takes part in bone bonding, forming strong chemical bonds with surrounding bone. Although the mechanical properties of bio-active ceramics have been found to be unsuitable for load-bearing applications such as in orthopedics, they are commonly used as surface coating on metallic implants to provide bonding with tissue, while the metallic component bears the load[17, 26].

2.3.1 Calcium Phosphate Bioceramics

Calcium phosphate (CaP) has been used in medicine and dentistry for more than 20 years and it has been used as artificial bone since 1970s[62]. It has been synthesized and used for manufacturing various forms of implants and also coating for implants[7-9, 17, 26, 63]. Depending on the Ca/P ratio, water content, impurities, and temperature, calcium phosphate can be crystallized into different forms[6]. There are several calcium phosphate ceramics that are considered biocompatible. Of these, most are bio-resorbable and will dissolve when exposed to physiological environments. Some of these materials include:

amorphous calcium phosphate ACP, dicalcium phosphate DCP ($CaHPO_4 2H_2O$), octacalcium phosphate OCP ($Ca_8H_2(PO_4)_6 5H_2O$), tetracalcium phosphate TTCP ($Ca_4P_2O_9$), alpha-tricalcium phosphate α-TCP ($Ca_3(PO_4)_2$), beta-tricalcium phosphate β-TCP ($Ca_3(PO_4)_2$), and hydroxyapatite HA ($Ca_{10}(PO_4)_6(OH)_2$). These forms of CaP are summarized in Table 2.3-1[64].

Table 2.3-1. Various calcium phosphate bioceramics

Chemical Name	Abbreviation	Chemical Formula	Ca/P Ratio
Amorphous calcium phosphate	ACP	-	-
Dicalcium phosphate	DCP	$CaHPO_4$	1.00
Dicalcium phosphate dihydrate	DCPD	$CaHPO_4 2H_2O$	1.00
Octacalcium phosphate	OCP	$Ca_8H_2(PO_4)_6 5H_2O$	1.33
Alpha-tricalcium phosphate	α-TCP	α-$Ca_3(PO_4)_2$	1.50
Beta-tricalcium phosphate	β-TCP	β-$Ca_3(PO_4)_2$	1.50
Hydroxyapatite	HA	$Ca_{10}(PO_4)_6(OH)_2$	1.67
Tetracalcium phosphate	TTCP	$Ca_4P_2O_9$	2.00

2.3.1.1 Bioresorption and Biodegradation

The dissolution products of CaP bioceramics can be readily assimilated by the human body. Bioresorption and biodegradation is generally controlled by *Physiochemical dissolution*- degradation depending on the local pH and the solubility of the biomaterial, *Physical disintegration*- degradation due to disintegration into small particles, and *Biological factors*- degradation cause by biological responses leading to local pH decrease, such as inflammation. All calcium phosphates degrade differently, the

degree of biodegradation in calcium phosphate ceramics is controlled by the aforementioned three factors, and also dependent on their properties such as surface area, density, porosity, composition, Ca/P ratio, crystal structure, and crystallinity[65, 66]. While various variables will have an effect on the biodegradation of calcium phosphate, the general order of solubility near-neutral pH environment is as follows (from highest to lowest):

$$ACP > DCP > TTCP > OCP > \alpha\text{-}TCP > \beta\text{-}TCP > HA$$

Stability of various forms of CaP as a function of pH is illustrated in Figure 2.3-1[67]. As seen in Figure 2.3-1 hydroxyapatite is relatively insoluble compare to other calcium phosphate phases, it is the only stable phase above pH 4.2. Below pH 4.2, dicalcium phosphate dihydrate (DCPD) is the stable phase. It is often observed that unstable phases of calcium phosphate will dissolve and re-precipitate into stable phase at a given pH. The pH of normal physiological environment is 7.2, however, this may decrease to as low as 5.5 in the region of tissue injuries or inflammation, and slowly return to 7.2 over time.

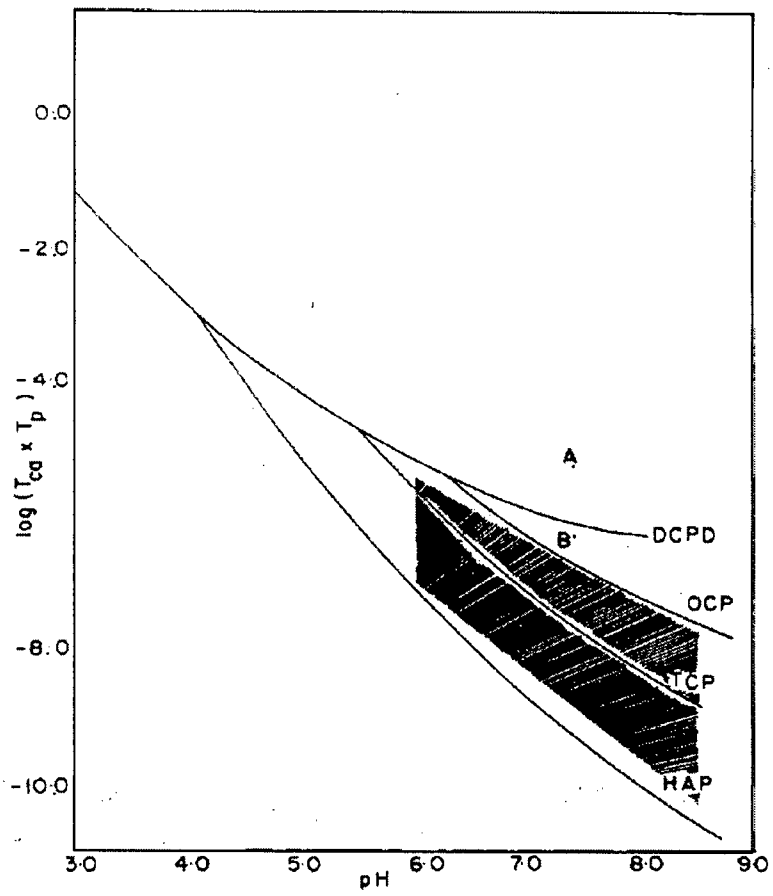

Figure 2.3-1. Logarithm of the product of calcium and phosphate concentrations plotted against pH values of solution saturated with respect to various calcium phosphate phases in the ternary system $Ca(OH)_2$-H_3PO_4-H_2O. Calculated for 37°C.

2.3.1.2 Mechanical Properties

The biomedical applications of calcium phosphates depend greatly on their mechanical properties; however, the poor mechanical properties of ceramic often limit its application. Table 2.3-2 summarizes the mechanical and physical properties of calcium

---

[1] Reprinted from Journal of Cystallinization of Calcium Phosphates, 102, P Koutsoukos, Z Amjad, MB Tomson, GH Nancollas, Crystallization of Calcium Phosphates. A Constant Composition Study, 1553 – 1557, Copyright (1980), with permission from American Chemical Society.

phosphates[6]. The wide range of variations in properties is due to the variation in structure, phase composition and manufacturing process. Tensile and compressive strength and fatigue resistance of HA (like most ceramics) are highly dependent on the total volume of porosity. For example, Jarcho et al reported compressive strength of HA as high as 917 MPa[68]. The HA specimen has been heat treated for 1 hour at 1100°C, while maintaining very fine grain size of 0.3 μm. In another study, a low compressive strength value of 138 MPa was reported by Rao et al, in which the HA specimen was heat treated at 900°C for 0.5 hour[69], and likely produced high porosity fraction in the material. Furthermore, the presence of porosity in form of either micropores (<1μm) or macropores (>10μm) can affect both the compressive and tensile strength of the material[10].

Table 2.3-2. Mechanical and Physical Properties of Calcium Phosphates

Property	**Value**
Elastic Modulus (GPa)	4.0 – 117
Compressive Strength (MPa)	70 – 300
Bending Strength (MPa)	147
Hardness (Vickers, GPa)	1.1 – 6.0
Poisson's Ratio	0.27
Bulk Density (g/cm^3)	1.90 – 3.27
Theoretical Density (g/cm^3)	3.16
Facture Strength (MPa)	12.8 – 60.4

2.3.2 Hydroxyapatite Bioceramics

Hydroxyapatite (HA) is chemically similar to the mineral component of bones and teeth, it is the most used phase among the various calcium phosphate bioceramic. HA is classified as the bio-active material, it exhibits good biocompatibility, bioactivity, and osteoconductivity[9, 64]. It has been intensely researched and used in orthopedic, dental, and maxillofacial applications. Hydroxyapatite crystallizes into hexagonal crystal structure and has a unit cell dimension a = 9.432 Å and c = 6.881Å. The Ca/P ratio of HA is 10:6 and the theoretical density is 3.219 g/cm^3 [6]. The mechanical properties of hydroxyapatite vary widely as many other calcium phosphates. Depending of the final heat treatment conditions, Ca/P ratio, and the presence of water and impurities, calcium phosphate can transform into HA or β-TCP. In many final products both HA and β-TCP phase coexist. A bioceramic consisted of a mixture of HA and β-TCP was first described as biphasic calcium phosphate (BCP) by Nery et al in 1986[70]. It was further researched and reported that the bioactivity of BCP maybe controlled by manipulating the HA/β-TCP ratios.

Hydroxyapatite exhibits excellent biocompatibility, it has the ability to integrate into bone structure and support bone ingrowth, and can form direct chemical bond with hard tissue[7, 8, 64]. It was reported that upon 4 to 8 weeks implantation, new lamellar bone and cancellous bone forms into the pore of hydroxyapatite implant[8]. Hydroxyapatite can be employed as bone substitute in forms of powders, porous blocks, or beads. Bone substitute or bone filler was most often used in the case of bone cancer and bone augmentation, where a large section of bone must be removed or reconstructed. Because

of the osteoconductive nature, HA bone filler can provide a scaffold and induce rapid filling of natural bone, reducing the healing time.

More recently, the effect of nanocrystals of HA on microvascular endothelial cell was studied. Pezzatini et al have exposed microvascular endothelial cells to stoichiometric HA nanocrystals and reported HA sustained endothelial survival without any cytotoxic effect[14]. Endothelial cell is a layer that lines the cavities of the heart and the blood vessels. The reaction of vascular endothelium cell to implanted biomaterial is of great importance because they interact in each step of tissue integration. It was concluded that HA nanocrystals exhibit high biocompatibility for microvascular endothelium, and do not acquire a proinflammatory or thrombogenic phenotype. Furthermore, endothelium was observed to be functioning toward angiogenesis – the formation of new blood vessels.

2.3.2.1 Thermal Stability

Hydroxyapatite is a hydrated calcium phosphate material. The stability of calcium phosphate depends on the temperature of preparation and the partial pressure of water. HA was found to be the stable phase up to 1360°C at 500mmHg partial pressure of water. And, in the absence of water content, β-TCP is found to be stable phase[71]. At dry environment and at elevated temperature above 900°C, HA will decompose and form other calcium phosphate as follows:

$$Ca_{10}(PO_4)_6(OH)_2 \Leftrightarrow 2\ \beta\text{-}\ Ca_3(PO_4)_2 + Ca_4P_2O_9 + H_2O$$

$$Ca_{10}(PO_4)_6(OH)_2 \Leftrightarrow 3\ \beta\text{-}\ Ca_3(PO_4)_2 + CaO + H_2O$$

At dry environment and at temperature above 1350°C, β-TCP will form. Both HA and β-TCP are very tissue compatible and osteoconductive[6, 71]. Therefore, heat treating HA under vacuum condition can induce decomposition at lower temperature, promoting the formation of water vapor. Whereas, heat treating in a high water content environment can counteract this effect and delay decomposition. Thus, it is important to control the atmospheric water content in order to prepare the desired final calcium phosphate phase.

2.3.2.2 Mechanical Properties

Hasimah et al have conducted a study on the effect of heat treatment temperature on the mechanical properties of hydroxyapatite[72], it was reported that upon heat treating HA from 1100°C to 1300°C, the compressive fracture strength increases from 12.87 MPa to 60.36 MPa and the porosity decreased from 37.7% to 5.5%. It was concluded that the increase in fracture strength was due to the increased bulk density as pore has a tendency to initiate crack. Similar study was also performed by Muralithran et al[73]. It was observed that when HA was heat treated from 1000°C to 1450°C, the relative density increased from 77.3% to 98.5% and the average grain size was 2.03 μm and 12.26 μm respectively. The authors suggested a definite positive correlation between hardness and grain size, however, the hardness was found to have decreased when a critical grain size is reached.

2.4 Biomaterial Coatings

Manufacturing of medical devices often incorporates a surface coating process. The design of medical devices is generally based on the bulk properties of material, it is often difficult to have a material that is both mechanically and biologically suitable. Since the biomaterial-biological medium interface is complex and usually involves reactions such as adsorption of water, protein-blood clot, inflammation, ion exchange, cell adhesion, corrosion, and decomposition, the surface properties of medical device plays a key role in determining its success. A biomaterial coating can tailor the surface characteristic of a medical device for a specific application without detrimentally affect the bulk properties of the biomaterial. Table 2.4-1 summarizes the purposes of biomaterial coatings. The ultimate objective of biomaterial coatings on medical devices is to combine the mechanical advantages of metallic implant and the biocompatible properties of coating to achieve the best desired biocompatible environment.

Table 2.4-1. Purposes of biomaterial coatings.

Wettability	Permeability
Bio-stability	Chemical inertness
Adhesion	Biocompatibility
Drug Delivery	Electrical Characteristics
Optical Properties	Frictional Properties

Biomaterial coatings can be categorized into two classes: passive surface coatings and active surface coatings. In general, passive coatings are used to alter selected properties of the implant surface without delivery of therapeutic or other agents.

Whereas, active surface coatings are aimed to deliver bioactive compounds or drugs to influence the biological response in order to achieve the desired function. In coronary stent applications, passive coating has often been applied as a thromboresistant coating; phosphorylcholine (PC) is one of the examples. In a six month implantation study, Grenadier et al have reported stents coated with phosphorylcholine appears to be safe and efficacious in the treatment of complex coronary lesions[74]. Drug eluting coatings are the one of the latest active coating developments in the medical industry, where formulated therapeutic agents are embedded into the coating reservoirs or matrix to enable site specific delivery. The drugs are gradually and locally released from the coating and simultaneously being absorbed by the surrounding tissues[40].

2.4.1 Hydroxyapatite Coatings

Due to the highly bioactive and biocompatible nature of HA, a medical device coated with HA is less likely to be recognized as foreign object by the body. Clinical data have shown that if an implant is coated with HA, it is possible to allow for positive material connections to establish between inorganic material and vital bone, and hence achieve long term osteointegration. In the case of osseous applications, hydroxyapatite coating can prevent fibrous tissue encapsulation on metallic implant, at the same time improves the integration of bone into the implant, and thus provides a strong bond between them[8]. In 1991, Furlong et al have performed a histological section of HA coated stem, which shown good osteointegration and formation of new vital bone. There was no evidence of an inflammatory reaction or of fibrous tissue formation[75]. Further

study on HA coated porous metallic implant demonstrated a clear acceleration of new bone ingrowth[75].

It is known that various metal ions can affect the functionality of osteoblast cell[76], and HA coating was also observed to be able reduce the release of metallic ions from the implant into the physiological surrounding. Sousa et al have reported that a film of 50μm HA coating can act as an effective barrier to metal ion release[76]. In their study, Ti_6Al_4V alloy was coated with 50μm HA by plasma spraying. No titanium, aluminum or vanadium was detected in by electrothermal atomic absorption spectroscopy. Similar study with 305 stainless steel coated with 50μm HA also found no release of metallic ion [77]. This barrier effect of HA was claimed to be a result of metal phosphate formation or incorporation of metal ions in the HA structure.

2.4.2 Processing of Hydroxyapatite Coatings

In the past, many different HA deposition methods have been reported, for example: plasma spray[15-17], sol-gel[18], pulse laser deposition[19], chemical vapor deposition, sputtering[20], electrophoretic deposition[21], and electrochemical deposition[22-24]. Among these methods, pulse laser deposition, sputtering, and chemical vapor deposition all involve a two step process. The first step involves synthesizing the desired coating material in bulk form, and in second step a pellet of coating material is irradiated by a high power source. Therefore these methods consume high amount of energy, and often require an ultra-high vacuum system, increasing the capital cost intensively. Furthermore, the coating composition frequently varies from the target material due to

the different sputtering speed. These methods are also not suitable for deposition on complex surface. Most of all, the high temperature of deposition may lead to detrimental effects on the of target substrate.

Plasma spray deposition of HA has become the most popular and commercial method for coating HA on orthopedic devices, however, technical issues still remain. One of the issues is the formation of other calcium phosphate phases other than HA resulting from the extremely high temperatures (>10,000 K) used in the plasma spray process. Ji et al have reported a microstructural study of plasma sprayed HA on titanium alloy and found that other than crystalline HA, amorphous calcium phosphate with Ca/P ratios of 0.6 – 1.0 are present, also a calcium titanate phase was detected at the coating-substrate interface[78]. Another issue is the poor adhesion of HA by plasma spray. Radin et al have found delamination of HA coating from titanium substrate in an in-vitro stability study[79]. Table 2.4-2 summarizes the general advantages and disadvantages of the techniques used for the deposition of hydroxyapatite.

Table 2.4-2. Summary of techniques used for deposition of hydroxyapatite coatings

Technique	*Thickness Range*	*Advantages*	*Disadvantages*
Plasma Spray	10 – 1000μm	▪ Rapid deposition rate ▪ Dense under well control ▪ spray very high melting point materials ▪ Wide range of applications	▪ Line of sight process ▪ High temperature induced ▪ High cost ▪ May decrease fatigue life of substrate ▪ High capital cost
Sol Gel	<1μm	▪ High purity ▪ Low cost process ▪ Low heat treatment process temp. (200 – 600°C)	▪ Expensive raw materials ▪ May require control atmosphere
Pulsed Laser Deposition	0.5-2mm	▪ Cost effective ▪ Rapid deposition rate ▪ Uniform coating thickness on flat substrate	▪ Line of sight process ▪ Cannot coat complex or porous substrate ▪ High capital cost
Sputtering	0.02-1mm	▪ Coating same composition as the source material ▪ Rapid deposition rate ▪ Uniform coating thickness on flat substrate	▪ Line of sight process ▪ Cannot coat complex or porous substrate
Electro-deposition	0.1-50μm	▪ Uniform coating thickness ▪ Rapid deposition rate ▪ Can coat complex substrate ▪ Low cost	▪ Sometime require high temperature heat treatment ▪ Difficult to produce thick crack-free coatings

2.5 Electrochemical Deposition

The electrochemical deposition (ECD) is done by passing an electric current between two electrodes separated by an electrolyte, and the deposition process takes place at the electrode-electrolyte interface. The electrochemical synthesis can be a reduction or an oxidation reaction. By manipulating the applied potential, the ECD reaction can be continuously varied. There are a number of features that differentiate ECD from other deposition technologies: (1) The reaction of electrochemical process takes place within the electric double layer of the electrode, which has a high potential gradient. Electric double layer is the layer which forms at the solid/liquid interfaces as a

result of a net charge on the solid surface (usually negative) causing a localized layer of neutralizing counter-ions (usually positive) from the solution phase to form near the solid surface[80]. (2) The deposition process occurs in a solid-liquid environment, which facilitates the growth of conformal coating on complex shaped substrates. (3) Process temperature is often low (<70°C) since it is limited by the boiling point of applicable electrolyte. (4) The electrolyte bath composition can be varied to control the coating composition. (5) Equipments are simple, inexpensive, and readily available. However, there are some disadvantages in the ECD process. The deposition product is often poorly ordered, making structural characterization difficult and sometimes contain amorphous impurties[80]. Furthermore, the deposition process can only be done with a conductive substrate.

Since coronary stent is a three-dimension mesh tube, the ability of ECD to deposit conformal films on complex non-planar devices is advantageous. Coronary stents can be coated relatively quickly (in minutes) and at relatively low (40°C) temperature. Capital cost of deposition instruments are relatively low compared to other technologies. Film thickness can be tailored over a wide range from ~0.1 μm up to millimeter range while still maintaining its usefulness for a desired application[23, 26]. The thickness and chemical composition of the ECD coatings can be well controlled through adequate selection of the process parameters, such as substrate composition and electrolyte composition, electrolyte concentration, pH, and temperature, and mode of applied potential (constant or periodic). The two most important parameters in determining the course of ECD

reactions are current density and applied potential, either one of these parameters can be controlled as a function of time to control the rate of coating deposition.

2.5.1 Electrochemical Deposition of Hydroxyapatite Coatings

In ECD, metal ions or complexes are hydrolyzed to form deposits on cathodic substrates[23, 25, 26]. In the electrochemical deposition process, the pH in the bulk solution is relatively low (typically 4.0<pH<6.0). The hydrolysis reaction and various cathodic reactions will consume water and produce OH^-, resulting in an increase of pH near the cathode.

In general, acidic solutions containing calcium and phosphate ions were used for the electrolyte for ECD-HA. Redepenning et al have reported the use of an aqueous solution saturated with $Ca(H_2PO_4)_2$ as an eletrolyte[81]. Shirkhanzadeh prepared an electrolyte for bioactive calcium phosphate coating by dissolution of hydroxyapatite into NaCl solution and further adjusted the pH by HCl[82]. A solution saturated with $CaHPO_4 \cdot 2H_2O$ and added KNO_3 and $NaHCO_3$ was prepared as electrolyte by Royer el at[83]. Electrochemical deposition of hydroxyapatite (HA) has been conducted in the mixed aqueous solution of $Ca(NO_3)_2\ 4H_2O$ and $NH_4H_2PO_4$[23, 84, 85].

According to a study by Shirkhanzadeh et al, the pH value within the diffusion layer of the cathode during ECD will be increased by the following two reactions:

$$2H_2O + 2e^- \rightarrow H_2 + 2OH^- \quad (1)$$

$$2H^+ + 2e^- \rightarrow H_2 \quad (2)$$

The concentration of phosphate HPO_4^{2-} is determined by the following reactions:

$$H^+ + PO_4^{3-} \Leftrightarrow HPO_4^{2-} \quad (3)$$

$$HPO_4^{2-} + OH^- \rightarrow H_2O + PO_4^{3-} \quad (4)$$

With the extra OH^- being produced, solubility limit of HA is reached (as illustrated in Figure 2.3-1) and consequently HA is deposited on the cathodic surface by the following reaction:

$$10Ca^{2+} + 6PO_4^{3-} + 2OH^- \rightarrow Ca_{10}(PO_4)_6(OH)_2 \quad (5)$$

Although this has been accepted as the general reaction sequence leading to HA deposition, details of cathodic reactions have been studied via cathodic polarization study to suggest further process controls. In a cathodic reactions study done by Yen et al, hydroxyapatite was coated via electrochemical method on pure titanium[23]. Yen et al reported that the cathodic reaction changes for different applied voltage:

(1) *Applied Voltage at [-0.1 to -0.3 V]*

$$O_2 + 2H_2O + 4e^- \rightarrow 4OH^-$$

$$H_2PO_4^- + H_2O + 2e^- \rightarrow H_2PO_3^- + 2OH^-$$

(2) *Applied Voltage at [-0.3 to -1.1 V]*

$$2H^+ + 2e^- \rightarrow H_2$$

$$H_2PO_4^- + e^- \rightarrow HPO_4^{2-} + \tfrac{1}{2} H_2$$

(3) *Applied Voltage at [-1.1 to -1.5 V]*

$$2HPO_4^{2-} + 2e^- \rightarrow 2PO_4^{3-} + H_2$$

(4) *Applied Voltage at [-1.5 to -3.0 V]*

$$2H_2O + 2e^- \rightarrow H_2 + 2OH^-$$

It was found that at an applied voltage of -0.7 V, $Ca(HPO_3H)_2 \cdot H_2O$ and $Ca(H_2PO_4)_2 \cdot H_2O$ were formed. At -1.25V, $CaHPO_4 \cdot 2H_2O$ were found to be the major phase and HA were found to be the minor phase. And, at -1.55V, HA became the major phase of deposition[23]. A purer HA was claimed at a lower deposition current density ($2mA/cm^2$) after being annealed at 300°C for 4 hours.

Kuo et al have also performed the cathodic polarization test, and suggested three stages of the reaction[26]:

(1) *Reduction of oxygen at [-0.4 V]*

$$O_2 + 2H_2O + 4e^- \rightarrow 4OH^-$$

(2) *Reduction of $H_2PO_4^-$ and $2HPO_4^{2-}$ at [-0.4 to -1.6 V]*

$$2HPO_4^{2-} + 2e^- \rightarrow 2PO_4^{3-} + H_2$$

$$2H_2PO_4^- + 2e^- \rightarrow 2HPO_4^{2-} + H_2$$

(3) *Reduction of water at [-1.6 to -3.0 V]*

$$2H_2O + 2e^- \rightarrow H_2 + 2OH^-$$

It can be seen that both Yen et al and Kuo et al have suggested very similar cathodic reactions. Figure 2.5-1 shows the cathodic polarization curve of titanium substrate in the electrolyte compose of $Ca(NO_3)_2$ $4H_2O$ and $NH_4H_2PO_4$. It was found that the greater amount of hydroxyls produced from reduction of water at voltage -1.6 to 3.0 V promotes the formation of a purer HA[26].

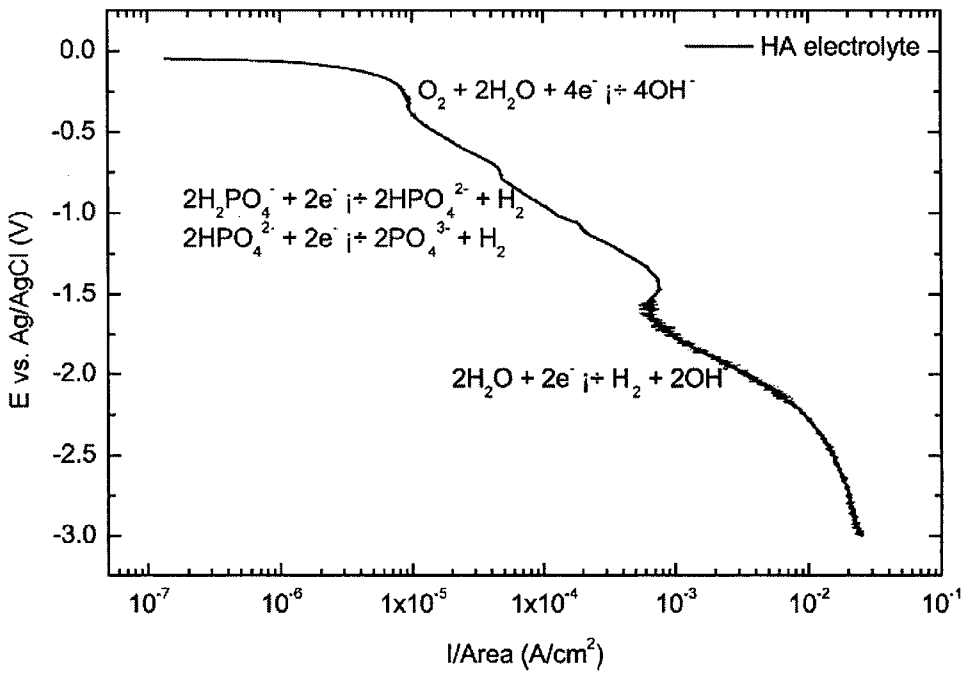

Figure 2.5-1. Cathodic polarization curve of Ti substrate in a $Ca(NO_3)_2$ $4H_2O$ and NH_4-H_2PO_4 electrolyte.

The electrochemical deposition of HA has also been conducted in an electrolyte composed of calcium acetate, acetic acid, and sodium phosphate[84]. Manso et al have subsequently dried the coated sample at 100°C and 900°C, X-ray diffraction (XRD) of the samples have shown that the 900°C dried sample exhibits HA phase with higher crystallinity. Surface force microscopy (SFM) was used to study the surface morphology of the coating. The analyses have proven that with the application of higher voltage a more compact film was produced, reducing the root mean square (rms) roughness from 90 nm to 20 nm[84].

---

[2] Reprinted from Journal of Materials Science and Engineering C, 20, Kuo M.C., Yen S.K., The process of electrochemical deposited hydroxyapatite coatings on biomedical titanium at room temperature, 153 – 160, Copyright (2002), with permission from Elsevier.

2.5.2 Microstructure and Phase of ECD Calcium Phosphate Coatings

As aforementioned, current density is one of the important parameters in controlling the rate of electrochemical deposition and the phase deposition. Yen et al have performed a series of experiments at different current densities to investigate the difference in phases and microstructures of ECD-CaP[23]. Electrolyte composed of $Ca(NO_3)_2 \cdot 4H_2O$ and $NH_4H_2PO_4$ was used for deposition of CaP on pure titanium substrate, and current densities were selected as 0.3, 1.0, 2.0, and 3.0 mA/cm^2 for a deposition time of 1000s. It was found that at 0.3 mA/cm^2, $Ca(HPO_3H)_2 \cdot H_2O$ monocalcium phosphate monohydrate (MCPM) was the main phase and revealed a flake dendrite structure. A major DCPD and minor HA phase was found at $1mA/cm^2$, and a fine loose plate-like structure was observed. At 2 mA/cm^2, a dense plate-like structure was found, and HA became the major phase. At 3 mA/cm^2, HA was again found to be the major phase, but "volcano-like" microstructures were observed. It was claimed that this is due to the "bubble-effect" from the increased current density and as a result generated higher production rate of hydrogen bubbles[23]. The "bubble-effects" were also experienced by others electrochemical deposition studies when high current or voltage was applied to the system[86-88]. Among these studies, "bubble effect" was generally observed to have a negative impact on coating surface coverage and coating structure. Optimization was attempted by Huo et al, in which the substrate was rotated at high speed, and thus the centrifugal force could clear away hydrogen bubbles.

A study of electrochemical deposition of calcium phosphate in modified simulated body fluid (SBF) was done by Peng et al[89]. SBF is an acellular fluid that has

inorganic ion concentrations similar to those of human extracellular fluid. Instead of applying a constant potential, a periodic pulsed potential was used for the deposition of calcium phosphate in SBF for duration of 30 minutes. The growth of coating was observed from 8 to 20 min of deposition. Sparsely distributed calcium phosphate deposits (nuclei) were found at 8 min, and the coalescence of these nuclei after 10 min of deposition has increased the surface coverage. At 20 min of deposition, coalescence continues and an interconnected porous coating was observed. The pore size was in the range of a few nanometers to 1μm[89]. XRD analysis has shown that the coating consists of OCP and amorphous HA phases.

Similar to the work done by Yen et al, Huang et al have conducted an electrochemical deposition study with an electrolyte composed of the same reagents. However, the applied voltage ranged from 1.0 to 10V and the time of deposition varied from 1 to 3 hours. Furthermore the coated specimens were subsequently treated with a hydrothermal process at various pH and temperatures. It was found that coating prepared at 60°C, 2.0 V, and 2.5 hours, contain essentially pure DCPD, and the coating morphology appeared as plate-like crystals with an estimated thickness of approximately 50 μm[90]. After post-hydrothermal treatment at 180°C, the coatings were found to consist of both needle-like and plate-like crystals. XRD results have demonstrated that the needle-like crystals corresponded to HA phase, and the plate-like crystal were DCPD phase. After 200°C hydrothermal treatment, the coating reveals an interlocking network of non-oriented needle-like crystals and it was proven by the authors that these crystals consist entirely of HA[90].

Kuo et al have conducted electrochemical deposition in an electrolyte composed of $Ca(NO_3)_2\ 4H_2O$ and $NH_4H_2PO_4$. Pure titanium was used as substrate and coating was deposited at current density 1 – 20 mA for duration of 5 – 40 minutes at room temperature. XRD analyses of the coatings are shown in Figure 2.5-2[26]. With a current density of 1 mA/cm^2, DCPD was observed to be the major phase and HA was the minor phase. The same was observed with current density 5 mA/cm^2, but with an increased peak intensity at $2\theta = 25.88°$ and $2\theta = 31.77°$. At current density above 10 mA/cm^2, DCPD peaks were not found and HA became the main phase of deposition. The authors have suggested that only at current density above 10 mA/cm^2 there will be high enough concentration of OH^- to convert HPO_4^{2-} into PO_4^{3-} to subsequently precipitate HA[26].

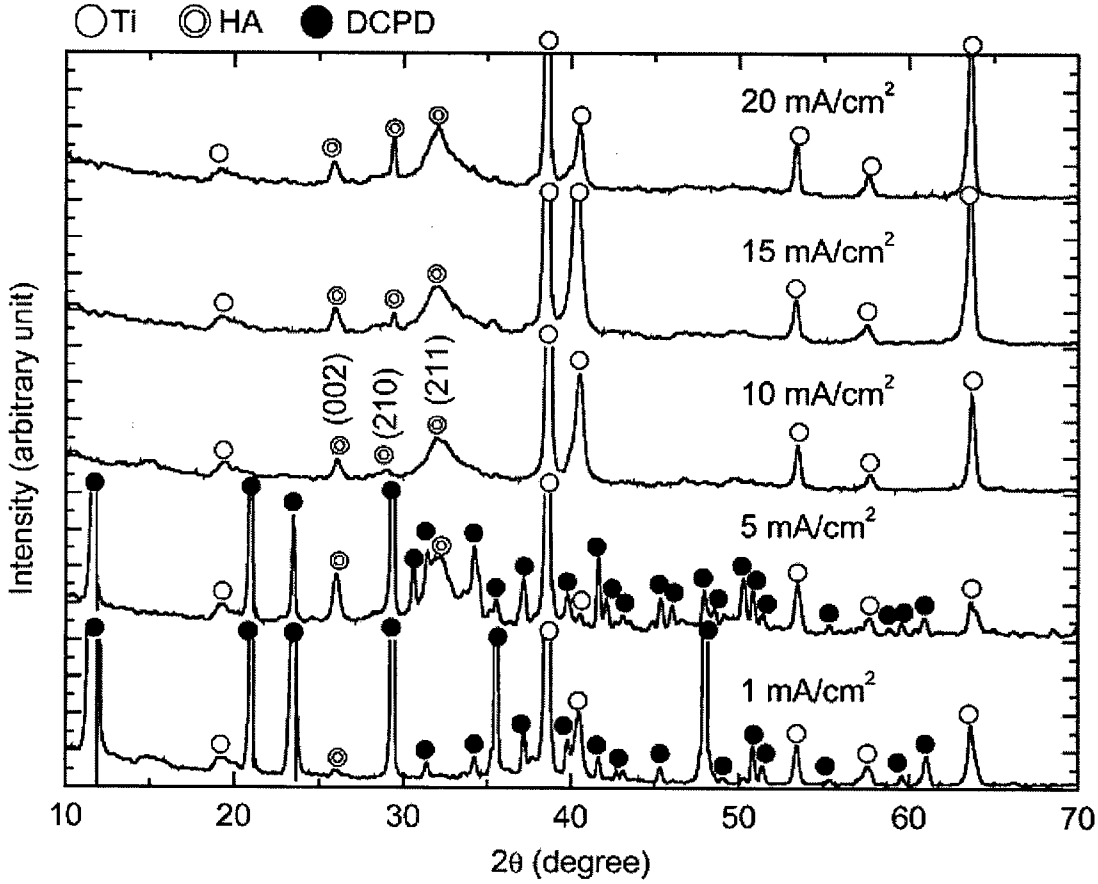

Figure 2.5-2. XRD analysis of coatings deposited at current density of 1, 5, 10, 15, and 20 mA/cm2 for 30 min.

© Journal of Materials Science and Engineering C, 2002, adapted by permission[3].

2.5.3 Adhesion of HA Coatings

Due to the brittle nature and adhesion concerns of HA bioceramic, there exists a challenge for the ECD hydroxyapatite coating to survive under the mechanical stress, i.e. in particular under coronary stent expansion during the angioplasty procedure. As well known, it is difficult to form a stable bonding at interface between ceramic and metal[91].

[3] Reprinted from Journal of Materials Science and Engineering C, 20, Kuo M.C., Yen S.K., The process of electrochemical deposited hydroxyapatite coatings on biomedical titanium at room temperature, 153 – 160, Copyright (2002), with permission from Elsevier.

The adhesion mechanism can be divided into three groups: (1) mechanical interlocking (2) physical bonding (3) chemical bonding. To overcome the difficulty of stable bonding, an interfacially modified surface is necessary between the stainless steel metallic surface and the hydroxyapatite ceramic, for the two surfaces to bond and adhere. Interfacial adhesion is influenced by numerous variables. These variables included: stress in film (both residual stress due to deposition conditions, and due to deformation of the substrate), contamination on substrate, chemical bonding between coating and substrate, physical properties, surface roughness, and precleaning method allowing chemically modified surface[92].

Lin et al have conducted a study on the growth of HA on 316L stainless steel in simulated body fluid, and alkaline treatment method was used to promote the adhesive strength of HA coating[91]. Alkaline treatment was performed by soaking the substrate in 10M NaOH aqueous solution at 60°C for 24 hours and heat treat at 600°C. The purpose of such treatment was to form an interfacial compound to bridge the 316L stainless steel (with metallic bond) and the HA (with covalent bond). It was found that an interfacial compound of Na_4CrO_4 formed after the alkaline treatment, and the following reaction was suggested[91]:

$$8Na(OH) + Cr_2O_3 \Rightarrow 2Na_4CrO_4 + 3H_2O + H_2$$

Tensile tests were performed to measure the tensile bonding strength of the coating, in comparison between 10M NaOH treated surface and 10M NaOH treatment followed by 600°C, the bonding strength increased from 25 MPa to 38 MPa[91].

The poor adhesion of electrochemically deposited HA can be also attributed to the "bubble effect" while high current (or voltage) was applied. In high current applications, the rate of OH^- and H_2 generation increases. When OH^- generation rate exceeds the rate of PO_4^{3-} formation, the excess OH^- groups would migrate away from cathode because of electric field and diffusion[89]. Therefore, the high pH boundary will shift away from the substrate and as a result calcium phosphate precipitation will take place away from the substrate surface, leading to poor coating adhesion. As hydrogen generation in electrochemical deposition happens at the electrolyte-substrate interface, the increased generation of H_2 often led to a heterogeneous and loose coating structure. Attempts have been made in the past to eliminate such phenomena. These included ECD processing with periodic pulse voltage by Shirkhanzadeh et al[93], and cathode rotation electrodeposition process by Recently, Hou et al[87]. In the process, the substrate was rotated at high speed (up to 1000 rpm) to remove both hydrogen bubbles and poorly adhered deposit particles. It was observed that the modified process produced a more homogenous and compact coatings which were more difficult to scrub from the substrates[87].

3 SCOPE AND OBJECTIVES

3.1 Scope of the Investigation

The principal motivation of the present work is search for better coatings for coronary stents, in particular search for bioceramic coatings such as hydroxyapatite, HA. Bioceramics, such as HA have been used in the medical industries for more than 20 years primarily because of their excellent biocompatibility. However, due to inferior mechanical properties such as low fracture toughness (<1.12 MPa$\sqrt{m}$) and low flexural strength (<140 MPa), the use of hydroxyapatite has been limited to no-load or low-load bearing applications. Hydroxyapatite coatings have a broad range of applications in medical devices and can provide superior biocompatibility in combination with the advantage of bulk material to achieve the best desired functions of the medical device. Electrochemical deposition (ECD) of uniform hydroxyapatite coating can be achieved on complex substrates. ECD also bears other advantages, such as good control of film thickness in 0.1 – 10 μm range, low temperature of processing (20 – 60°C), uniformity, and deposition rate and owing to low cost of equipment and starting materials. The combination of the potential advantages of ECD for uniform thin film HA coating on complex substrates motivated us to investigate this process for coating coronary stents. There are strong indications that hydroxyapatite thin film coating on coronary artery stents can reduce or eliminate restenosis. Hence, the process for electrochemical deposition of hydroxyapatite has been studied and optimized in the present thesis. The most significant process parameters (solution chemistry and concentration, temperature, current density, deposition time) were investigated and their effects on coating characteristics (thickness, uniformity, adhesion, phase composition) were evaluated.

Although there were previous studies of electrochemical deposition, very few have focused on thin film (<0.5 μm) hydroxyapatite coating and none of these have focused on coatings for stents. The uniqueness of present study is to combine the technique of surface modification, electrochemical deposition, and phase optimization to produce thin film hydroxyapatite coating for cardiovascular applications. The technology has been transferred to MIV Therapeutics, a Vancouver biotechnology company, which currently evaluates the method in a series of in-vitro and in-vivo trials.

3.2 Objectives

The broad objective of this study is to achieve a well-controlled and reproducible process to obtain thin film hydroxyapatite coatings via electrochemical deposition, on coronary stents made of 316L stainless steel. The specific objectives of the present thesis are as follows:

1. To develop reproducible hydroxyapatite coating process via electrochemical deposition with full coverage, optimum thickness (<0.5 μm), porous (~50vol%) microstructure, and sufficient adhesion to stent surface such that the coatings survive without delamination in the in-vitro stent deployment.
2. To determine the effects of electrochemical deposition (ECD) process parameters on the evolution of the resulting calcium phosphate coating. To develop an optimized electrochemical deposition process to deposit thin film hydroxyapatite coating on coronary stents by studying the process parameters, such as current density, time of deposition, electrolyte concentration, pH, and temperature.

3. To determine the resulting hydroxyapatite coating basic properties, such as coating thickness, microstructure, elemental composition, crystallinity, mechanical integrity, and phase composition.
4. To assess the effect of substrate surface pre-treatment on the deposition process and resulting coating in terms of physical (microstructure and phase) and mechanical (adhesion) properties. To apply a substrate surface pre-treatment to achieve high level of adhesion of ECD-HA coatings.
5. To apply a post-treatment process to the coatings to attain desired phase composition (i.e. pure phase HA), as well as improved adhesion and mechanical integrity of the coatings.
6. To perform further characterization of the coating in industrial setting:
    - Qualitative mechanical assessment based on in-vitro crimping and expansion tests.
    - Rate of dissolution based on in-vitro dissolution tests.
    - Overall performance qualification based on in-vitro stent deployment and 40 million cycles fatigue test.

4 EXPERIMENTAL METHODOLOGY

The following experimental methods were employed:

1. Measurement of the weight and thickness of electrochemically deposited coatings for different process parameters, such as current density, time of deposition, electrolyte concentration, pH, and temperature. The process stability, reproducibility and ease of control were monitored.
2. Evaluation of microstructural morphology such as uniformity and porosity, and phase composition of various ECD thin film coatings, deposited at different current densities and deposition times, and coatings deposited with substrate (316L stainless steel) surface pre-treatment and coating post-treatment.
3. Qualitative characterization of mechanical behavior of ECD coating with various substrates surface pre-treatments and coating post-treatment.
4. ECD process optimization, based on the outcome of the above steps 1 – 3. Application of the optimum ECD process for deposition of HA on coronary stents for further evaluation.
5. In-vitro evaluation of ECD thin film coating on coronary stents, such as crimping and expansion tests, dissolution tests, and fatigue tests.
6. In-vivo evaluation of the coated stents in porcine models (this step done entirely by the collaborating company MIV Therapeutics, Vancouver, B.C.)

4.1 Sample Preparation

Two types of substrates made of 316L medical grade stainless steel were used in this study, i.e. plate and a real coronary stent. The nominal chemical composition of 316L stainless steel is given in Table 4.1-1.

Table 4.1-1. Nominal chemical composition of 316L stainless steel

Element	C	Mn	Si	P	S	Cr	Mo	Ni	N	Fe
Weight% (max.)	0.030	2.000	0.750	0.045	0.030	18.000	3.000	14.000	0.100	Balance

Stainless steel plates were cut into rectangles with a width of 2.5 cm, a height of 3.0 cm and thickness of 0.1 cm. The actual plate area being coated was a square with 2.5 cm width and thickness of 0.1 cm. Unless otherwise stated, all plate specimens were polished with LECO® silicon carbide abrasive paper followed by a final 1 μm mirror polish with LECO® diamond suspension. The polished specimens were degreased by detergent and further ultrasonically cleaned in distilled water and absolute ethanol, then dried.

Stainless steel coronary stents were provided by MIV Therapeutics of Vancouver, B.C. All received coronary stent specimens were laser cut and electropolished using proprietary MIVT procedure. The MIVI 700 Series Coronary Stent had a 1.7 mm outside diameter, 1.5 mm inside diameter and a length of 14 mm. The MIVI stent is comprised of a series of sinusoidal-ring geometries with two discs forming a single module, a flexible curlicue was fabricated to join two modules together. A 14 mm MIVI stent consists of four modules. A schematic diagram of the stent is illustrated in Figure 4.1-1.

The strut of the stent had a width of 100 μm and the disc had a diameter of 500 μm. Unless substrate surface treatment was performed, all stent specimens were used as-received after cleaning. Stents specimens were cleaned ultrasonically in absolute ethanol, and then dried in air.

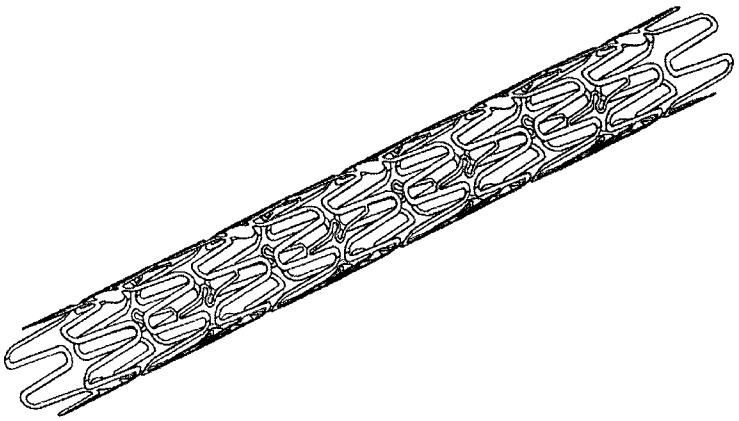

Figure 4.1-1. Schematic diagram of MIVI 700 Series Coronary Stent

4.1.1 Substrate Surface Modification

In order to create a better interfacial bond between the electrochemically deposited coating and the substrate, a substrate surface modification was performed with the use of 10N NaOH alkaline solution[91]. The 316L stainless steel substrates were soaked in 10N NaOH aqueous solution at 60°C for 24 hours. After the alkali treatment, the substrates were ultrasonically cleaned with distilled water and dried at 40°C. The alkaline treated substrates were subsequently heat-treated to 500°C for 20 minutes. Surface characterizations were conducted on the alkaline treated substrates. Electrochemical depositions were performed on the alkaline treated coronary stent

specimens for mechanical evaluation and in-vitro characterizations, and compared with those deposited on as-received stents.

4.2 Electrochemical Deposition

Electrochemical deposition was conducted in a water based electrolyte containing 0.02329M $Ca(NO_3)_2$ $4H_2O$ and 0.04347M $NH_4H_2PO_4$. The pH of the electrolyte was measured by Beckman 260 pH meter with accuracy ± 0.004 pH (Beckman 260, Beckman Coulter, Inc., Fullerton, California). The electrolyte pH was controlled at 4.5 with the addition of sodium hydroxide to the electrolyte solution. The electrolyte temperature was maintained at 45°C ± 2°C. The stainless steel substrate was used as the cathode, and a platinum foil was used as the anode. The cathodic electrochemical deposition was carried out using a current source with 0.01 mA resolution (IET Model VI-700, IET Lab Inc., Westbury, New York). All coated specimens were rinsed in distilled water to remove residual electrolyte and dried in oven at 40°C for 1 hour. Unless otherwise stated, all depositions were performed under the above generic ECD conditions. Figure 4.2-1 illustrates a schematic diagram of the electrochemical deposition.

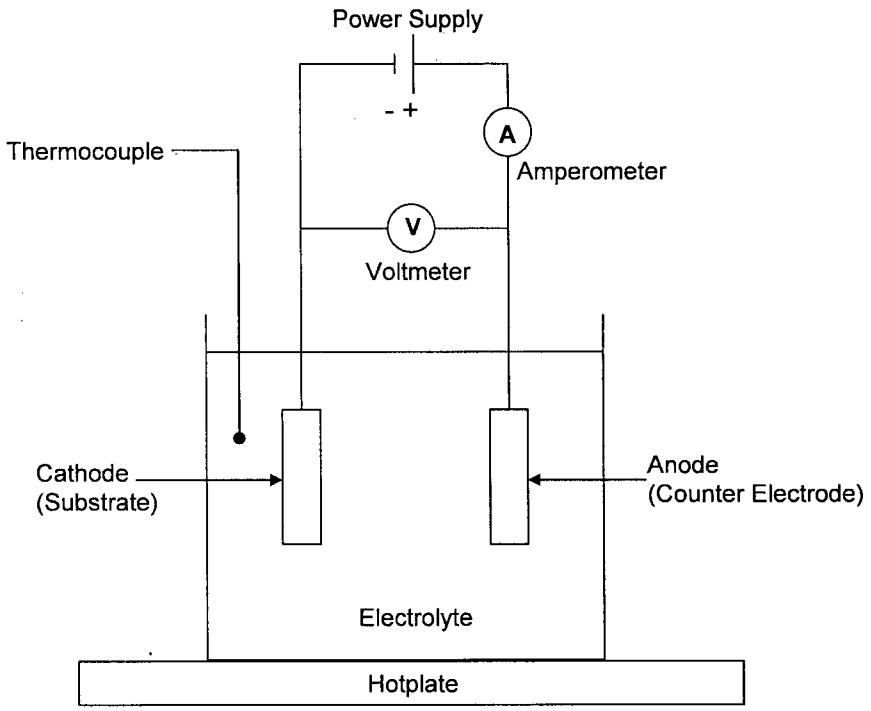

Figure 4.2-1. Schematic diagram of electrochemical deposition setup

4.2.1 Electrochemical Deposition Process Parameters Investigation

In order to gain the knowledge of electrochemical deposition for the coronary stent application, understanding the influence of basic process parameters on the resulting coating is essential. Based on the generic electrochemical deposition process the following process parameters were investigated:

- *Current density.* ECD was conducted at current density of 1 – 15 mA/cm^2 for 5 minutes deposition time.
- *Deposition time.* ECD was conducted for duration of 1 – 15 minutes with a current density of 1 mA/cm^2.
- *Electrolyte concentration.* Concentration of ECD electrolyte was adjusted based on the calcium to phosphors (Ca/P) ratio. ECD was conducted with electrolyte

Ca/P ratio of 2.92, 2.63, 1.95 and 0.49, at current density of 1 mA/cm^2 for 2 minutes

- *Electrolyte pH.* Electrolyte pH values of 3.0 – 6.0 with 0.5 increment were used for ECD at current density of 1 mA/cm^2 for 2 minutes. The specific range of pH was chosen for investigation to ensure a stable electrolyte was obtained without precipitation.
- *Electrolyte temperature.* ECD was conducted at current density of 1 mA/cm^2 for 2 minutes deposition time with electrolyte temperature at 25, 45, and 70°C.

All of the above electrochemical depositions were initially conducted on 316L stainless steel plates for the purpose of microstructural and phase characterization and process observation. The weight measurement and thickness estimation was performed based on the two main reaction rate determining parameters, i.e. current density and deposition time. The measurement of weight was performed on the coated specimens with various current densities and deposition times, and it is based on the weight gain per area (mg/cm^2), with a Sartorius ME235P-SD balance with 0.01 mg accuracy. The thickness (μm) estimation was also performed based on weight gain on coated specimens with various current density and deposition time, and through scanning electron microscopy examination of the cross-section area.

Evaluation of microstructural morphology such as uniformity and porosity, and phase characterization of the resulting coatings was conducted for all of the above specimens; the process stability and ease of control were also closely monitored for

process optimization. For the purpose of process consistency investigation, ECD coating was performed on five batches of ten coronary stent samples using process parameters listed in Section 5.2 (Table 5.2-1), and the coatings were characterized.

4.2.2 Electrochemical Deposition Optimization

The optimization of electrochemical deposition process parameters was chosen and detailed in Chapter 5 "Results and Discussion". The optimized parameters were applied and evaluated on electropolished stainless steel coronary stent provided by MIV Therapeutics of Vancouver, B.C.

The generic ECD process was performed as discussed in Chapter 4.2.1. Optimized parameters were applied on all stent substrates with a 0.90 mA applied current, and a deposition time of 1 minute. The applied current was specified to assure suitable current density was applied to the stent surface. The deposition time was adjusted to achieve desired thickness of the deposit, i.e. about 0.5 μm for the 1 minute deposition for the above conditions.

4.2.3 Phase Conversion Process

It is known that crystalline HA, among various calcium phosphate phases, has the longest resorption life of approximately 2 – 3 years under in-vitro environment. To ensure the resulting electrochemically deposited coating is of stable crystalline

hydroxyapatite, a phase conversion process was introduced[81, 100]. The phase conversion process was accomplished by soaking the coated substrates into 0.1N NaOH aqueous solution at 75°C for 12, 24, 48, and 72 hours. The measured pH of the 0.1N NaOH solution is approximately 12.5. The converted specimens were gently rinsed with distilled water and dried at 40°C. The converted specimens were then heat treated at 300°C, 500°C, and 700°C for 20 minutes for crystallization.

4.3 Microstructural and Phase Characterizations

The microstructural morphology and elemental analysis of the resulting coatings were observed by scanning electron microscopy equipped with energy dispersive x-ray spectroscopy (SEM/EDX, Hitachi S-300N, Hitachi Ltd., Tokyo, Japan). Crystallography of the resulting coatings was analyzed by X-ray diffractometer (XRD, Siemens D5000, Siemens, now Bruker-AXS, Germany) with Cu K_α radiation (λ = 1.5418 Å) and operated at a tube voltage of 40kV and a current of 30mA. The range of 2θ was from 5° - 50° with a scanning rate of 0.02°/s.

4.4 In-vitro Evaluations

For the application of coronary stents, the ECD-HA coating not only has to withstand deformation during manufacturing stage (i.e. stent crimping), but also at the implantation stage. Furthermore, the coating has to maintain its integrity and resist fatigue stresses in concern with the heart beat over the years after implantation in human.

In-vitro evaluations were targeted to assess the coating with crimping and expansion test, dissolution test, and fatigue test.

4.4.1 Crimping and Expansion Test

In order to implant and deliver a coronary stent in the percutaneous transluminal coronary angioplasty procedure, a stent must be first mounted onto a balloon catheter. This procedure in the manufacturing stage is often referred as the crimping process where the stent is crimped under external pressure. The crimping procedure was performed by MIV Therapeutics of Vancouver, B.C. with MSI stent crimping machine (Machine Solutions Inc., MSI SC 513, Arizona, USA). The MSI stent crimping machine applies an external pressure by using a pneumatic crimp mechanism. The ECD-HA coated stents were crimped from an original diameter of 1.7 mm to 1.0 mm onto a balloon catheter (Arriva™, InSitu Technologies Inc., Minnesota, USA).

Coronary stent mounted onto a balloon catheter is termed a stent delivery system (SDS). After implantation of the SDS into desired position, surgeon will expanded the coronary stent with an inflation device in order to keep the artery open. The expansion test for ECD-HA coated SDS was conducted with Encore™ inflation device (Encore™ 26 inflation device, Boston Scientific, Maple Grove, MN). The stent was expanded from a crimped diameter of 1.0 mm to 3.0 mm with 14 atm pressure.

4.4.2 Dissolution Test

Solubility of various calcium phosphates differs greatly, which affect the biodegradation of ECD coating. The variables that affect the dissolution not only consist of the phase and crystallinity of the coating, but variables such as pH, the specific nature of the buffer, temperature, and porosity are also important.

Dissolution tests were performed with Varian dissolution apparatus (Varian VK750D, Varian Inc., California, USA). Key features of the apparatus included precise bath temperature and rotation speed control, and the use of seal bottles to prevent dissolution media from evaporation. Dissolution tests were conduct at a bath temperature of 37°C and rotation speed at 20 rpm. Phosphate buffer saline (PBS) was used as the dissolution media because it helps to maintain constant pH (7.4) and it is isotonic. PBS contained 10mM phosphate, 140mM NaCl, and 3mM KCl. ECD coated stents were placed into dissolution apparatus with sealed bottles of 10 mL PBS, and ECD coated stents were weighted between 30 minutes to 4 weeks.

4.4.3 Fatigue Test

The objective of fatigue testing is to meet the requirements as per the "FDA Draft Guidance for the Submission of Research and Marketing Applications for Interventional Cardiology Devices" [94] for in vitro mechanical fatigue testing. The test should demonstrate the safety of the device from mechanical fatigue failures for at least one year of implantation life. The fatigue test is intended to provide empirical evidence for the continued structural integrity of the ECD-HA coated stents when subjected to mechanical

fatigue such as that which they would receive *in vivo*. The test is designed to simulate the stent fatigue due to the expansion and contraction of the vessel in which it is implanted. The test is accelerated in order to obtain results in a reasonably short time period. The environment for the test is phosphate buffer saline (PBS) at 37°C ± 3°C. The in-vitro simulated fatigue test was equivalent to one year of in-vivo implantation, i.e. approximately 40 million cycles of fatigue stress, which simulates heart beat rates from 50 – 100 beats per minute.

Six stent specimens were divided into three pairs for ECD coating. One stent from each pair was implanted into the proximal end of the simulated vessel, another into the distal end. All three pairs were ECD coated under the optimum deposition conditions, substrates surface were modified and subsequently treated with the phase conversion process. Final ECD coated stent specimens were then tested with 40 million fatigue cycles.

In fatigue testing, the objective was to determine if the ECD-HA coating is able to survive 40 million cycles in a vessel that dilated with an average percent outer-diameter (%OD) strain of 0.48%. The fatigue test was performed with a commercial EnduraTec fatigue testing machine (ElectroForce® 9100 Series, EnduraTec System Corporation, Minnesota, USA). A coronary stent with the optimum ECD-HA coating was first crimped onto a balloon catheter as described in Chapter 4.4.1, and then it was deployed into a simulated vessel (artery). A high performance laser was used to continuously monitor and measure the change in outside diameter of the simulated vessel, information

was subsequently feedback to the control computer to calculate the percent radial stain of stent. Two linear actuators were used to pressurize a saline test solution linked to the test vessel, a pump assembly converts the actuator displacement to test pressures, which simulated 40 million cycles.

At the end of the test cycles, the stent sample was retrieved and the PBS test solution was subsequently passed through a 0.4 μm micro-filter to trap potential debris from the ECD-HA coating. Scanning electron microscopy (SEM) was used to examine both the coating microstructure and the saline filters for any lose debris. SEM observation was made at ×100, ×800, and ×3000 magnification to examine the microstructure of coating at the end of the test to identify any existing micro-cracks or micro-peels. Energy dispersive x-ray spectroscopy (EDX) was used to identify the elemental composition of the coating surface or an area of interest such as filtered debris. Both SEM and EDX analyses were used to demonstrate the existence of remains of coating after the fatigue test. Filter specimen was carbon coated to create a conductive surface to avoid charging in SEM.

5 RESULTS AND DISCUSSION

5.1 ECD of Calcium Phosphate Coatings – Process Parameters Investigation

5.1.1 Current Density

Current density, applied voltage, and electrolyte concentration are the principal variables controlling the rate of reaction in the ECD process[25]. In order to achieve consistent results, current density instead of applied current, was chosen for investigation because different substrates (stents and plates) were interchangeably used throughout the study. The surface areas of different substrates were determined with the assumption of negligible surface roughness.

The SEM observation of plate specimens deposited at current density 15, 10, 5, 3, and 1 mA/cm^2 are shown in Figure 5.1-1 (a) – (e), respectively (other process parameters are listed in Table 5.2-1). The "bubble effects" were found on the coating surface of specimen deposited at 15 mA/cm^2, as shown in Figure 5.1-1 (a), where the vertical axis of specimen was horizontally aligned in the figure. Previous studies also reported similar phenomenon[23, 86-88]. This effect was attributed to the increased reaction rate with increasing current density, and as a result, hydrogen bubbles generated at a vigorous rate[23, 86]. The hydrogen bubbles rise to the surface and disturbed the formation of uniform coating.

In general, the microstructure of coating deposited at 15 mA/cm^2 exhibits a fine and loose structure. Figure 5.1-1 (b) illustrates the microstructure of coating deposited at

10 mA/cm^2. "Bubble effect" was not observed at such current density, the coating exhibits a fine and loose structure similar to 15 mA/cm^2, but with flakes growing on top. At 5 mA/cm^2, the coating exhibits a dense and non-oriented plate-like structure, as shown in Figure 5.1-1 (c). At 3 mA/cm^2, the microstructure was also non-oriented plate-like, but less dense and reveals an under-layer of coating (Figure 5.1-1 (d)). At the lowest current density of 1 mA/cm^2, a thin layer (~1 μm) of porous coating was observed as shown in Figure 5.1-1 (e). The morphology of this thin layer was similar to the under-layer in Figure 5.1-1 (d), but more porous. Other than some small amount of plate-like structures displayed at the deposition boundary (Figure 5.1-1 (e) [left]), the overall microstructure exhibits high porosity and good coverage. Due to technical difficulties, the stainless steel plates were used as-received in this study.

A trend of microstructure evolution can be clearly noticed from Figure 5.1-1, as current density changes. Figure 5.1-1 (b) – (d) indicated that the current of 10 – 3 mA/cm^2 facilitate the growth of plate-like crystals, and such microstructure is mechanically unstable since it can be easily detached from the substrate. Thus, to avoid the bubble effect and to prevent growth of plate-like crystals, 1 mA/cm^2 is more desirable for thin film uniform coating. Figure 5.1-2 illustrates the weight gain of ECD coated specimens deposited with current density 1 – 15 mA/cm^2 for 5 minutes deposition. The weight gain of coatings increases with increased current density. It was observed that the weight gain slightly reduced with 15 mA/cm^2, which can be explained by the "bubble effect" where fragments of the coating were flaked off by the large volume of hydrogen bubbles generated. This observation agrees with previous studies[86-88]

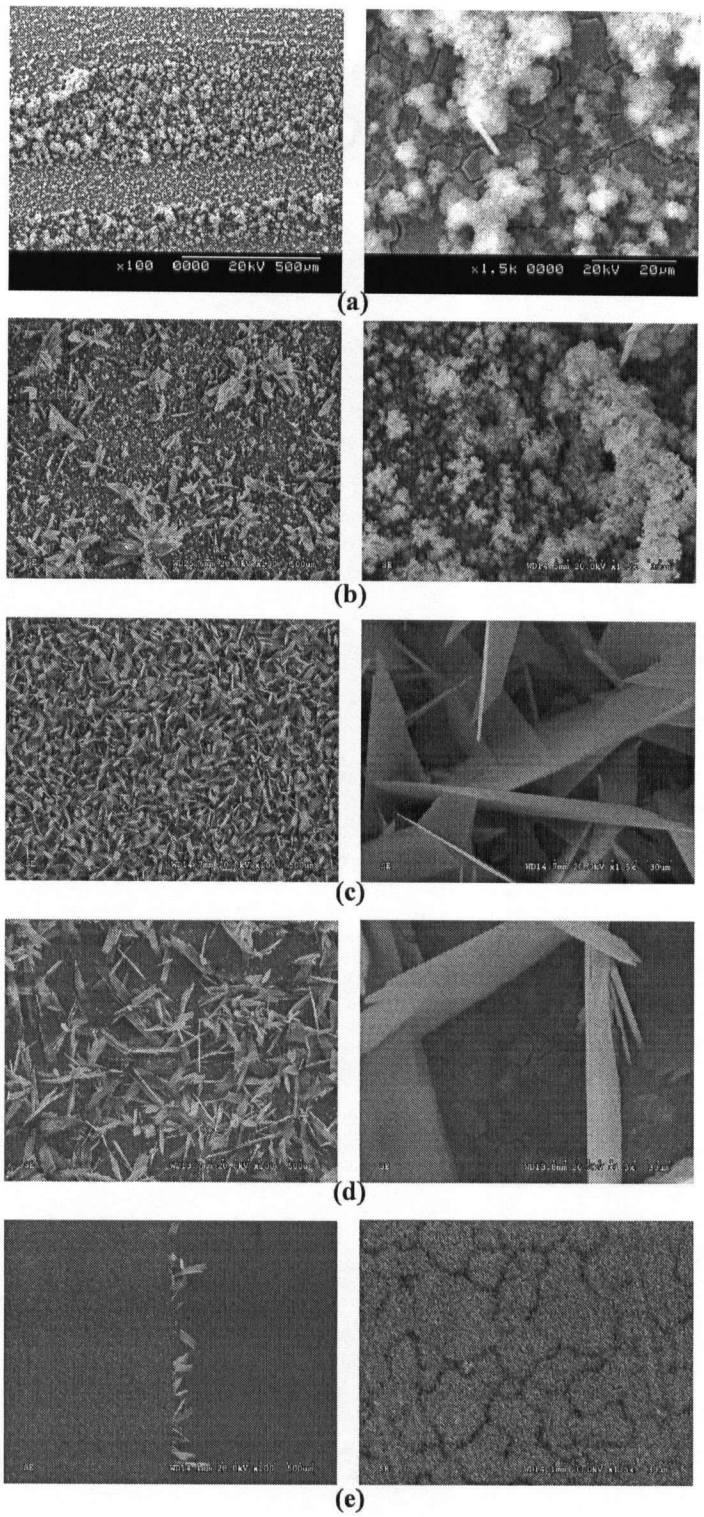

Figure 5.1-1. SEM images of ECD coating deposited at various current densities: (a) 15 mA/cm^2, (b) 10 mA/cm^2, (c) 5 mA/cm^2, (d) 3 mA/cm^2, (e) 1 mA/cm^2 [Left: ×100; Right: ×1,500]

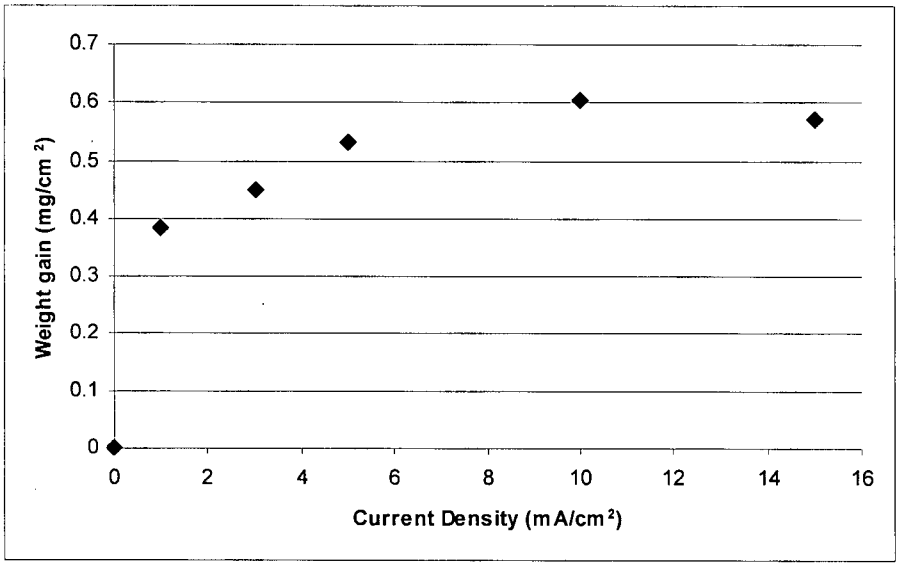

Figure 5.1-2. Weight gain of ECD coated specimens versus current density with 5 minutes of deposition.

5.1.2 Deposition Time

Scanning electron microscopy images were obtained for ECD coatings deposited at various times to evaluation the growth morphology and structural characteristics of the evolving film on plate specimens. Current density of 1 mA/cm^2 was selected for this study based on the resulting uniform thin film. The SEM observation of plate specimens deposited for 15, 10, 5, 3, and 1 min are shown in Figure 5.1-3 (a) – (e), respectively (other process parameters are listed in Table 5.2-1). From the observation of the deposition process, an "initiation period" (~15 seconds) for formation of coating was noticed. This phenomenon was also reported in other previous studies[89, 95]. An initiation period corresponds to the time from the application of current to the beginning of calcium phosphate deposition. It is believed that the initiation period is related to the initial kinetic of reduction of water, hydrogen gas generation and increase of pH around the electrode, and consequently precipitation (deposition) of calcium phosphate[89].

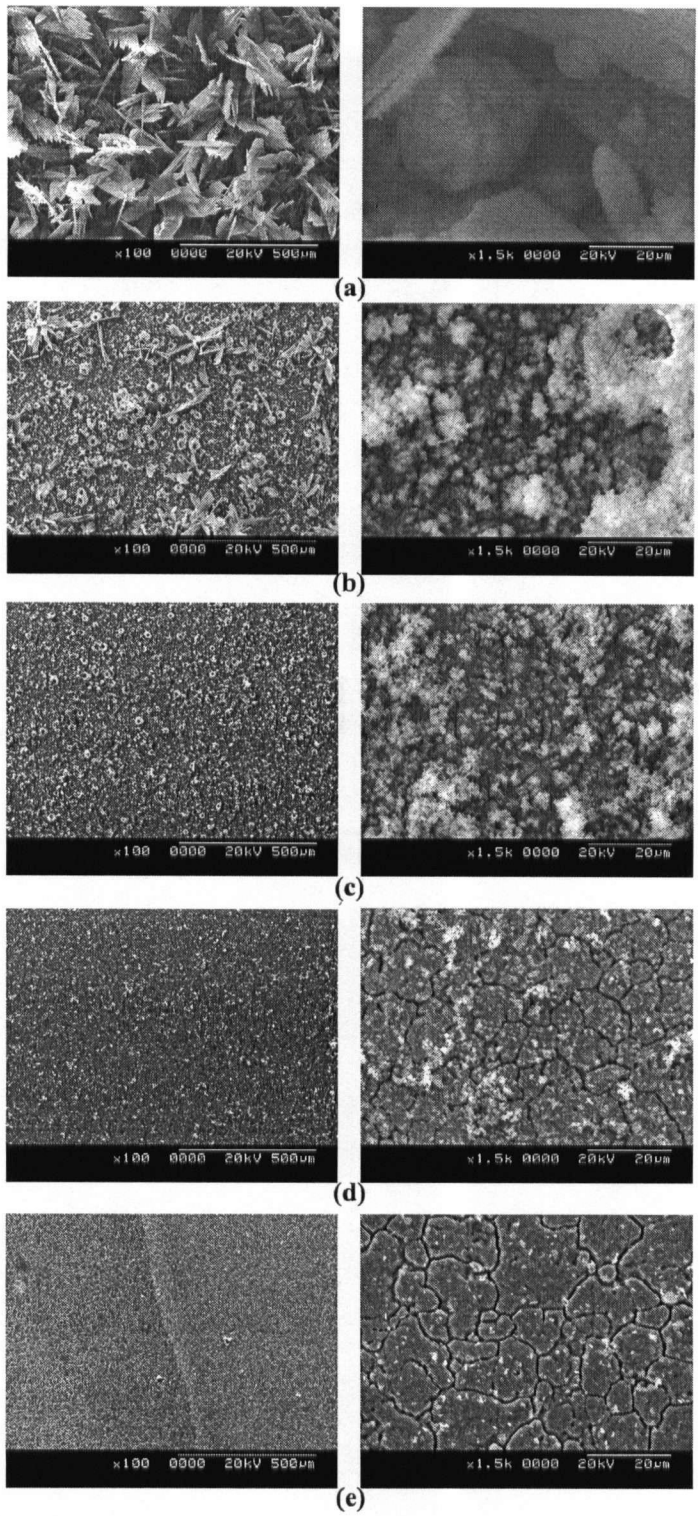

Figure 5.1-3. SEM images of ECD coating deposited with various deposition time: (a) 15 min, (b) 10 min, (c) 5 min, (d) 3 min, (e) 1 min [Left: ×100; Right: ×1500] at 1mA/cm^2.

Figure 5.1-3 (a) shows the ECD microstructure after 15 min of deposition; plate-like flake structure was observed with a dense under-layer similar to Figure 5.1-1 (d). As the deposition time decreased to 10 min, the amount of plate-like structure visibly decreased, and revealed the under-layer (Figure 5.1-3 (b)). The under-layer exhibits some "volcano-like" structure, which is also observed in Figure 5.1-3 (c). This is likely due to the bubble effect where the H_2 bubbles were trapped during the deposition process[89]. When the deposition time decreases to 3 min, "volcano-like" structure was no longer seen, instead sparsely distributed deposit was observed as illustrated in Figure 5.1-3 (d). Microstructure of 1 min deposit is shown in Figure 5.1-3 (e). Under ×1,500 magnification, very little material seems to be deposited, however, under ×100 magnification, a noticeable uniform film boundary was observed. Figure 5.1-4 illustrates a ×20,000 magnification SEM micrograph of the 1 min deposition, and reveals a thin and uniform porous coating. Due to technical difficulties, the stainless steel plates were used as-received in this study.

The weight gain of ECD specimens coated for 1 – 15 minutes with 1 mA/cm^2 is shown in Figure 5.1-5. With increase of deposition time, an increased in weight gain was observed. A more drastic increase of weight gain was seen from 3 minutes to 5 minutes of deposition; this is believed to be a result of the growing crystals on top of the thin film observed in Figure 5.1-4. It is also expected that increasing surface resistance (due to increasing coating thickness) slows down the deposition reaction. It appears that in order to avoid loosely attached plate-like structures and bubble effects, process parameters

should be chosen towards lower end, i.e. current density 1 mA/cm^2 and with 1 minute deposition time.

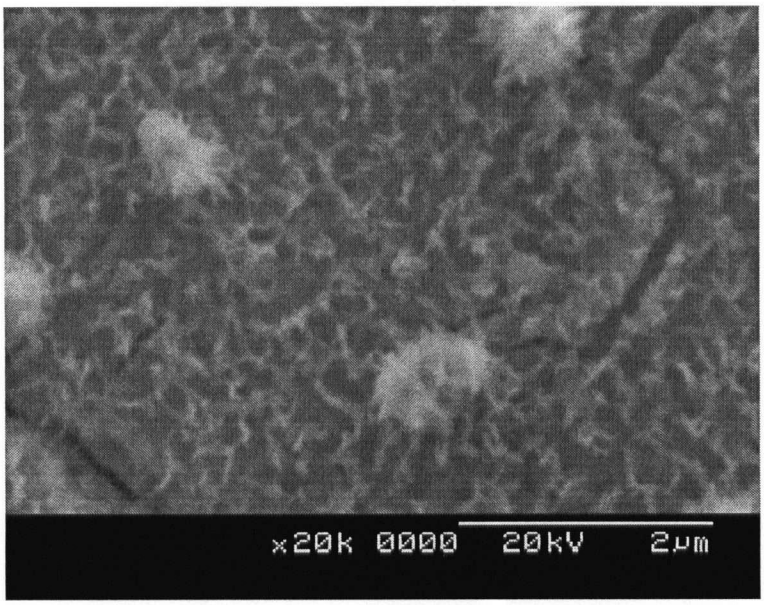

Figure 5.1-4. High magnification SEM image of ECD coating with deposition of 1 min [×20,000] at 1mA/cm^2.

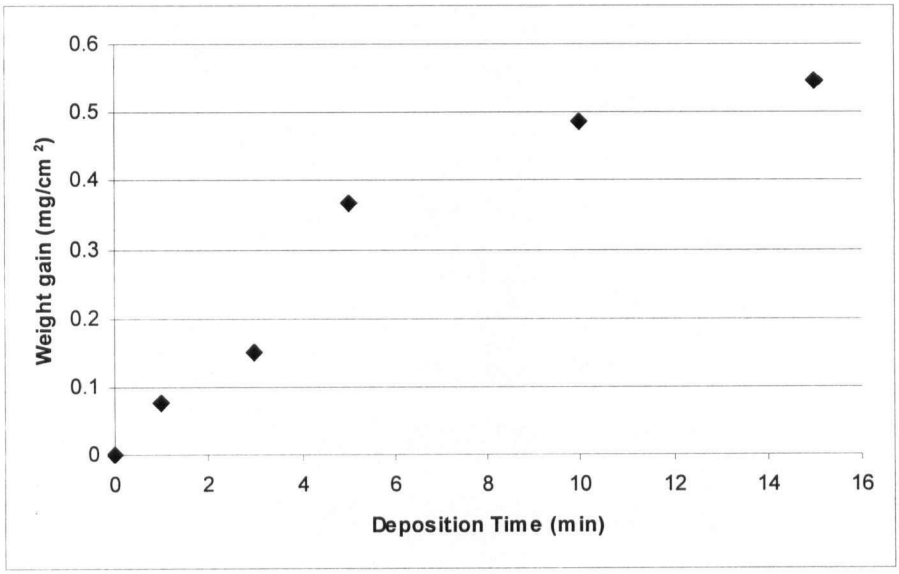

Figure 5.1-5. Weight gain of ECD coated specimens versus deposition time deposited at 1 mA/cm^2.

5.1.3 Ca/P Ratio

The composition and properties of the resulting deposit was previously found to be dependent on the composition of electrolyte[23, 82, 83, 89, 96]. However, it was observed that for electrolyte composed of $Ca(NO_3)_2$ $4H_2O$ and $NH_4H_2PO_4$, the Ca/P ratio of the resulting deposits were nearly independent of the Ca/P ratio of the electrolyte. Figure 5.1-6 illustrates the different Ca/P ratio of the resulting deposits for various Ca/P ratio electrolytes evaluated in this work through EDX. Table 5.1-1 shows the concentration of $Ca(NO_3)_2$ $4H_2O$ and $NH_4H_2PO_4$ for the preparation of different Ca/P electrolytes. The Ca/P ratio of the deposits ranged from 1.41 – 1.57, independent of the Ca/P ratio of the electrolyte. SEM images of the various resulting deposits deposited with electrolyte of Ca/P ratio 2.92, 2.63, 1.95, and 0.49 are shown in Figure 5.1-7 (a) – (d), respectively. Among the four results, the deposit for electrolyte Ca/P 1.95 appears to be most porous (Figure 5.1-7 (c)), but all exhibit similar microstructure. It appears that, within the parameters in this study, the different Ca/P ratio of electrolyte has minimal effect on the Ca/P ratio of the resulting deposit and the resulting microstructure.

In the present study, the surface of the stainless steel plate samples was polished to 1 μm mirror finish, however a surface roughness created by the deposited ECD coating may cause unnecessary absorption of the generated X-ray signal, which is difficult to account for in the EDX quantification analysis. The accuracy of EDX quantitative analysis with the use of well-polished standards having a composition similar to the sample has been reported to be greater than 2% relative for major concentrations[105]. The analysis of elements with concentrations less than 5wt% will typically yield relative

accuracies of ~10%, even with standards. It was also reported that for samples with rough surfaces, i.e. fracture samples or small particles, the relative accuracy may be as low as 50% [105]. Therefore, the EDX analysis in this study may not reflect the true concentration and should only be considered as an relative indicator.

Table 5.1-1. The concentration of $Ca(NO_3)_2\ 4H_2O$ and $NH_4H_2PO_4$ for the preparation of different Ca/P ratio electrolytes.

Electrolyte Concentration (M)		Electrolyte Ca/P ratio
$NH_4H_2PO_4$	$Ca(NO_3)_2\ 4H_2O$	
0.0217	0.0635	2.92
0.0217	0.0572	2.63
0.0217	0.0423	1.95
0.0435	0.0212	0.49

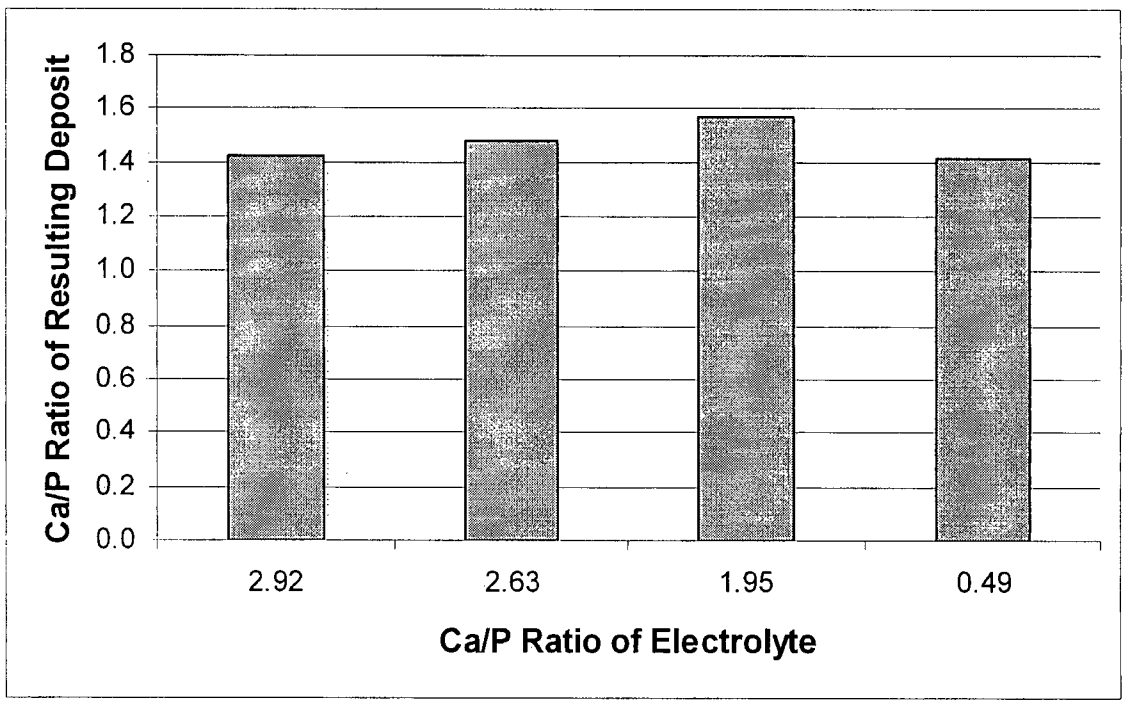

Figure 5.1-6. Ca/P ratio of resulting deposit with the use of various Ca/P ratio electrolytes. Ca/P ratio was derived from EDX spectra.

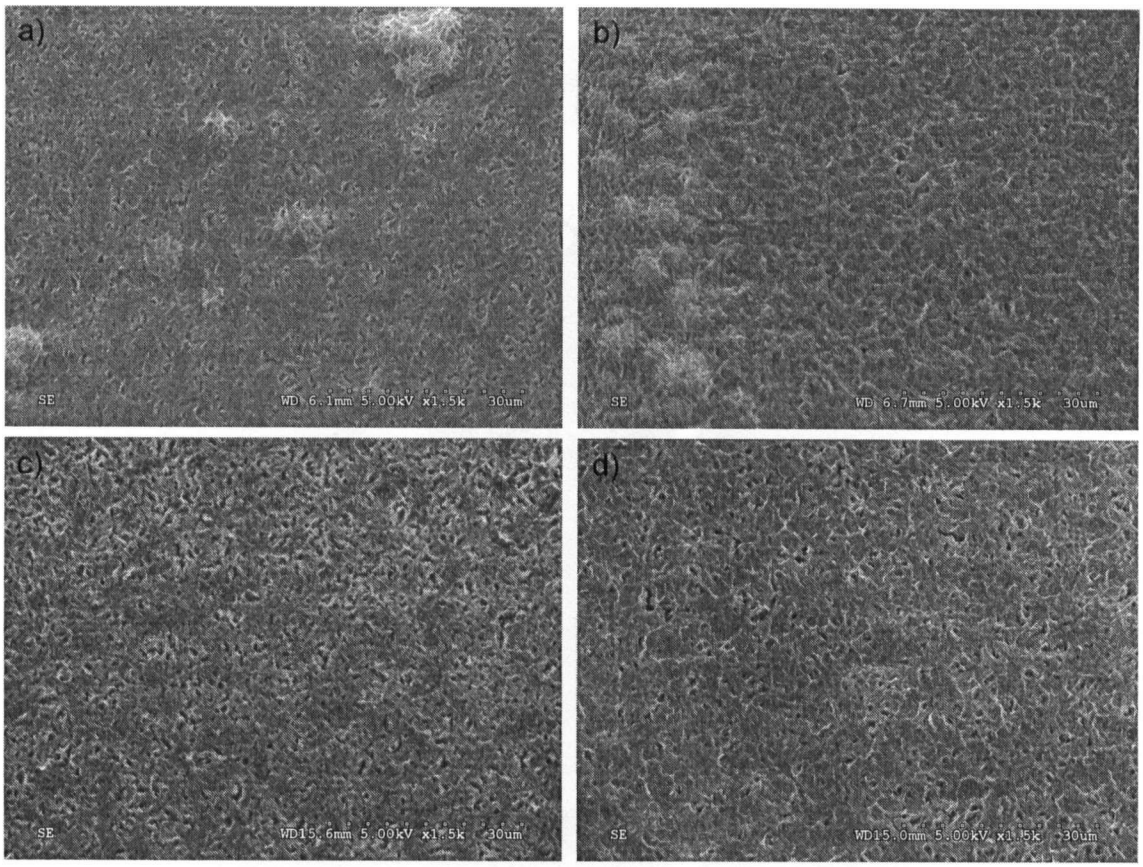

Figure 5.1-7. SEM images of resulting deposits from various Ca/P ratio electrolytes; a) 2.92, b) 2.63, c) 1.95, and d) 0.49. [×15,000]

5.1.4 Temperature

The electrolyte temperature in the ECD process was found to be influential on the uniformity of coverage and on the coating microstructure. Figure 5.1-8 illustrates the microstructure of coatings deposited at 25°C, 45°C, and 75°C, respectively (other process parameters included: current density = 1 mA/cm^2, deposition time = 5 minutes, electrolyte pH = 4.2, electrolyte Ca/P ratio = 1.95). It can be observed that the coating uniformly improved from Figure 5.1-8 (a) to (b), however, the microstructure appears to be denser and exhibit cracks in Figure 5.1-8 (c).

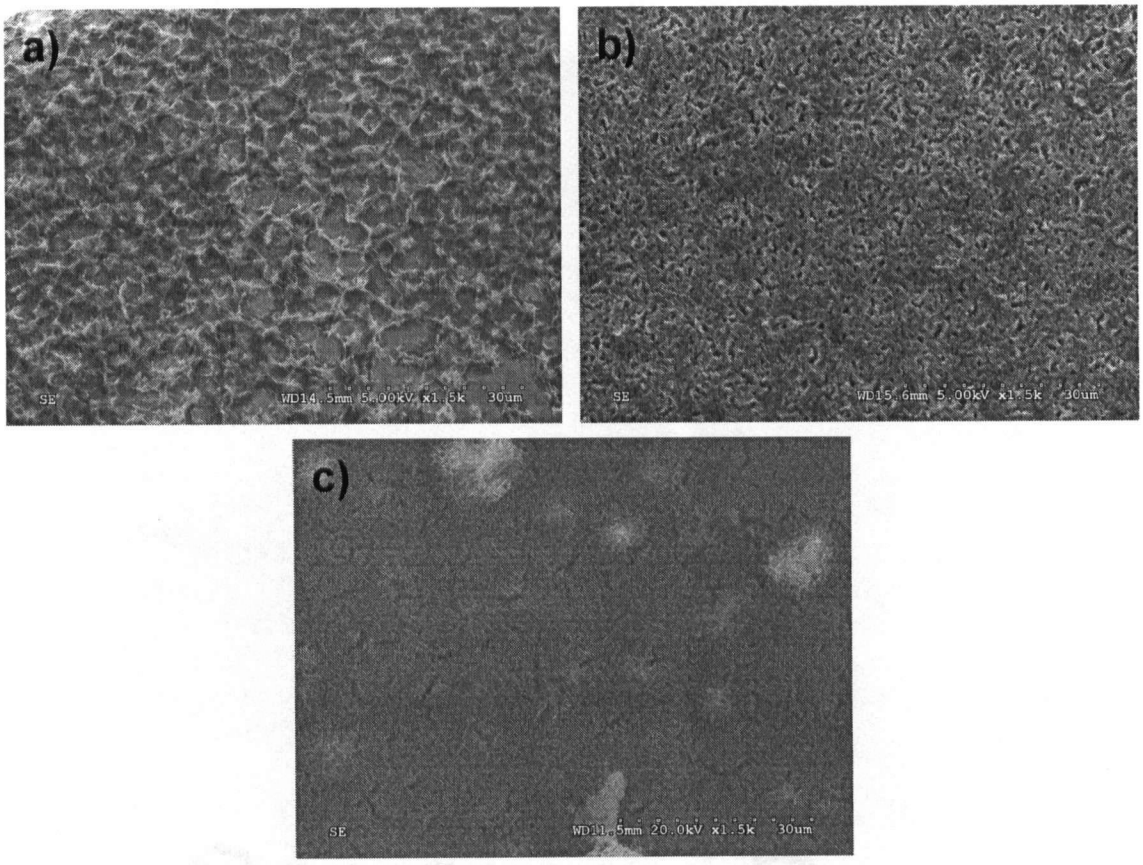

Figure 5.1-8. SEM images of resulting CaP deposits conducted in electrolyte with temperature a) 25 °C b) 45°C, c) 75°C. [×15,000]

While a constant current density was applied (i.e. constant current source, for a fixed geometry substrate), the influence of temperature on the supplied voltage was noticed. Figure 5.1-9 shows typical influence of the electrolyte temperature on the measured supply voltage. The voltage decreases as the electrolyte temperature increases, possibly due to decrease of water resistivity, as previously suggested[97].

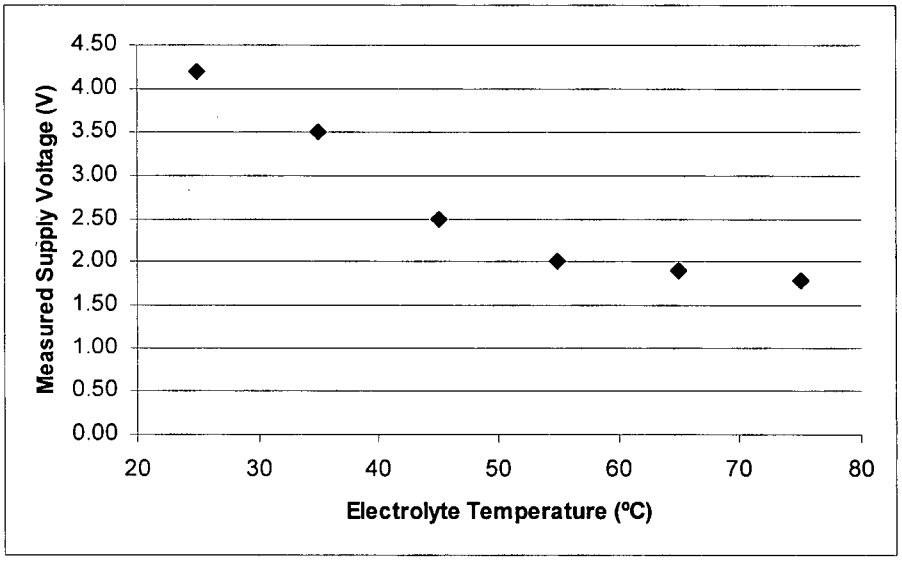

Figure 5.1-9. Influence of electrolyte temperature on measured supply voltage, for constant current source (I = 13.77 mA).

5.1.5 The Influence of Electrolyte pH

In general, hydroxyapatite is known to dissolve in an acidic environment with pH < 2 and precipitate in a basic environment with pH > 9 [67] (Figure 2.3-1). However, the phase composition, crystallinity, nature of solution, temperature, and porosity also plays a role in dissolution and precipitation of calcium phosphates[6]. In the process of electrolyte preparation, slight precipitation was observed when the pH reached 6.0 at 45°C. A stable electrolyte without precipitation was found to lie between pH 4.0 – 5.5 at 45°C. ECD conducted with electrolyte pH 3.0 at 45°C has demonstrated non-uniform surface coverage as shown in Figure 5.1-10. SEM images of ECD coating deposited with electrolyte of pH 4.0, 4.5, and 5.5 are shown in Figure 5.1-11 (a) – (c), respectively (other process parameters are as follows: current density = 1 mA/cm^2, deposition time = 5 minutes, electrolyte temperature = 45°C). All coatings exhibit uniform surface coverage, there were no distinctive microstructural differences observed among the three deposits.

Therefore the range of pH 4.0 – 5.5 was concluded to be optimal for the process under consideration.

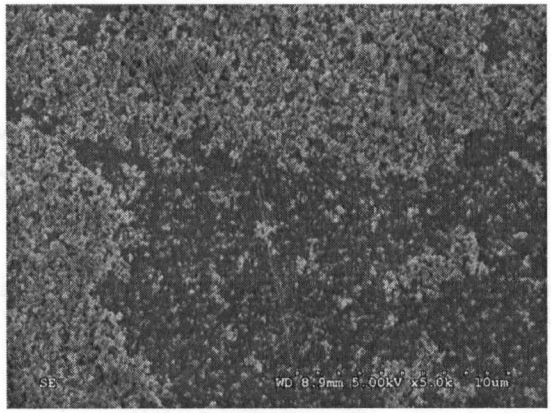

Figure 5.1-10. SEM Image of ECD conducted with pH 3.0 electrolyte at 45°C. [×5,000]

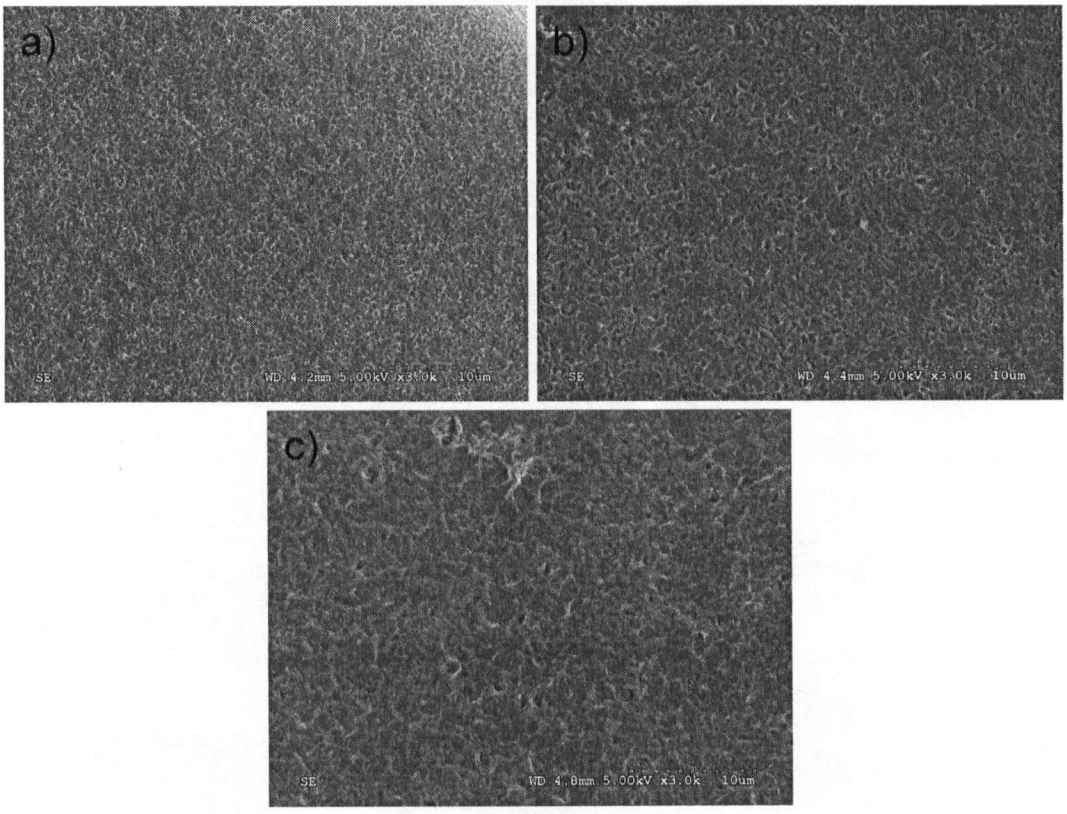

Figure 5.1-11. SEM images of ECD coatings deposited with various electrolyte pH: a) 4.0, b) 4.5, and c) 5.5. [×3,000]

5.2 ECD of Calcium Phosphate Coatings on Coronary Stents

5.2.1 Deposition Process Optimization

It is obvious from the microstructural observations that both current density and deposition time plays an important role on the amount and microstructure of the ECD coatings. In order to achieve thin film (<0.5 μm) coating and to maintain a desire coating microstructure (i.e. porous structure without large plates of crystal over-growth), it was determined that current density should be 1.0 mA/cm^2, and deposition time should be 1 minute (other standard ECD parameters kept constant, as listed in Table 5.2-1). It was observed that the application of different current densities had a more significant effect on the coating microstructure compared to deposition time, whereas the deposition time had more control of weight (or thickness) of the resulting coatings. For the purpose of depositing thin porous coating as illustrated in Figure 5.1-1 (e) on coronary stent, current density of 1 mA/cm^2 was chosen for deposition with various deposition times. The Ca/P ratio of ECD electrolyte was chosen to be 1.95. Although there was no remarkable microstructural difference observed with various Ca/P ratio (refer to Chapter 5.1.3), the coating with Ca/P 1.95 exhibits the most porosity and highest Ca/P ratio (Figure 5.1-6., Figure 5.1-7) Deposition temperature for the optimized process was selected at 45°C, as such electrolyte temperature showed high consistency through the five batches of ECD coatings (Appendix B), and at the same time provides a crack-free uniform resulting coating (Figure 5.1-8). The electrolyte pH was determined to be 4.5, as this electrolyte pH was found to facilitate uniform deposition.

Table 5.2-1. Optimum parameters for ECD of calcium phosphate coatings*.

ECD Process Parameters	Value
Electrolyte Ca/P ratio	1.95
Calcium Nitrate [$Ca(NO_3)_2$ $4H_2O$]	0.04347M
Ammonium phosphate [$NH_4H_2PO_4$]	0.02329 M
Current Density	1.0 mA/cm^2
Deposition Time	1 minute
Electrolyte pH	4.5
Electrolyte Temperature	45°C

*Electrolyte solution was prepared with distilled water, typical volume of electrolyte = 400mL.

Figure 5.2-1 shows SEM images of 316L stainless steel bare metal stent manufactured by MIV Therapeutics, Vancouver, BC. Minor bumps can be observed on the edge areas as seen in Figure 5.2-1 (b) & (c), believed to originate from the laser cutting process. Figure 5.2-2 to Figure 5.2-5 illustrates the ECD coating deposited with the optimum parameters (Table 5.2-1) on coronary stents for 1, 2, 3, and 5 minutes, respectively, at magnifications of ×100, ×300, ×800, and ×1,500. As can be observed in Figure 5.2-2, a thin film (~0.5 μm) coating was indeed achieved with the use of optimum parameters, for 1 minute deposition (coating thickness was estimated based on cross-section evaluation of stent coating, Figure 5.2-8). The coating is observed to be covering the entire stent surface uniformly, loosely attached crystals were not found. The high conformance of coating can also be seen on the edges of the stent where the laser cutting bumps were found. The coating exhibits a porous structure demonstrating a possibility for drug encapsulation. Figure 5.2-6 shows the EDX surface analysis results for the 1 minute deposition. Calcium and phosphorous were found, confirming the existence of a calcium phosphate coating. Increasing the deposition time to 2 minutes clearly increased the density of the coating as seen in Figure 5.2-3. Nevertheless, full coverage and

uniformly was achieved again. Non-uniformity was observed when the deposition time was further increased to 3 and 5 minutes (Figure 5.2-4 and Figure 5.2-5). Nucleation of loosely attached structures was observed sparsely distributed over the entire stent surface in Figure 5.2-4. Large crystal plates were seen with 5 minutes deposition as observed in Figure 5.1-3 for prolonged deposition time. From the observation of both Figure 5.2-4 and Figure 5.2-5, it is noticed that the laser cutting bumps were no longer visible, indicating the increasing of thickness and density of the coating as deposition time increased.

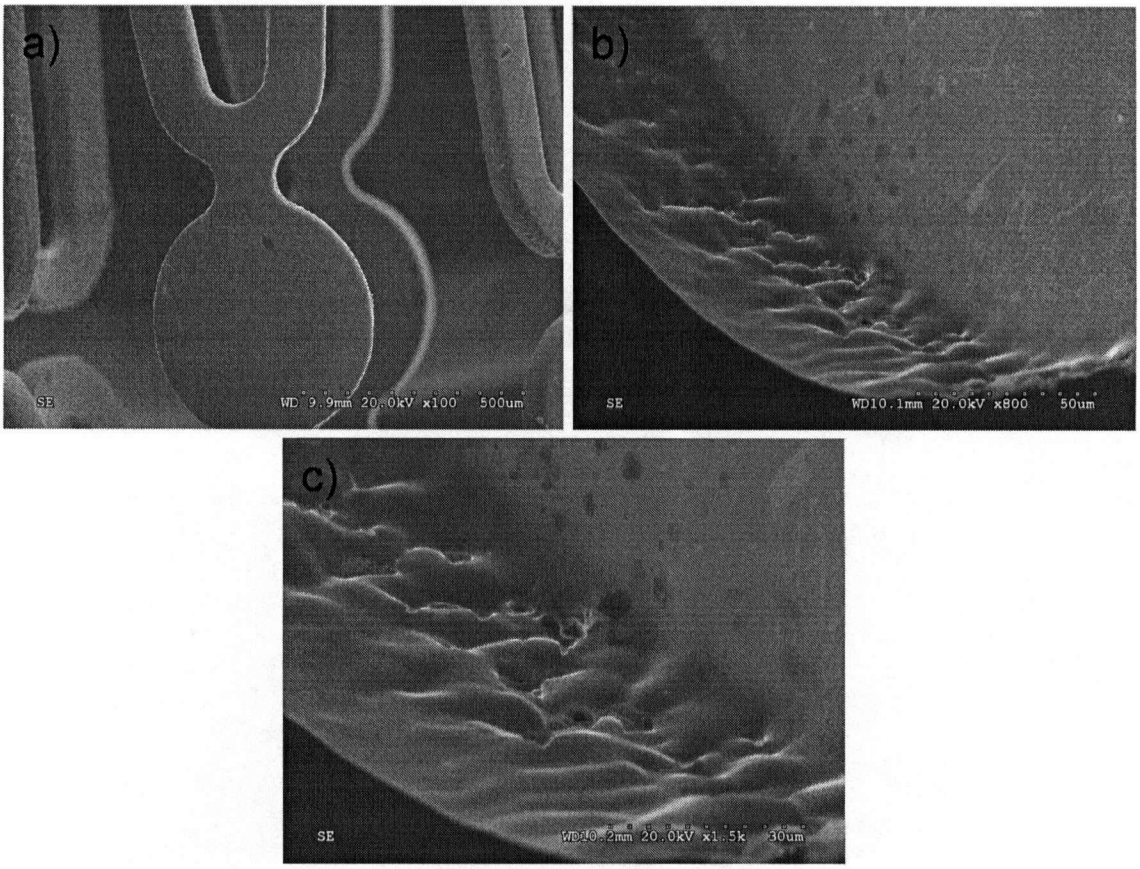

Figure 5.2-1. SEM images of bare metal stent with various magnification: a) [×100], b) [×800], c) [×1,500].

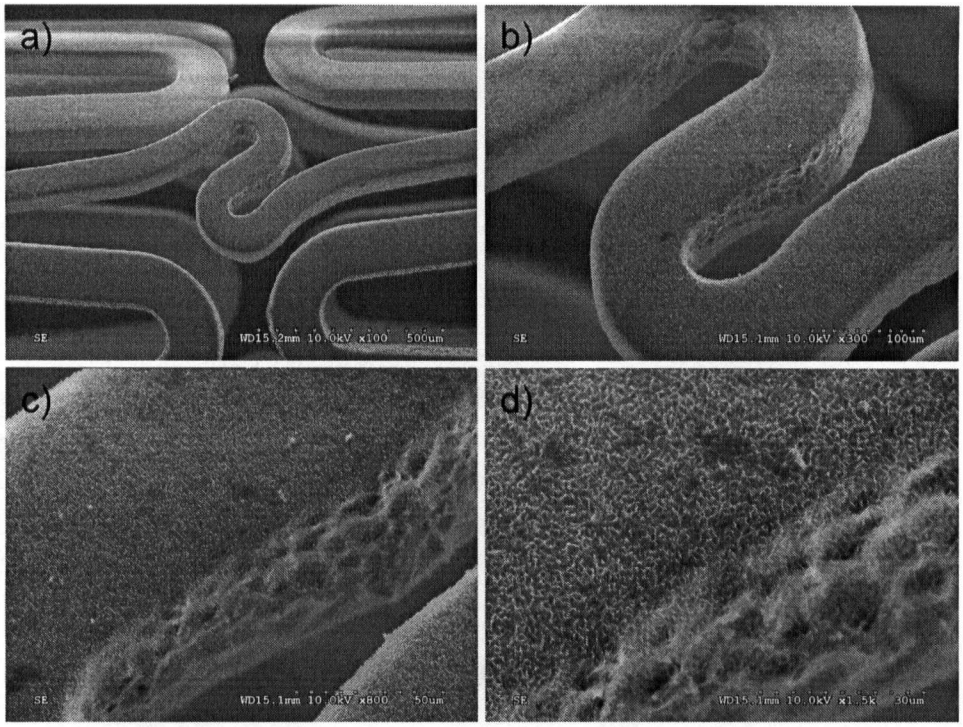

Figure 5.2-2. SEM images of ECD coating deposited on coronary stent with optimum parameters for 1 minute. (a) [×100], (b) [×300], (c) [×800], and (d) [×1,500]

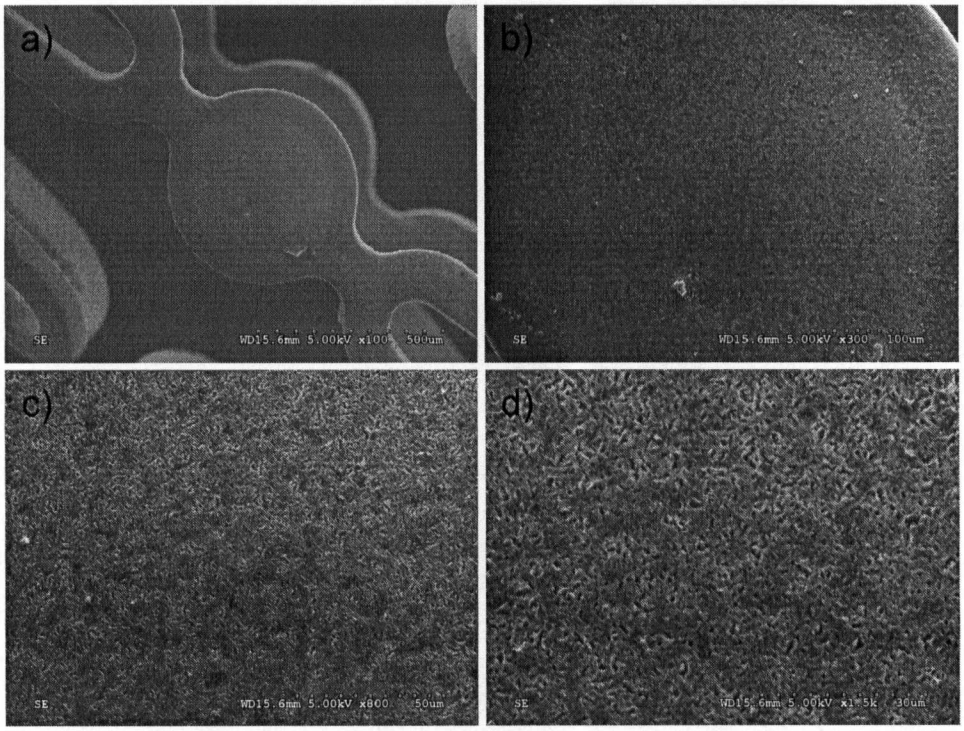

Figure 5.2-3. SEM images of ECD coating deposited on coronary stent with optimum parameters for 2 minutes. (a) [×100], (b) [×300], (c) [×800], and (d) [×1,500]

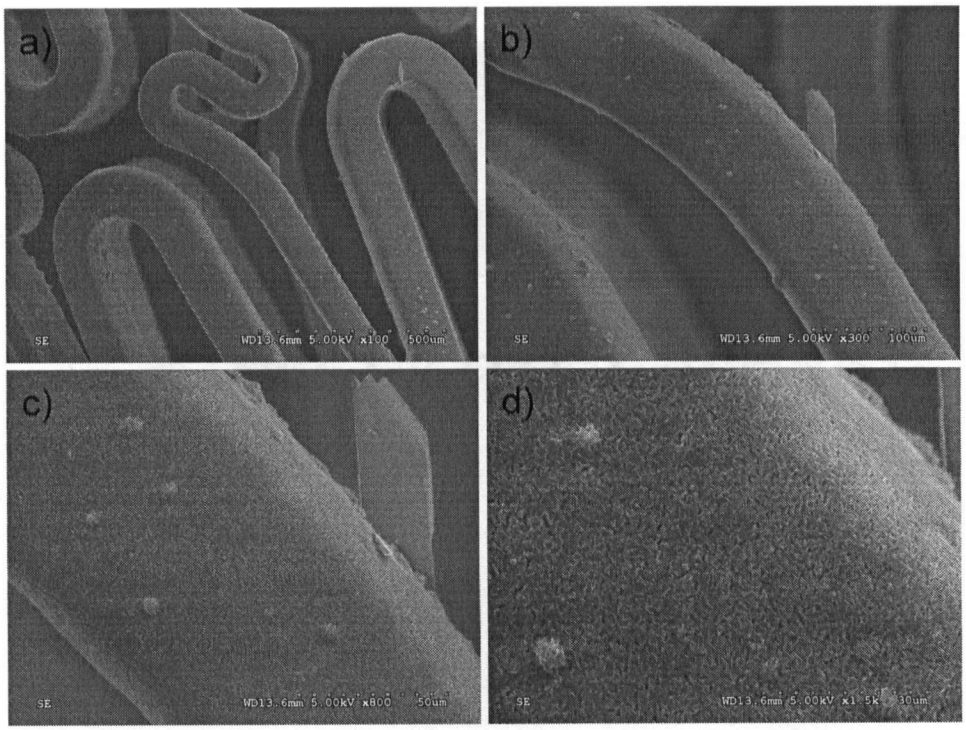

Figure 5.2-4. SEM images of ECD coating deposited on coronary stent with optimum parameters for 3 minutes. (a) [×100], (b) [×300], (c) [×800], and (d) [×1,500]

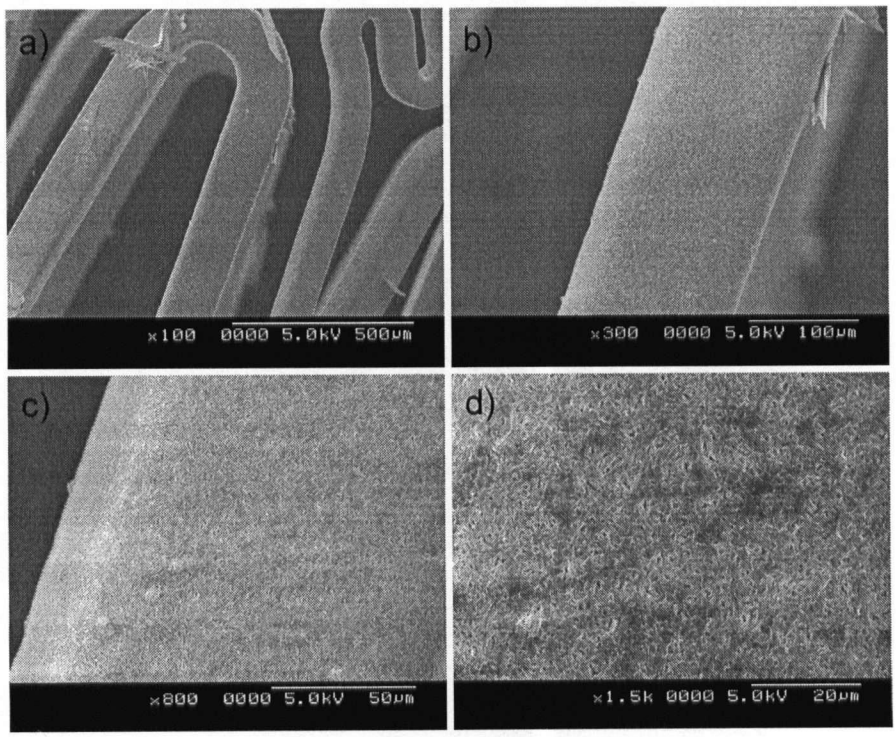

Figure 5.2-5. SEM images of ECD coating deposited on coronary stent with optimum parameters for 5 minutes. (a) [×100], (b) [×300], (c) [×800], and (d) [×1,500]

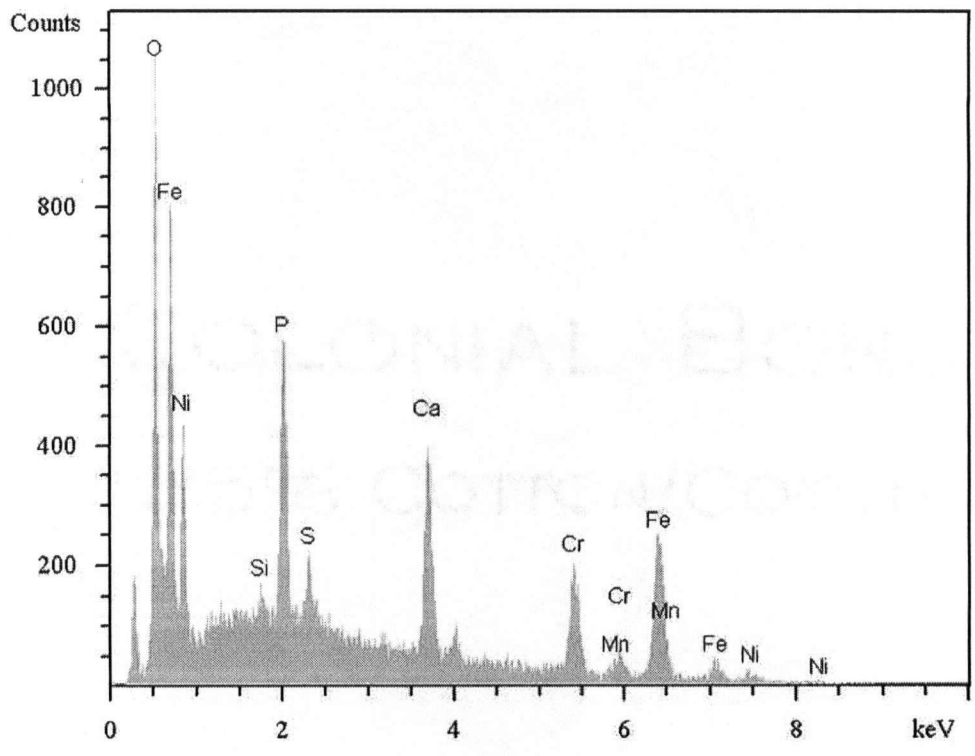

Figure 5.2-6. EDX surface analysis of the ECD coating deposited on coronary stent with optimum parameters for 1 minute.

Figure 5.2-7 shows the X-Ray diffraction pattern of the ECD coating deposited with optimum process parameters (Table 5.2-1), for 1 minute. Due to the technical difficulty of X-Ray diffraction analysis on thin film (~0.5 μm), ECD coating was conducted on ten stainless steel plate substrates (as described in Chapter 4.1), then scraped off and collected onto a stainless steel plate for analysis. Two phases can be clearly noticed in the coating; the DCPD peaks (JCPDC# 01-072-0713) are at 2-theta 11.64°, 20.95°, 29.28°, 34.16°, and 41.78°, the HA peaks (JCPDC #009-0432) are at 2-theta 25.98° and 31.94°. Stainless steel substrate has a peak at 2-theta 44.52°. However, due to the similarities of HA and OCP X-ray diffraction patterns (2-theta 25 – 40°), the two phases can not be clearly distinguished. As indicated by the peak width, the HA

phase was poorly crystallized. Similar XRD analyses on HA were also reported previously, where poorly crystalline HA was characterized and identified by the broad peak width[23, 73, 84, 98]. Since the coating consisted of highly soluble DCPD phase and poorly crystallized HA phase, it is reasonable to believe that such coating bears high solubility. Further dissolution test results (Section 5.2.4 – Table 5.2-2) have shown that the coating lost 50% of its weight ($D_{1/2}$) within 20 minutes, and was totally dissolved (D_{Total}) in approximately 40 minutes, in phosphate buffer saline.

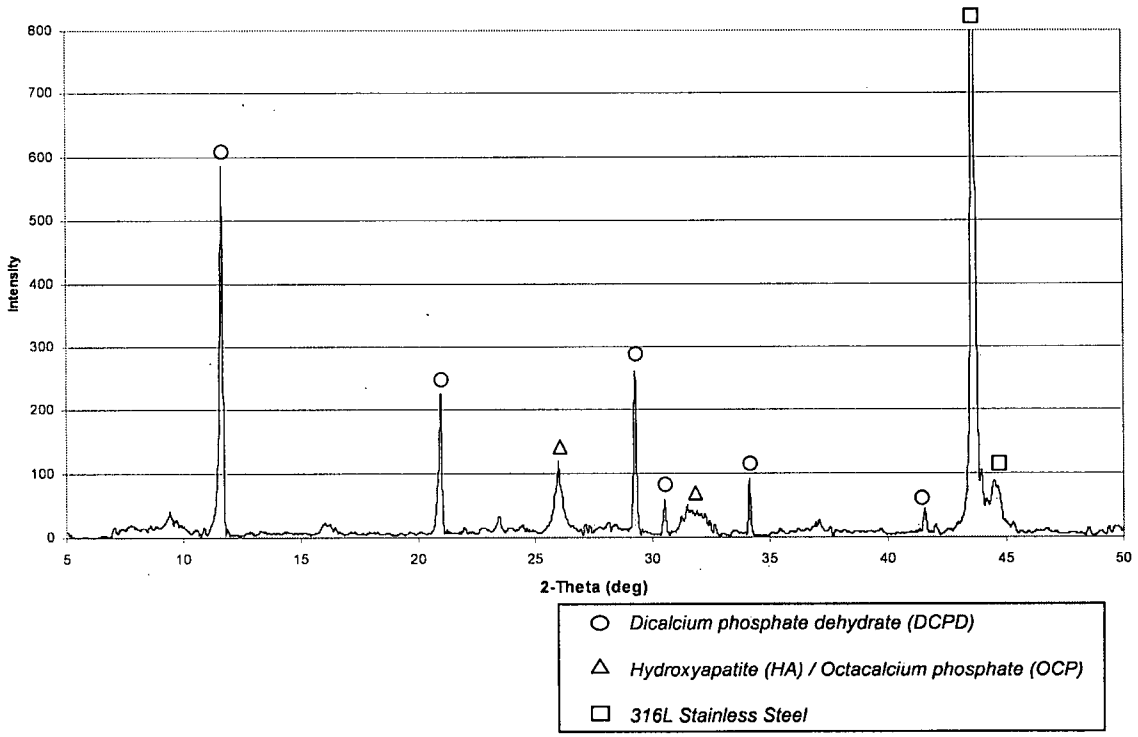

Figure 5.2-7. X-Ray diffraction of the ECD coating deposited with optimum parameters (Table 5.2-1), for 1 minute, showing a mixed phase of DCPD and HA.

In addition, cross-section study was performed on the ECD coating deposited with the optimized parameters for 1 minute. Figure 5.2-8 illustrated the SEM image of the

coating cross-section. It was revealed that the coating thickness of an ECD coating with 1 minute deposition was approximately 0.5μm.

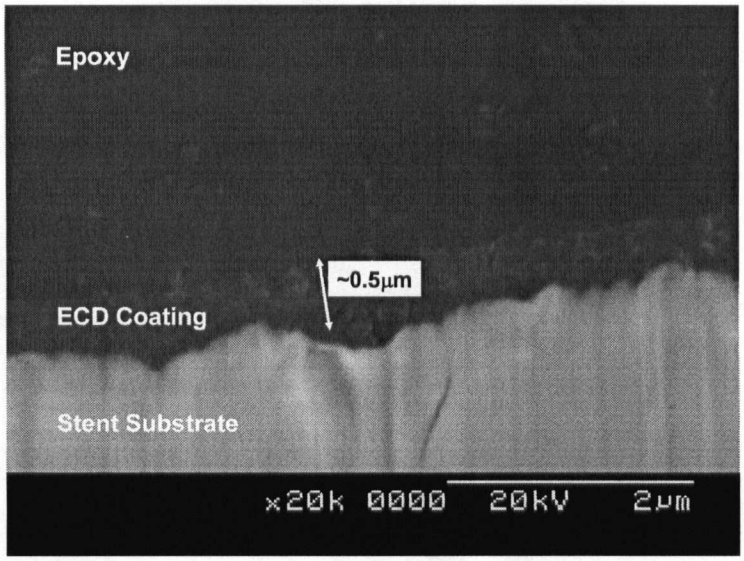

Figure 5.2-8. Cross-section SEM image of ECD coating deposited on stent. Estimated coating thickness was approximately 0.5μm.

5.2.2 In-vitro Crimping and Expansion Tests on ECD Coated Stents

A qualitative coating adhesion assessment was performed by in-vitro stent crimping and expansion test on an ECD coated stents with CaP deposited at optimum parameters (Table 5.2-1). The simulation tests performed by MIVT indicated that the maximum strain experienced by stent during expansion may reach up to 15% in the bottom of "V" section of the stent[27].

Figure 5.2-9 illustrates an expanded bare metal stent. It can be seen that upon expansion, the metal surface suffers significant plastic deformation (i.e. the slip bands), which leads to delamination of coating shown in Figure 5.2-10. The deformation of a

coated stent after expansion can be seen in Figure 5.2-10 (a) and (b) and can be compared with a stent before expansion in Figure 5.2-1 (a). Two distinctive deformation areas can be observed: a compressive stress area in Figure 5.2-10 (c) and a tensile stress area in Figure 5.2-10 (d). The compressive stress area exhibits a buckle delamination effect as illustrated schematically in Figure 5.2-11[99]. Observations in Figure 5.2-10 (c) have indicated that the interfacial adhesion is low and the coating buckling lead to the loss of large coating section. The tensile stress in brittle films can lead to through-thickness cracking as illustrated schematically in Figure 5.2-12[99]. Figure 5.2-10 (d) shows tensile stress causing a series of parallel cracks with approximately uniform spacing (~5 μm) indicating a poor interfacial bonding. The delamination allowed better estimation of the coating thickness, observed again to be ~0.5 μm, which agrees with the cross-section evaluation illustrated in Figure 5.2-8.

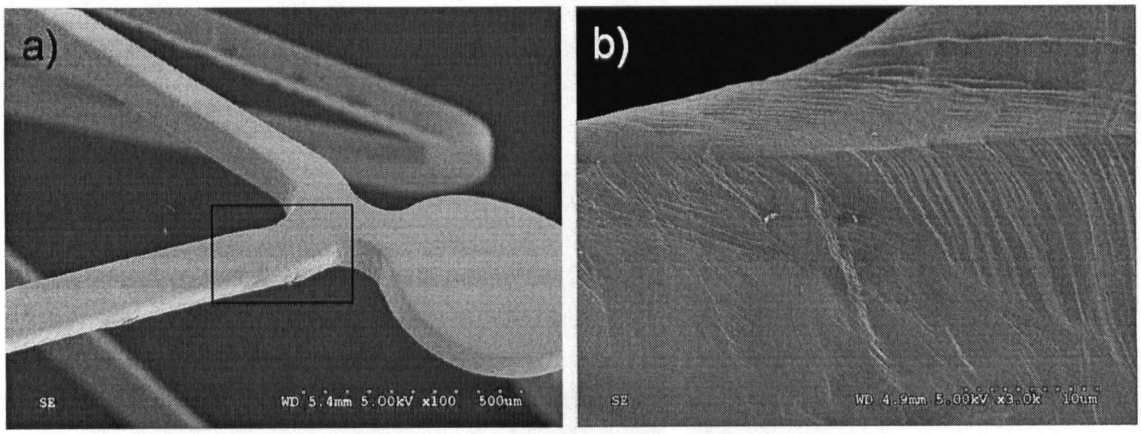

Figure 5.2-9. (a) SEM images of an expanded bare metal stent [×100], (b) high magnification revealing a significantly deformed surface [×3,000].

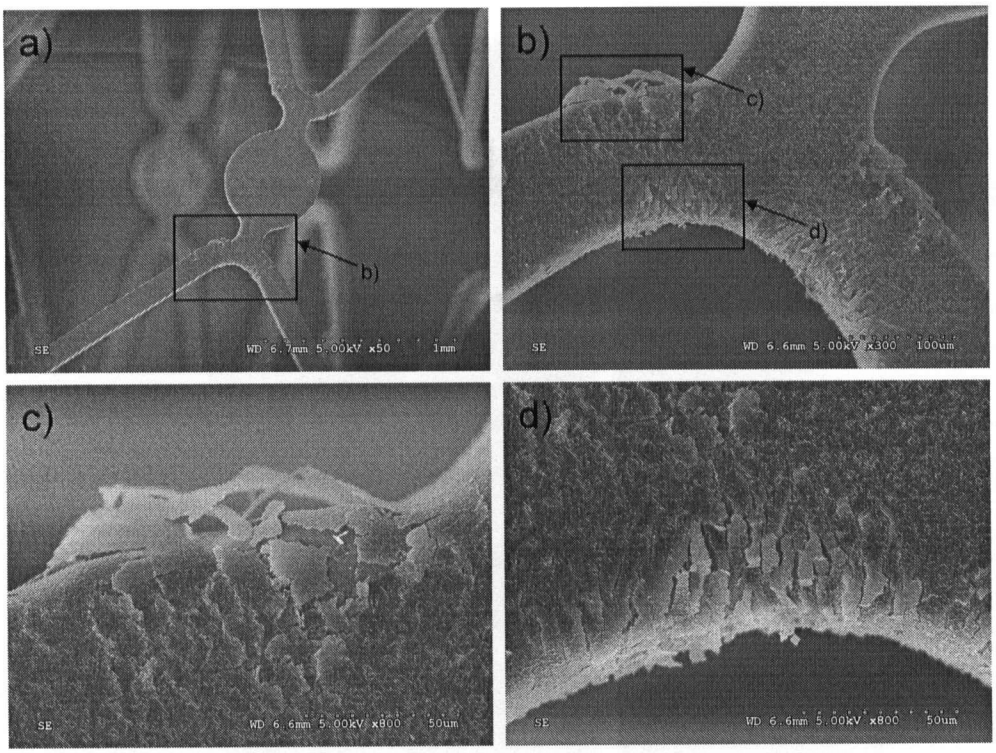

Figure 5.2-10. SEM images of expansion test result from an ECD coated stent specimen deposited with optimum parameter for 1 minute deposition. (a) Expanded area [×50] (b) Expanded area [×300] (c) Compressive stress area showing coating delamination [×800] (d) Tensile stress area showing coating delamination [×800]

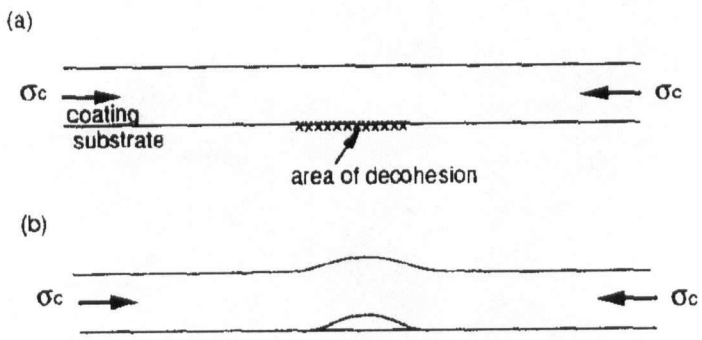

Figure 5.2-11. Compressive spallation by buckling showing localized interfacial decohesion.

© Journal of Engineering Failure Analysis 2, 1995, adapted by permission[4].

---

[4] Reprinted from Journal of Engineering Failure Analysis 2, 2, Strawbridge A, Evans H.E., Mechanical failure of thin brittle coatings, 85 – 103, Copyright (1995), with permission from Elsevier.

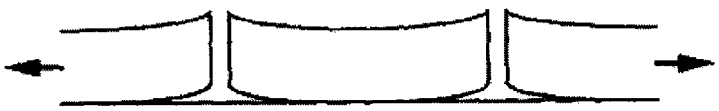

Figure 5.2-12. Tensile stress in brittle film causing through-thickness cracking and interfacial delamination.

© Journal of Engineering Failure Analysis 2, 1995, adapted by permission[5].

5.2.3 Substrate Surface Modification for Improvement of Coating Adhesion

Substrate surface modification (as described in Chapter 4 Experimental Methodology) was employed in this study to enhance the interfacial adhesion between the coating and the substrate[91]. Figure 5.2-13 shows the SEM image of a stent surface treated with 10M NaOH aqueous solution at 60°C for 24 hours and after subsequent heat treatment at 500°C for 20 minutes. It was observed that the pretreated metal surface exhibits a nano-rough surface structure, with the characteristic size of the surface pattern on the order of 100 nm. Figure 5.2-14 illustrates the EDX analysis of the pretreated 316L stainless steel surface. While Fe, Ni, and Cr are the main constituents of 316L stainless steel, it was reasonable to believe that the surface included a new compound Na_4CrO_4 as reported by Lin et al formed on the stent surface after surface modification[91]. The nano-rough surface structure formed during the surface modification process is believed to promote mechanical interlocking and thus physical bonding. Additionally, the inter-compound layer of Na_4CrO_4 may act as a chemical bonding bridge between the metal and ceramic. However, it has not been clarified in the present work which factor specifically

---

[5] Reprinted from Journal of Engineering Failure Analysis 2, 2, Strawbridge A, Evans H.E., Mechanical failure of thin brittle coatings, 85 – 103, Copyright (1995), with permission from Elsevier.

(i.e. nano-roughness or modified surface chemistry) helps to improve the coating adhesion to stent surface.

In-vitro stent expansion was performed on a bare metal stent with surface modification as illustrated in Figure 5.2-15. Under the high magnification of 10,000×, a surface layer can be clearly seen with cracks (Figure 5.2-15 (d)). Such layer was not observed in the bare metal stent expansion test illustrated in Figure 5.2-9. It was therefore reasonable to believe that the cracked inter-compound layer observed was the indeed the ceramic Na_4CrO_4 layer.

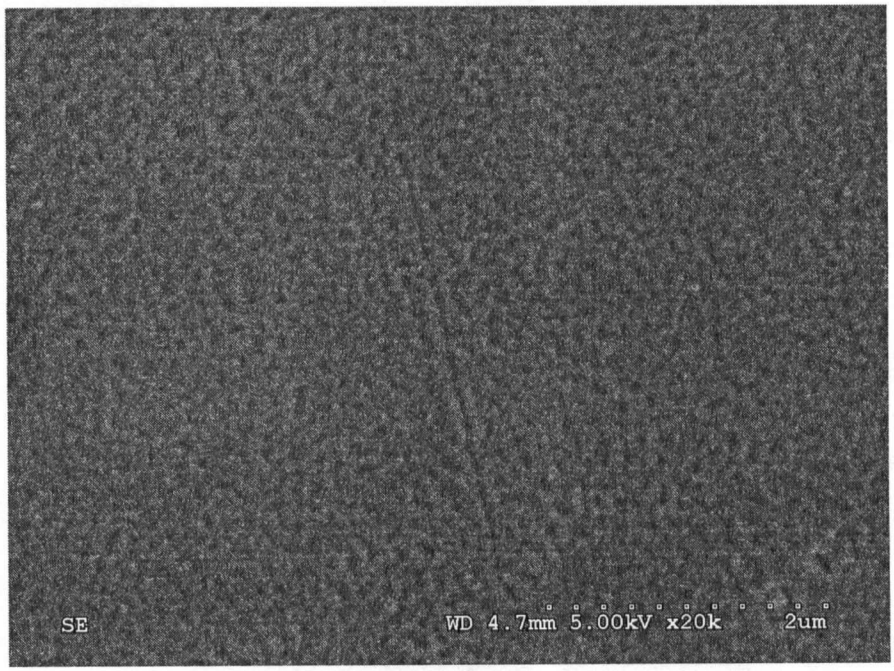

Figure 5.2-13. SEM image of a stent surface after surface modification [×20,000]. The surface showed a nano-size roughness.

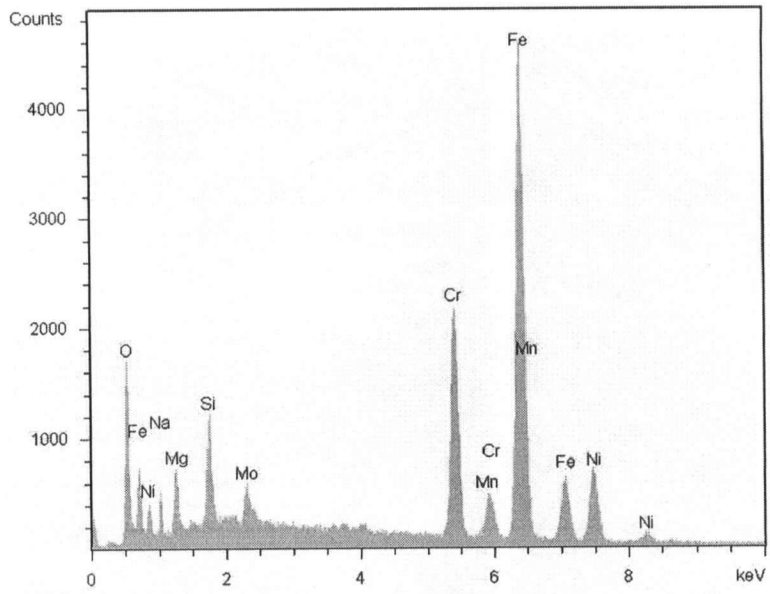

Figure 5.2-14. EDX surface analysis of a surface modified stent.

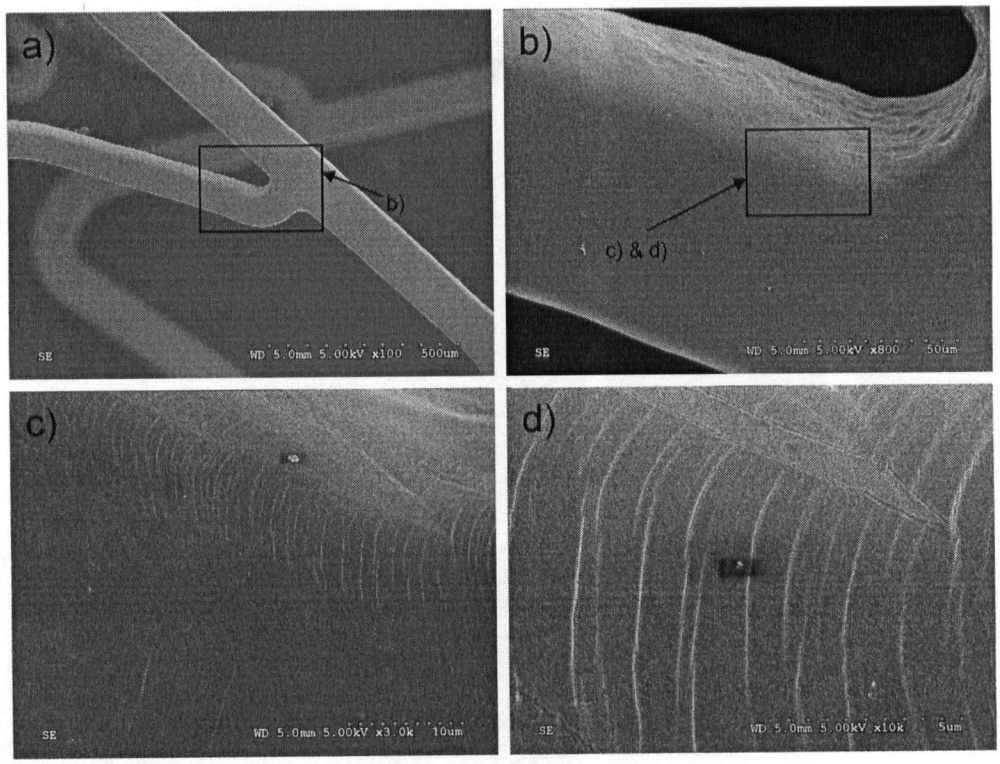

Figure 5.2-15. Expansion test result from a bare metal stent specimen after surface modification. (a) [×100], (b) [×800], (c) [×3,000], and (d) [×10,000]. The Na_4CrO_4 inter-compound can be seen with cracks.

Electrochemical deposition with the optimized deposition parameters (Table 5.2-1) was conducted on the surface modified stent (Figure 5.2-16). It was observed that the coating exhibits 100% coverage with excellent uniformity. The deposit on laser cut bumps as shown in Figure 5.2-16 (c) demonstrated high conformance. Observation under high magnification (×10,000) as illustrated in Figure 5.2-16 (d) revealed a ~50% porous microstructure. It appears that although electrically insulating, the Na_4CrO_4 surface layer is in no way disturbs the ECD process.

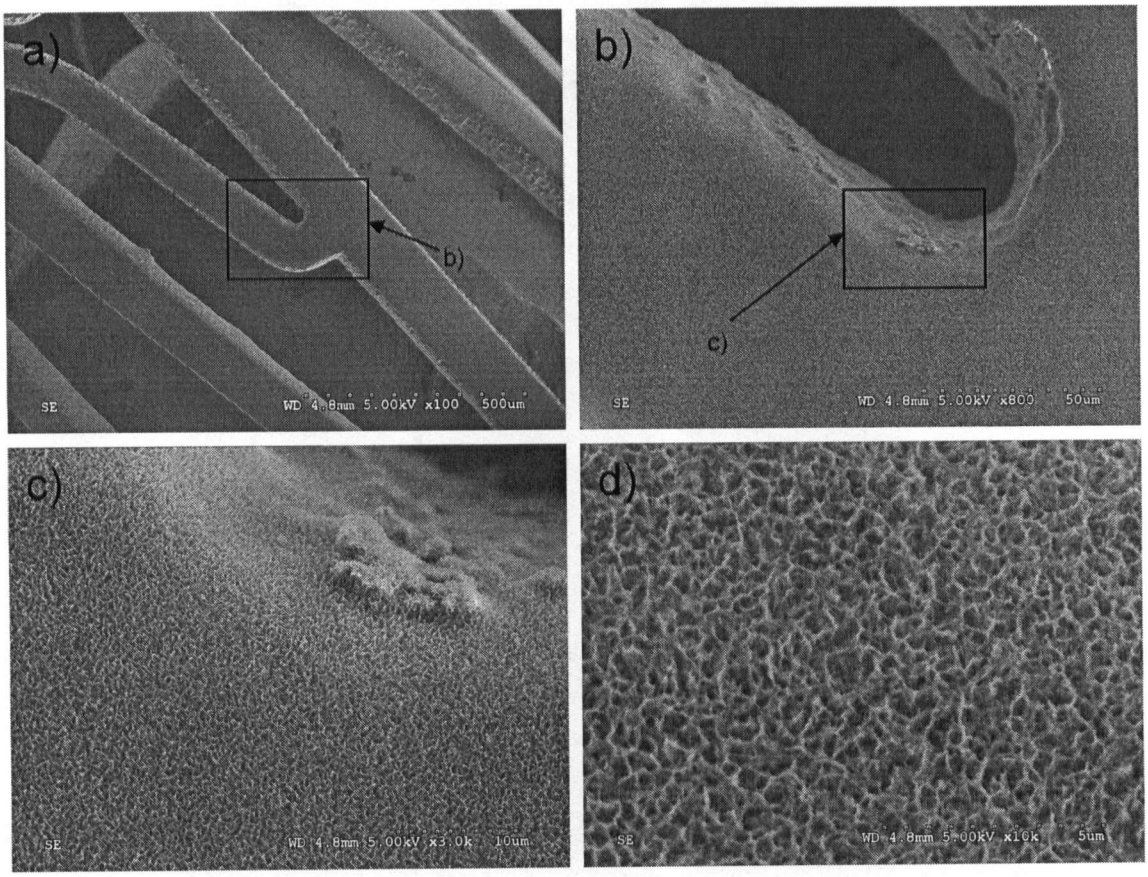

Figure 5.2-16. SEM images of ECD coating deposited with optimum deposition parameters on surface modified stent. (a) [×100], (b) [×800], (c) [×3,000], and (d) [×10,000]

Figure 5.2-17 shows the SEM images of the coated stent after expansion test (with the use of a 3.0 mm diameter catheter) with an ECD coating deposited using the optimum deposition parameter (Table 5.2-1), on surface modified stent. There is no coating buckling or delamination. However, both Figure 5.2-17 (c) & (d) revealed a series of parallel nano-cracks (<100nm) with approximately uniform spacing. The nano-cracking with no observed coating decohesion proved an improved interfacial bonding between the ECD coating and the surface modified stent. Figure 5.2-18 shows the SEM images of a more severe expansion test results (known as "over-expansion" in industry, with the use of a 3.5 mm diameter catheter) for an ECD coating deposited with optimum deposition parameters, on surface modified stent.

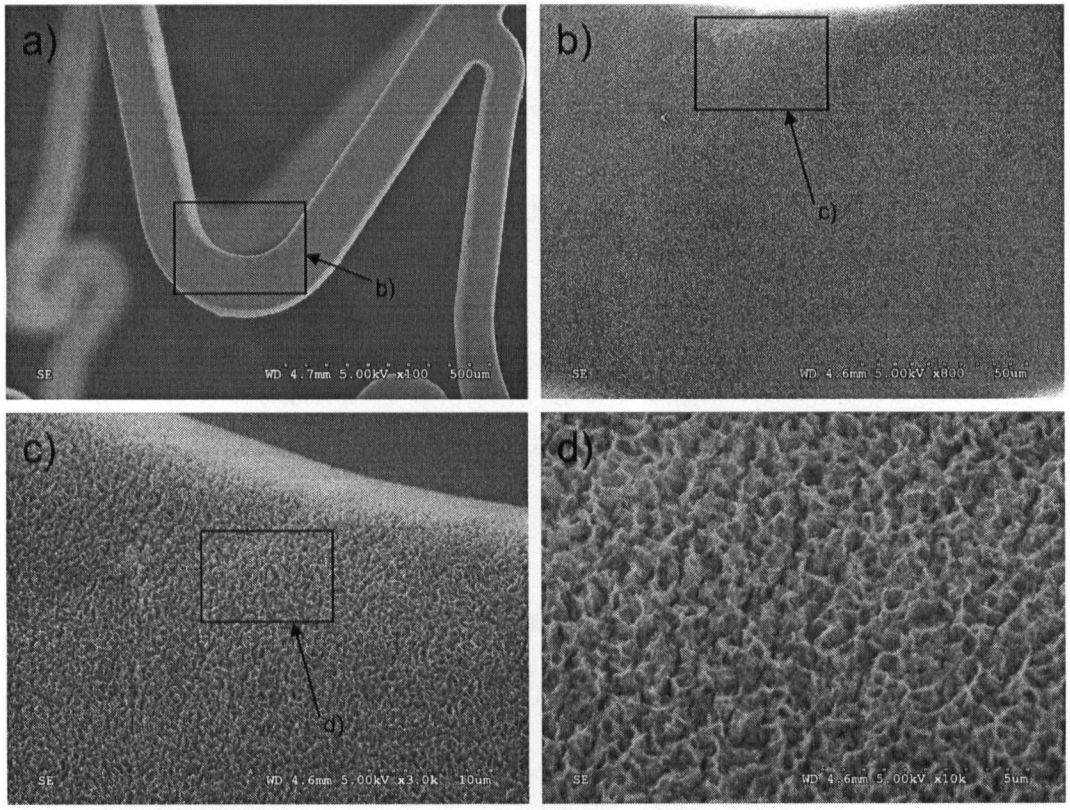

Figure 5.2-17. SEM images of expansion test result from an ECD coating deposited with optimum deposition parameters on surface modified stent. Expansion performed with a 3.0 mm diameter catheter. (a) [×100], (b) [×800], (c) [×3,000], and (d) [×10,000]

The degree of deformation in Figure 5.2-18 (a) was notably higher compared to Figure 5.2-17 (a), although the degree of strain can not be quantified. Even though there were obvious nano-cracks (<100nm) present in the coating, yet no delamination or separation of the coating was seen in Figure 5.2-18 (d). Fracture of such coating to accommodate the strain was observed to be localized, i.e. the nano-cracks were limited to small (<100nm) areas adjacent to the pores, in the areas of the highest strain on the expanded stent. It was observed that these nano-cracks may link to form larger, 1 – 10μm long cracks, but without separation of the coating from the substrate. It is concluded that, in comparison with coating deposited on non-surface modified stent (Figure 5.2-10) the adhesion of coating deposited on stent with surface modification has shown significant improvement. The increase in adhesion is believed to be due to (i) the surface nano-roughness created during the surface modification process, thus enhanced mechanical interlocking with the ECD coating; and/or (ii) the formation of the Na_4CrO_4 inter-layer that have changed the surface chemistry, promoting formation of a chemical bond between the modified surface and the coating during the ECD process.

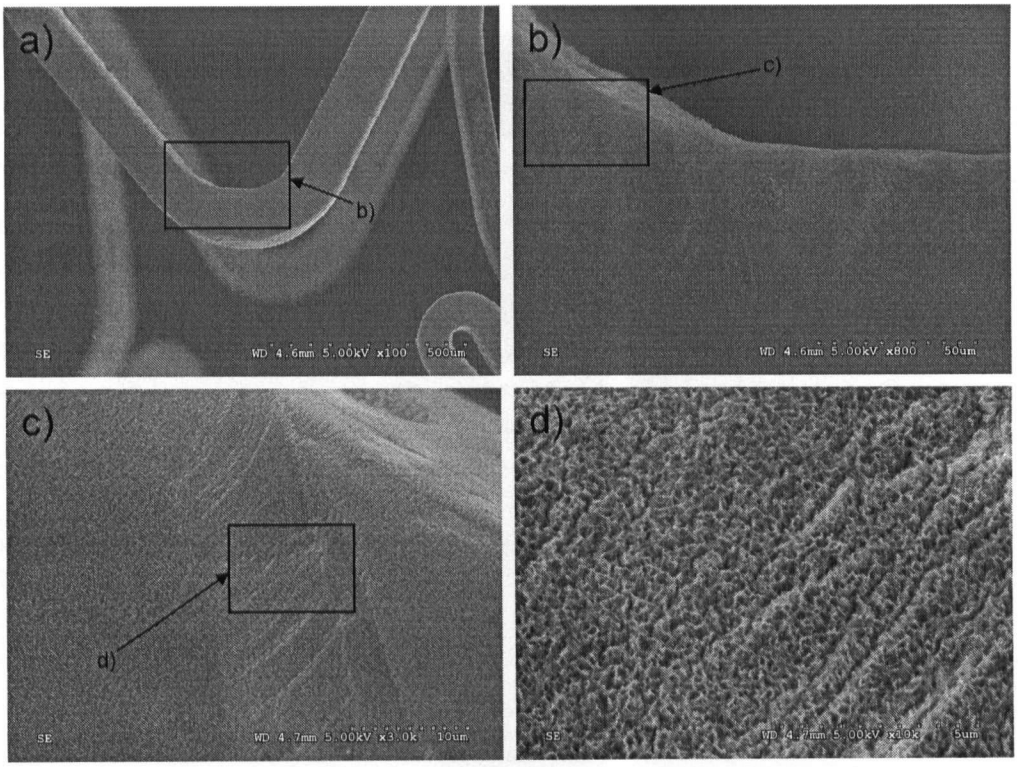

Figure 5.2-18. SEM images of expansion test result from an ECD coating deposited with optimum deposition parameters on surface modified stent. Expansion performed with a 3.5 mm diameter catheter. (a) [×100], (b) [×800], (c) [×3,000], and (d) [×10,000]

5.2.4 Phase Composition of ECD Calcium Phosphates Coatings

To prolong resorption of the ECD as-deposited mixed-phase calcium phosphate coatings, phase and crystallinity optimization was performed. As mentioned in Chapter 5.2.1, total dissolution of as-deposited ECD coating occurred within 40 minutes in phosphate buffer saline at 37°C (pH = 7.4). The high rate of dissolution was believed to be due to the mixed-phase of coating, including poorly crystalline HA and dicalcium phosphate dihydrate (DCPD). Here after, the ECD deposited coating with the use of the optimum deposition parameters will be described as the "as-deposited coating." In order to achieve phase conversion toward substantially pure HA, as-deposited calcium

phosphate coatings were submerged into 0.1M of NaOH aqueous solution at 75°C for 12, 24, 48, and 72 hours[81, 100].

Figure 5.2-19 illustrates the X-Ray diffraction patterns of as-deposited ECD coating and after various time of the above phase conversion process. Upon the phase conversion process, DCPD peaks were no longer found in the patterns and only the HA peaks were found. The intensity of HA peaks increased as the conversion time increased. With 72 hours conversion, the four most representative peaks of HA at 2-theta 25.87°, 31.77°, 32.19°, and 32.90°, were distinctively detectable. This can be attributed to the transformation according to the following reaction[96]:

$$5CaHPO_4 \cdot 2H_2O + 6OH^- \Leftrightarrow Ca_5(PO_4)_3OH + 2PO_4^{3-} + 15H_2O$$

It was reported that DCPD is an unstable phase above pH 6.9 and transforms to hydroxyapatite[81]. Our experimental results have demonstrated the same. Although the HA peaks were more distinctive comparing to that in the as-deposited coating, HA crystallinity (as indicated by the peak width) was still considerably low. Dissolution test results (Section 5.2.4 – Table 5.2-2) have revealed that the coating lost 50% ($D_{1/2}$) of its weight within 4 hours, and was totally dissolved (D_{Total}) in 6 ½ hours.

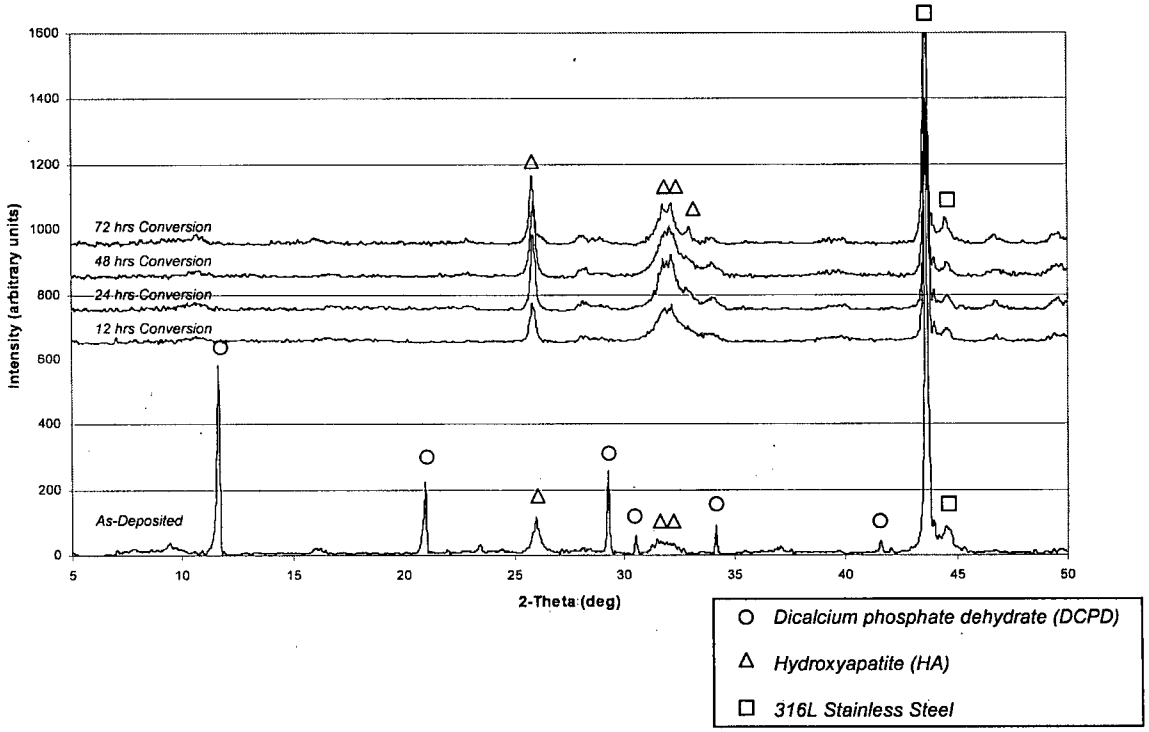

Figure 5.2-19. X-Ray diffraction patterns of as-deposited ECD coating and the resulting coating after 12, 24, 48, and 72 hours of $NaOH_{(aq)}$ phase conversion at 75°C.

The microstructure of the ECD coating on stent with 12 hours conversion process is illustrated in Figure 5.2-20. In contrast to the as-deposit sample, the pores size appear to be larger (i.e. 1.0 – 1.5 μm vs. 0.2 – 0.5 μm in the as-deposited coating). This maybe attributed to the phase transformation process in which the DCPD phase was dissolved and re-precipitated as HA[100, 101]. Similar patterns were also found in the microstructure of ECD coating after 72 hours of the conversion process as illustrated in Figure 5.2-21. SEM observations revealed that all the ECD coatings upon the conversion process have maintained full coverage and uniformity on the stent substrate.

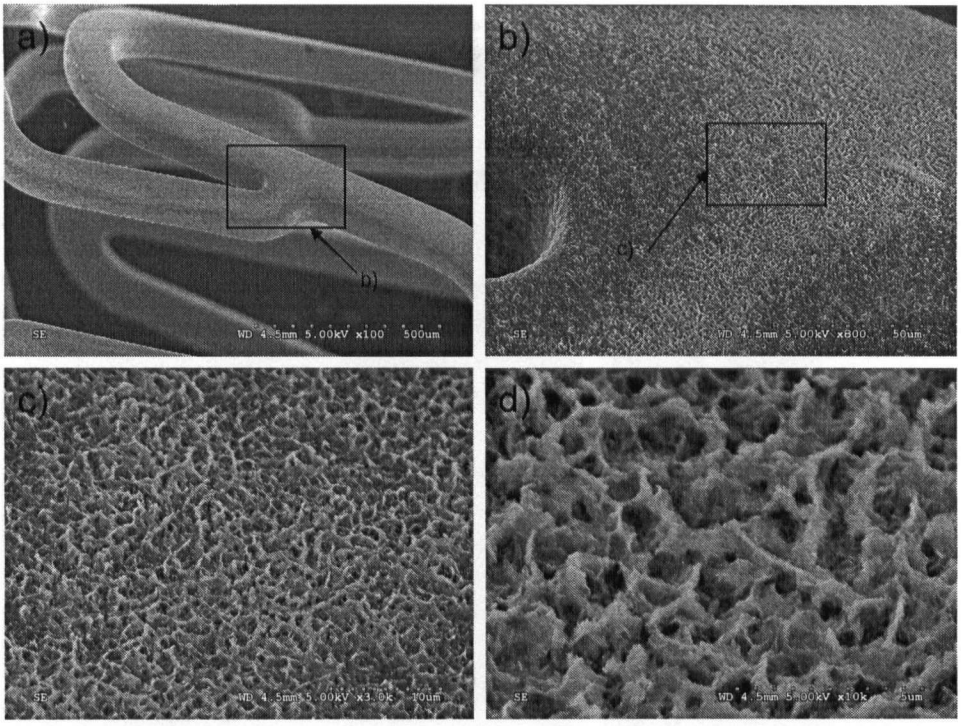

Figure 5.2-20. SEM images of a 12 hours phase conversion ECD coating deposited with optimum deposition parameters. (a) [×100], (b) [×800], (c) [×3,000], and (d) [×10,000]

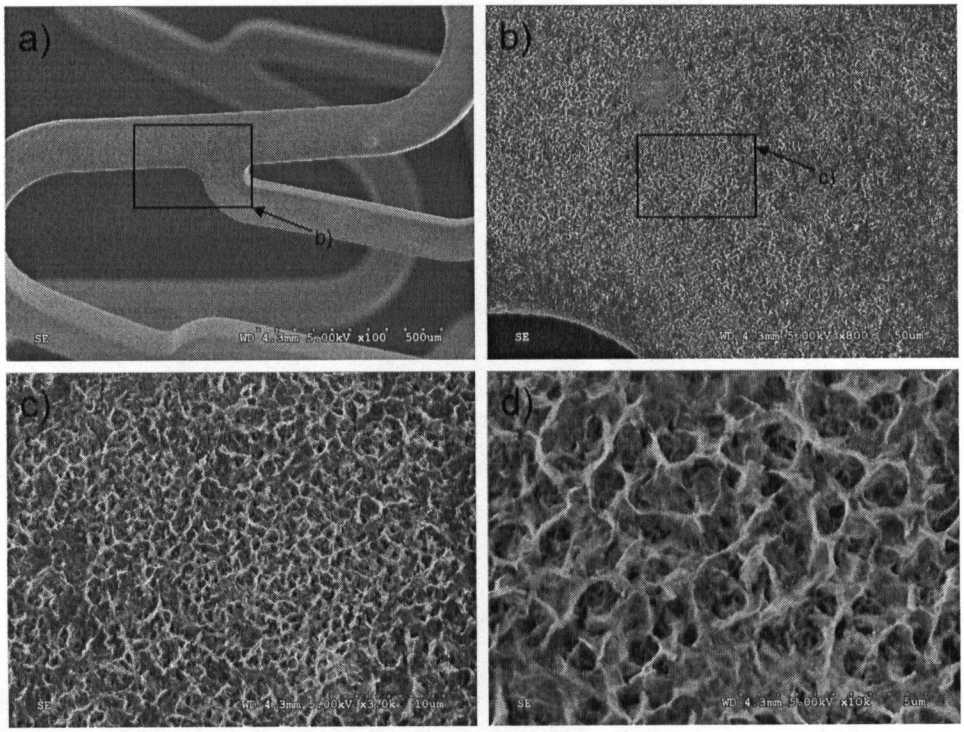

Figure 5.2-21. SEM images of a 72 hours phase conversion ECD coating deposited with optimum deposition parameters. (a) [×100], (b) [×800], (c) [×3,000], and (d) [×10,000]

It is generally believed that an amorphous HA coating has higher dissolution rate than a crystalline HA coating[65]. It is common to measure crystallinity by using diffraction techniques, such as x-ray diffraction: greater crystallinity yields a sharper diffracted beam[102, 103]. The higher the heat treatment temperature, the larger and more perfect the crystals and thus the lower the degradation (dissolution) rate. Therefore, easily resorbable calcium phosphate materials are usually heat-treated CaP materials[30]. High heat treatment temperatures induce HA crystals growth, and thus lead to the decrease of total porosity and pore size[73, 104]. Depending on the calcium to phosphorous ratio, presence of water and impurities, amorphous HA can be transform to crystalline HA[6, 30]. Therefore, a heat treatment after the NaOH conversion was also performed. Three as-deposited calcium phosphate coatings were converted with 0.1M NaOH aqueous solution for 12 hours at 75°C, followed by three different heat treatment temperatures at: 300°C, 500°C, and 750°C for 20 minutes.

Figure 5.2-22 illustrates the X-Ray diffraction patterns of the ECD coating after 12 hours of 0.1N $NaOH_{(aq)}$ phase conversion and after the subsequent 300°C, 500°C, and 750°C heat treatment of 20 minutes. As the heat treatment temperature increases, the peaks become narrower and individual peaks of HA become more distinctive. After 300°C heat treatment, no significant change occurred in the XRD pattern; it was observed that the sample still consisted of poorly crystallized HA. At 500°C, the signature peaks (as indicated by JCPDC #009-0432) of HA at 2-theta 25.87°, 28.96°, 31.77°, 32.19°, 32.90°, and 34.05° have became more distinctive and the intensity had notably increased. Furthermore, the width of the peaks was considerably narrower as compared to the 300°C

samples. Upon heat treating the coating at 700°C, a pure phase of HA was formed. It was observed that both the intensity and 2-theta have closely matched the reference XRD pattern of hydroxyapatite. The two higher intensity peaks at 31.77° and 32.19° were found to be well defined. Some of the peaks not noticeable at <700°C, i.e. at 2-theta 10.85°, 16.79°, and 46.71°, were found to have became more evidenced. This trend of phase evolution have suggested that the 0.1N NaOH conversion and the subsequent heat treatment does optimize the HA phase and does increase the crystallinity.

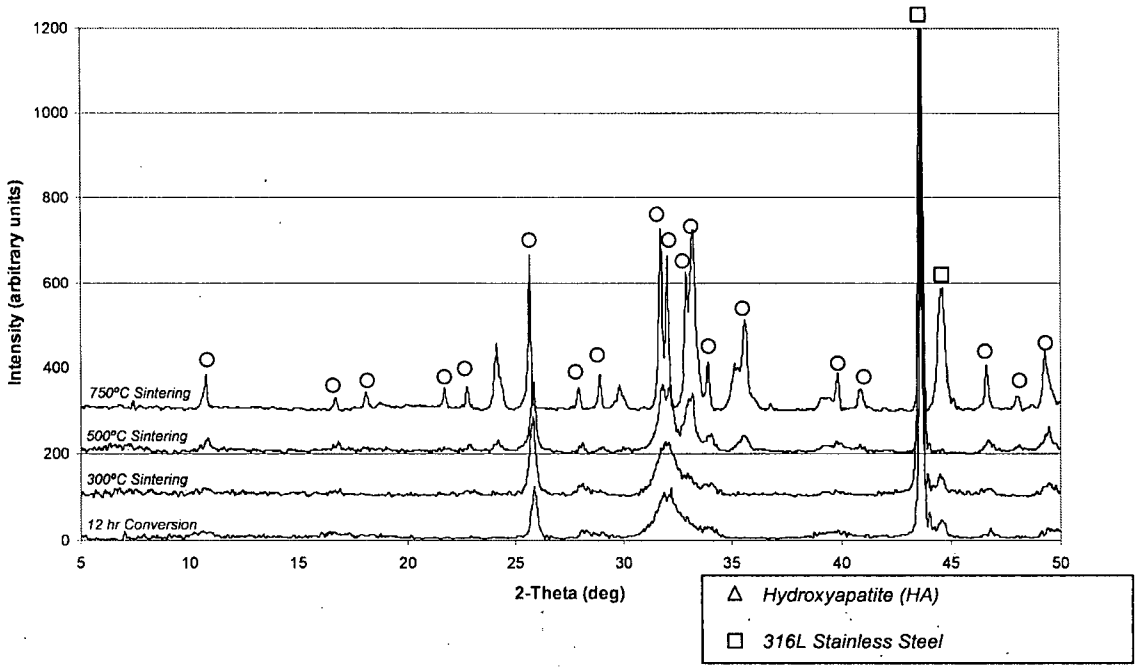

Figure 5.2-22. X-Ray diffraction patterns of 12 hours $NaOH_{(aq)}$ phase converted ECD coating and after 300°C, 500°C, and 750°C for 20 minutes of heat treatment of the coating.

Although the width of HA peaks became narrower as heat treatment temperature increases, it has not been clarified in the present work that it was due to the increase of crystallinity or grain size. Numerous studies suggested that the narrowing of HA peaks is

indication of higher crystallinity[23, 73, 84, 98]. Figure 5.2-23 (b) & (c) illustrates the microstructure of the 500°C and 750°C heat treated coating on stent, respectively. Although the overall microstructure of the heat treated coating was observed to be similar, the coating density was observed to have increased as compared to the pre-heat treated coating (Figure 5.2-23 (a)). It was also observed that the overall integrity of the coating appeared to have increased. The loosely attached structure found in the pre-heat treated coatings has formed a closely inter-connected porous structure. In the dissolution tests for ECD coating, it was found that the time needed for 50% coating dissolution ($D_{1/2}$) increased from 20 minutes to 4 hours upon $NaOH_{(aq)}$ treatment. Furthermore, the phase conversion process (with $NaOH_{(aq)}$ treatment + 500°C heat treatment) prolonged ECD-HA coating dissolution up to four weeks, with only ~6% weight lost during the test. Table 5.2-2 summarizes the dissolution results for the ECD coatings.

Figure 5.2-24 shows the SEM images of an ECD-HA coated stent after $NaOH_{(aq)}$ treatment and 500°C / 20 minutes heat treatment, after stent expansion. High degree of substrate deformation is noticed, since a 3.5mm diameter catheter was used for the expansion test. Examinations of both tensile and compressive areas have found no detrimental cracking or delamination of the coating. Although some fine cracks (~300nm) were noticeable, it is reasonable to believe that the heat treatment process has increased the integrity of the coating.

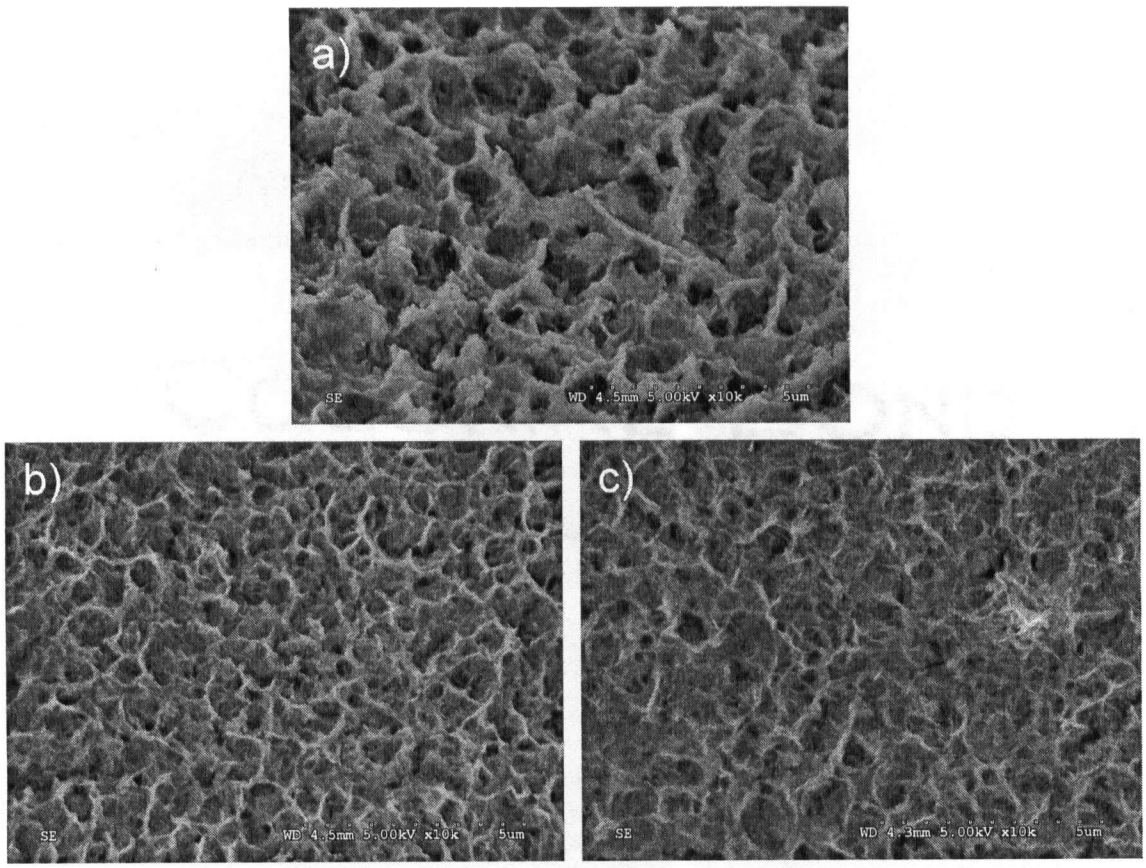

Figure 5.2-23. SEM images of ECD coating after phase conversion process [×10,000]. (a) 12 hours $NaOH_{(aq)}$ treatment (b) 12 hours $NaOH_{(aq)}$ treatment + 500°C heat treatment (c) 12 hours $NaOH_{(aq)}$ treatment + 750°C heat treatment.

Table 5.2-2. Summary of ECD coatings dissolution test data. Dissolution tests were conducted with 10 mL of phosphate buffer saline (PBS) at 37°C (pH = 7.4) with rotation speed at 20 rpm.

ECD Coating Description*	**Time to $D_{1/2}$****	**Time to D_{Total}****
As deposited ECD Coating	20 minutes	40 minutes
ECD Coating with $NaOH_{(aq)}$ Conversion	4 hours	6 ½ hours
ECD Coating with $NaOH_{(aq)}$ Conversion + 500°C heat treatment	> 4 weeks	> 4 weeks

* All Coatings were prepared as described in Table 5.2-1.

** $D_{1/2}$ denotes the time of 50% coating weight lost, D_{Total} denotes the time of total coating dissolution.

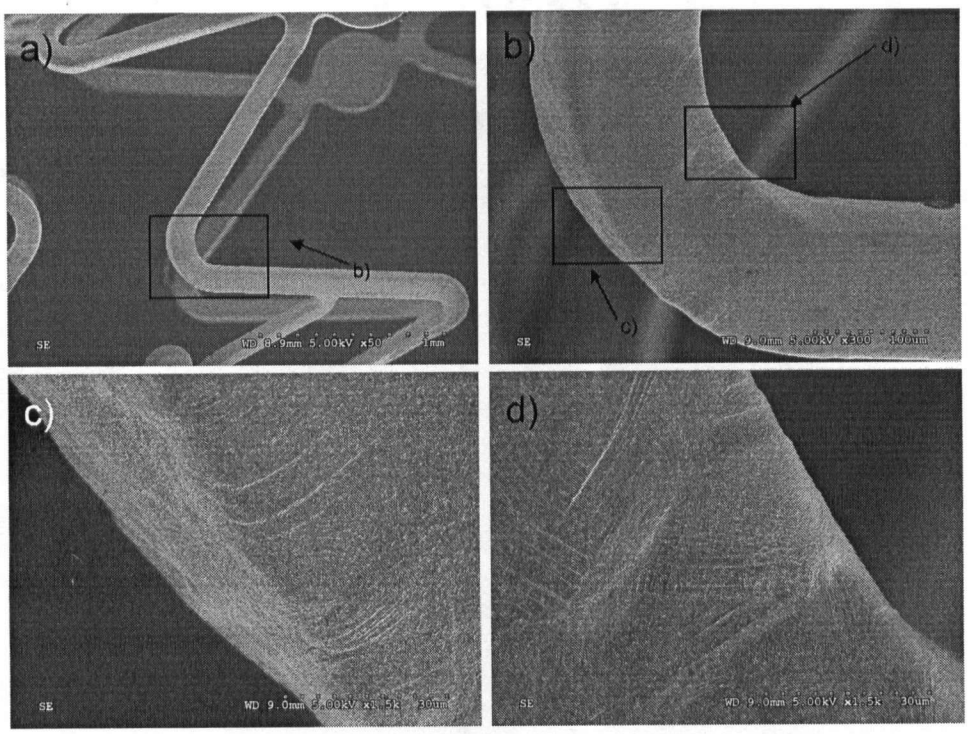

Figure 5.2-24. SEM images of expansion test result from an as deposited ECD coating upon $NaOH_{(aq)}$ treatment + 500°C heat treatment. Expansion performed with a 3.5 mm diameter catheter. (a) [×50], (b) [×300], (c) Showing the compressive stress area [×1,500], and (d) Showing the tensile stress area [×1,500]

5.2.5 In-vitro Fatigue Test

The purpose of this test was to ensure ECD-HA coated stents are fatigue-resistant in an accelerated 40 million cycles test, (i.e. simulating about 1 year of heartbeat), and to ensure no catastrophic failure occurred to the integrity of ECD-HA coating. This is to provide empirical evidence for the continued structural integrity of the ECD-HA coated stents when subjected to mechanical fatigue such as that would receive *in vivo.* SEM was used to examine the coating surface at the end of the test and to examine saline filters for any lose debris. EDX was used to identify the elemental composition of the coating

surface or an area of interest such as filtered debris. The test was performed at MIV Therapeutics, Vancouver, B.C.

As described in Chapter 4.4.3, six ECD-HA coated stent specimens were divided into three pairs, and one stent from each pair was implanted into the proximal end of the simulated vessel, another into the distal end. The target %OD strain of the fatigue test was 0.48%. Figure 5.2-25 summarizes the actual %OD strain of the six fatigue tested stent specimens. Percent OD strain for vessel #1 was found to be the closest to the target at ~0.515%, vessel #2 exhibits the highest strain at ~0.565% and vessel #3 shows the least strain at ~0.395%.

Specimen Position	Speimen ID	Average % OD Strain
Vessel #1 Proximal	1P	0.51
Vessel #1 Distal	1D	0.52
Vessel #2 Proximal	2P	0.57
Vessel #2 Distal	2D	0.56
Vessel #3 Proximal	3P	0.35
Vessel #3 Distal	3D	0.44

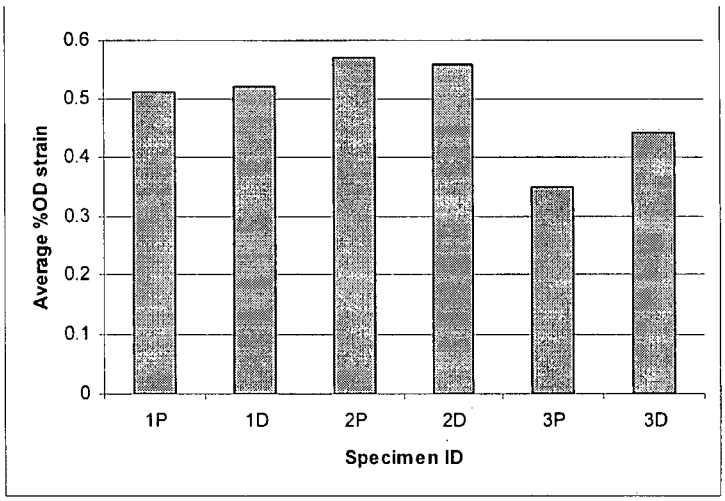

Figure 5.2-25. Summary of average %OD strain for the six fatigue tested stent specimens.

SEM images of specimen 1P after the fatigue testing are shown in Figure 5.2-26. Crystals of phosphate buffer saline (PBS) used as the test media, and NaCl were found on stent surface, as PBS contained 10mM phosphate, 140mM NaCl, and 3mM KCl. Due to salts buildup, it was not possible to evaluate the coating by weight measurement. Instead, since PBS did not contain any calcium, the content of calcium in ECD-HA was used as an indicator of the coating existence. Figure 5.2-26 (b) illustrates the area analysis by EDX. The results have shown a high count of calcium suggesting the ECD-HA coating still remains on the stent surface (Figure 5.2-26(d)). The side edge of stent 1P is shown in Figure 5.2-26 (c). While the coating microstructure on the edge area remains the same, the coating microstructure on the top surface was obviously thinner. The "thinning" of the coating was likely due to the contact between the vibrating vessel wall and the top coating surface. However, as indicated by EDX analysis, it was reasonable to conclude that the ECD-HA coating remains adhered to the stent surface.

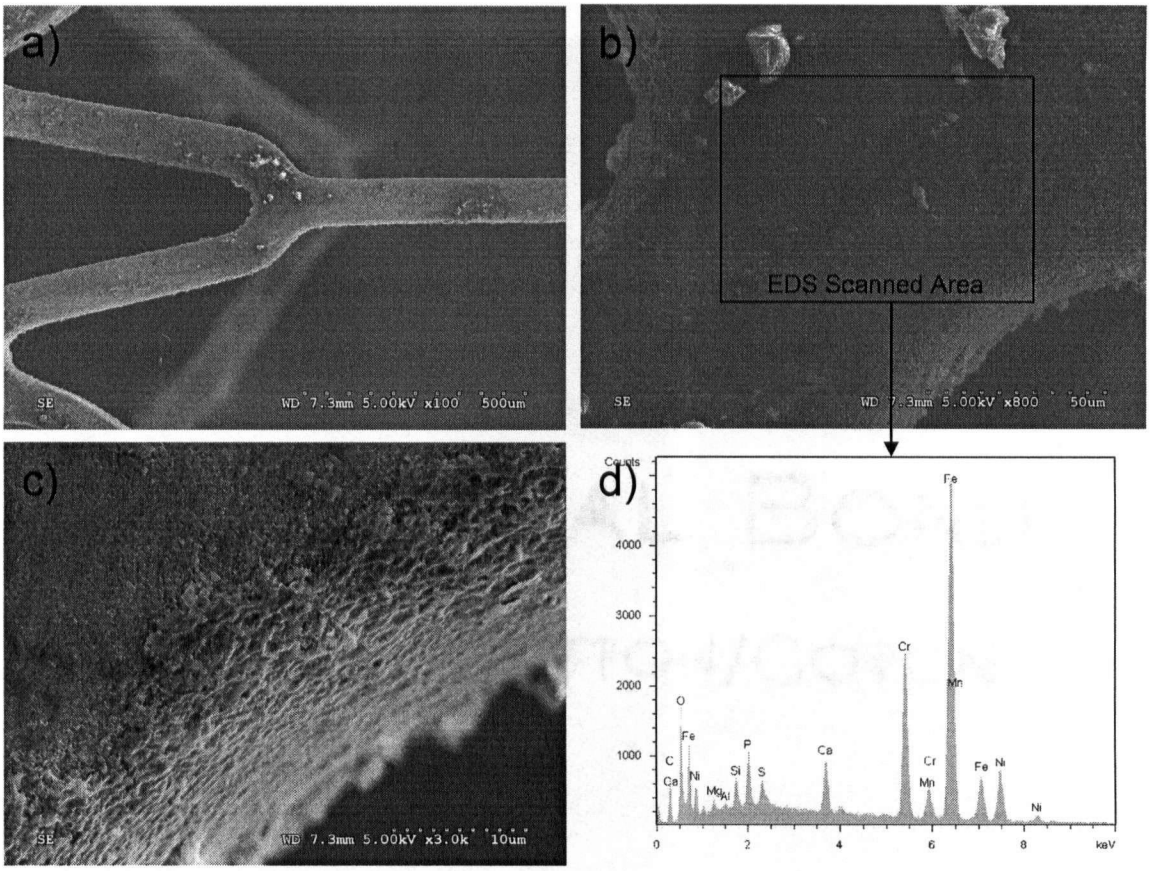

Figure 5.2-26. SEM images of explanted fatigue tested specimen 1P from vessel #1 proximal end (a) [×100], (b) [×800], (c) [×3,000] (d) EDX analysis from surface area scan.

Figure 5.2-27 illustrates the SEM image of specimen 2P after the fatigue test. Even though specimens in vessel #2 suffered the highest %OD strain, there was no cracking or peeling found in the 2P coating. Similar to specimen 1P, NaCl crystals were found on the stent surface. Figure 5.2-27 (b) shows the area analyzed by EDX, distinctive calcium content was found, indicating presence of ECD-HA coating. The characteristic porous microstructure of the ECD coating can be seen in Figure 5.2-27 (c). However, the coating was observed to be somewhat denser than before fatigue testing; this is believed to be due to the crystallized NaCl or KCl inside the pores during the

fatigue test. Nevertheless, both EDX and surface microstructure have suggested that the ECD-HA coating remains on the stent surface.

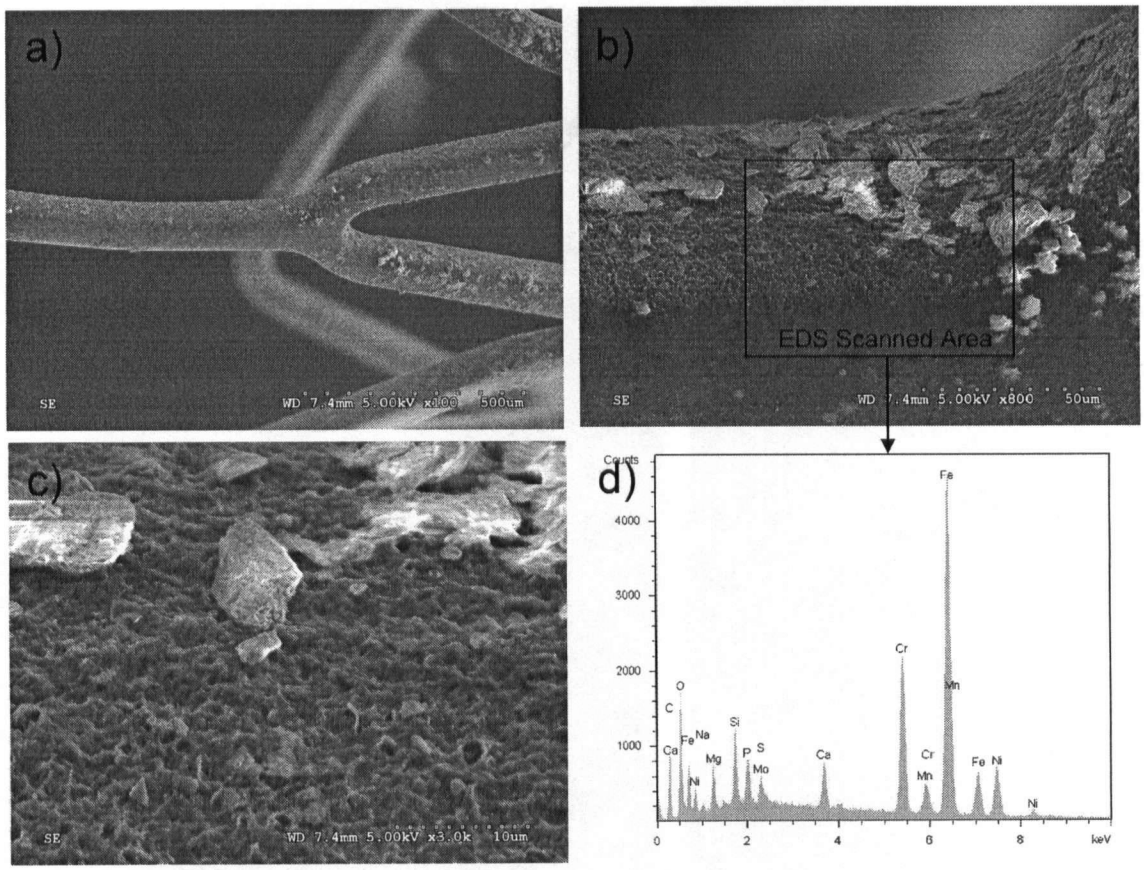

Figure 5.2-27. SEM images of explanted fatigue tested specimen 2 from vessel #2 proximal end (a) [×100], (b) [×800], (c) [×3,000] (d) EDX analysis from surface area scan.

The %OD strain of vessel#3 was the least among the three vessels, the SEM image of the specimen 3P after fatigue test is shown in Figure 5.2-28. Once again, NaCl crystals were found on the stent surface. And, similar to specimen 2P, a denser porous microstructure was observed (Figure 5.2-28 (c)). Unlike specimen 1P and 2P, the coating microstructure of specimen 3P in the stent edge area and stent surface area have shown

minimal difference. Closer examination of Figure 5.2-28 (b) reveals a uniform microstructure from the stent edge to surface, and no "thinning" was observed, Figure 5.2-28 (c). Surface area scan with EDX analysis suggested the ECD-HA still remains with high calcium content.

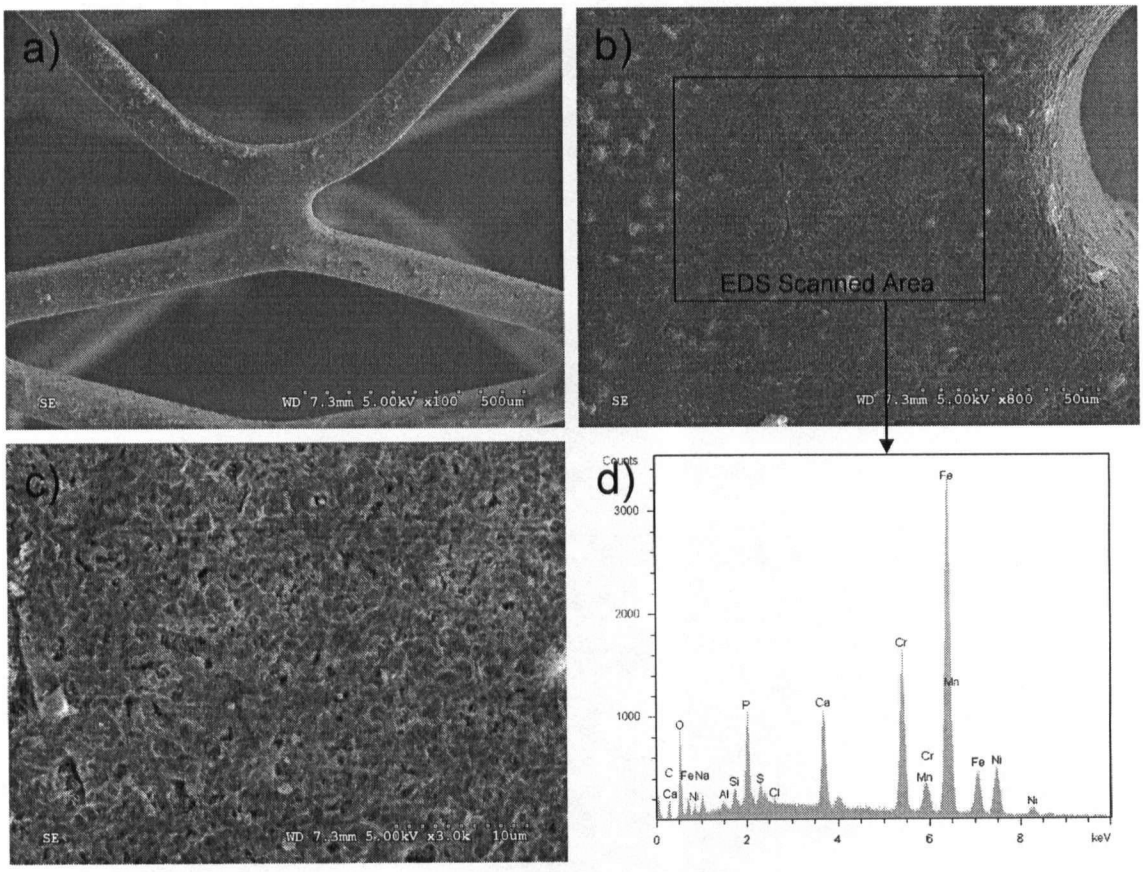

Figure 5.2-28. SEM images of explanted fatigue tested specimen 2 from vessel #3 proximal end (a) [×100], (b) [×800], (c) [×3,000] (d) EDX analysis from surface area scan.

At the end of the 40 million cycles fatigue test the PBS test solution was passed through a 0.4 μm micro-filter to trap potential debris released from the fracturing ECD-HA coating. Numerous debris were found on filter, and SEM and EDX characterizations

were performed over the different debris of interest (i.e. suspected HA debris and other contaminations). SEM and EDX characterizations indicated that there were several types of debris, varying in shape, morphology, and elemental content, present in the fatigue test system. In general, six categories of debris can be recognized. Figure 5.2-29 illustrates the six main categories of debris found, namely D1 – D6. Debris size was observed to range from 5μm – 30μm diameter. EDX analyses of the six debris were illustrated in Figure 5.2-30 respectively.

D1 and D3 both contain high silicon content, as shown in Figure 5.2-30 EDX-D1 and EDX-D3. It was believed that the silicon content was from the silicon-made vessel wall. The only debris found to contain calcium was D2, nevertheless, calcium content was minimal (0.37wt%). Judged from the high phosphorus content, it is believed that D2 was a PBS chlorine crystal buildup on coating surface, possibly detached during the test along with a trace of ECD-HA coating. Most important of all, none of the debris found on filter resemble the shape or microstructure of the ECD coating. Debris D2, D4, and D6 all contain high content of chlorine from PBS based on the EDX result in Figure 5.2-30 EDX-D2, EDX-D4, and EDX-D6, respectively. Other commonly found debris was D5 containing high sulphur content as illustrated in Figure 5.2-29. Additional elements such as copper, zinc, and magnesium were often found incorporated in debris, the origin of these elements was unknown.

Although EDX analysis was performed to determine the presence of different elements, due to the intensity overlap caused by the filter material (i.e. carbon and

oxygen), the concentration result may not be referred to as the exact percentage of each element in the analyzed area. In other words, the concentration presented in the EDX analysis, may not reflect the true concentration and should only be considered as an indicator. This is because the dispersion energy used in the EDX analysis was high enough to penetrate to the substrate (filter), the elemental analysis data of the debris may also contains elements of the substrate and the surrounding area. Therefore, as seen in Figure 5.2-30, a high content of carbon and oxygen from the filter material is clearly distinguishable. Also, it was reported that for rough surface samples or small particles, the relative accuracy of EDX may be as low as 50% [105].

From the microstructural observation and elemental analysis carried out on the fatigue tested stent specimens, there was no visible crack or delamination occurred on the coating surface at ×3,000 magnification. Although "thinning" of the surface coating was observed, EDX analysis have proved that the ECD-HA still remains attached to the stent surface. Furthermore, SEM observations of the debris filters have not found any debris resembling the ECD-HA coating. EDX analyses on the found debris have not suggested any debris with high calcium content originating from ECD-HA coating.

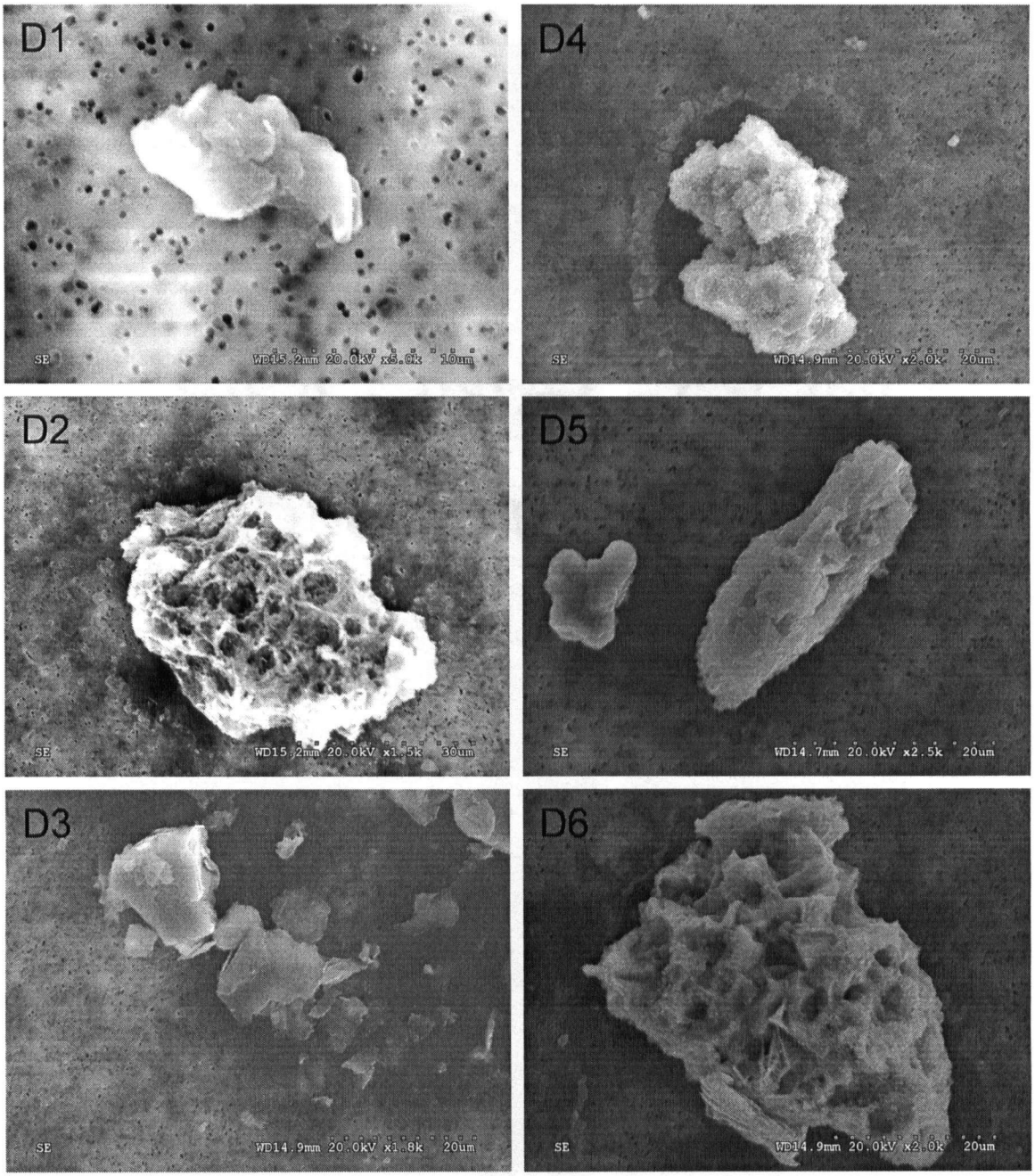

Figure 5.2-29. The six main categories of debris found on filter after the fatigue test.

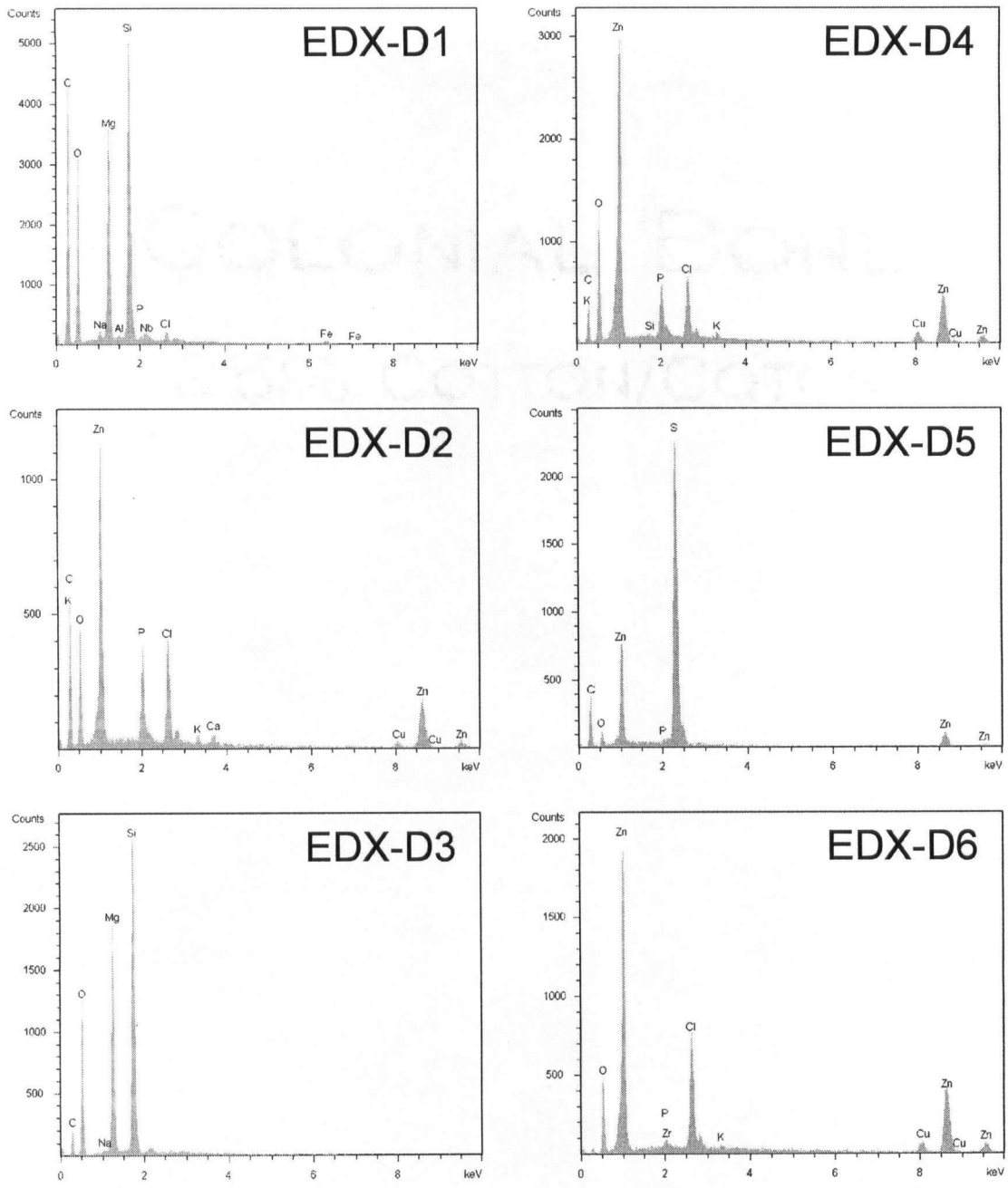

Figure 5.2-30. EDX analysis of the six main categories of debris found after the fatigue test.

5.2.6 Reproducibility and Consistency of ECD-HA Process

The ECD coating process (at optimum coating parameters as listed in Table 5.2-1) and the phase conversion process (i.e. 0.1N $NaOH_{(aq)}$ + 500°C heat treatment) on the surface modified stent, were run repeatedly to evaluate process reproducibility. Five batches of ECD coatings were produced and characterized. Each batch consisted of ten 316L stainless steel bare metal stents manufactured by MIV Therapeutics, Vancouver, BC. Each stent was weighted with Sartorius ME5 micro-balance (accuracy ±1 μg) before and after the ECD process. SEM qualification was performed with stent sample #1, #5, #10 from each batch, coating uniformity and microstructure were closely monitored.

Table 2.3-1 shows the summary of the average weight of ECD coating per each batch and their yield rate. Yield rate is defined as the fraction of coating processed within the specification limits. Details of records can be found in Appendix B. The qualification criterion for coating weight (specification) was set to be 62 μg ± 5 μg. All SEM observations of coating surface have shown uniform surface coverage and porous microstructure as illustrated in Figure 5.2-20. The average weight of the five batches was found to be 62.6 μg, with standard deviation 2.1 μg, and the average yield rate was found to be 94%. The coating on three stents (ECD-RP-002-08, ECD-RP-003-05, and ECD-RP-004-02) was found to have weighted outside of the acceptable range and was rejected. It was concluded that, in term of coating microstructure, uniformity and weight, the application of ECD-HA coatings on coronary stent exhibits high process reproducibility and consistency.

Table 5.2-3. Summary of five batches of ECD coating average weight and yield rate.

	Coating Weight of ECD HA Batch (μg)				
Stent Number	ECD-RP-001	ECD-RP-002	ECD-RP-003	ECD-RP-004	ECD-RP-005
01	62	60	61	64	65
02	63	62	59	23	64
03	66	63	61	63	64
04	65	61	64	67	63
05	64	60	73	65	65
06	60	62	61	62	62
07	61	61	60	61	59
08	62	42	62	63	61
09	66	65	63	61	65
10	65	64	62	66	59
Average (μg):	63.4	62.0	61.4	63.6	62.7
Overall Average (μg):	62.6				
Standard Deviation (μg):	2.0	1.6	1.4	2.0	2.2
Overall Standard Deviation (μg):	2.1				
Yield Rate:	100%	90%	90%	90%	100%
Overall Yield Rate:	94%				
* Rejected samples were excluded from average and standard deviation calculation					

5.2.6.1 Errors in ECD-HA Characteristics and Process Parameters Measurement

Within the group of 50 stents used for reproducibility study, stents weights were in the range of 15.243 mg – 16.897 mg. According to MIV Therapeutics, the weight variation was attributed to the stent manufacture process, i.e. laser cutting and electropolishing. It was also suggested by MIV Therapeutics that under these manufacture process variations, the surface area of the stent may vary as much as 5%. In consideration of the current density (1 mA/cm^2) applied under the optimum coating condition, the surface area variation can impose a 5% error in current density measurement.

Electrolyte temperature fluctuation was observed during the process reproducibility study. A two degree Celsius variation was observed while the optimum coating temperature (45°C) was being used. It was believed that the fluctuation was due to the hot-plate on/off cycling. Measurement of electrolyte pH was done with Beckman 260 pH meter with an inhered error of ± 0.004 pH. Chemical preparation for the ECD electrolyte was performed with Sartorius ME235P-SD balance with 0.01 mg accuracy. Time of deposition was controlled by switching the current supply on/off, human error was expected to be ± 2 seconds. Coating weight measurement for stent was performed with Sartorius ME5 micro-balance with ±1 μg accuracy.

Based on the reproducibility and consistency study of ECD-HA process, the cumulative errors described above were found to have no significant implication on the coating microstructure and coverage. The average weight measurement was found to be 62.6 μg, with standard deviation 2.1 μg. This measurement was found to be well within the qualification criterion for coating weight (62 ± 5 μg).

6 CONCLUSIONS

In this study, electrochemical deposition (ECD) was used to deposit uniform calcium phosphate coatings on 316L stainless steel coronary stents. The influence of the ECD process parameters (deposition time, current density, electrolyte temperature, pH, and Ca/P ratio) on the resulting deposition morphology was investigated. The research results in the following conclusions:

1. Hydroxyapatite coatings can be successfully deposited through ECD on 316L stainless steel coronary stents.

2. The ECD current density and deposition time play an important role on the coating characteristics, in particular the amount and microstructure of coating being deposited. In order to achieve uniform thin film (<0.5 μm) coating on the complex surface of coronary stents, current density should be 1.0 mA/cm^2 and deposition time should be 1 minute. These conditions were determined for the electrolyte concentration of 0.02329M calcium nitrate and 0.04347M ammonium phosphate (Ca/P 1.95), deposition temperature at 45°C, and pH = 4.5.

3. It was observed that the level of current density has a more significant effect on the resulting Ca/P microstructure, whereas the deposition time has more control of weight or thickness of the resulting coating. The coating microstructure exhibits plate-like crystals when high current density (> $3mA/cm^2$) was applied. The

optimum stent coating current density revealed a porous coating with uniform coverage on the complex stent surface.

4. ECD with electrolyte temperature at 45°C exhibits good reproducibility of coating microstructure and thickness (~0.5 μm), as demonstrated through a five batches of ten stents reproduction evaluation. The average weight of the five batches was found to be 62.5 μg, with standard deviation 2.1 μg, and the average yield rate was found to be 94%.

5. The electrolyte Ca/P ratio (0.49 – 2.92) and pH (4.5 – 5.5) selected for this study have not shown significant impact on the microstructure of the resulting ECD-HA coatings.

6. Stent surface modification was employed to improve coating adhesion and integrity. The modification involved soaking of stent in 10N $NaOH_{(aq)}$ at 60°C for 24 hours, and subsequently heat-treatment at 500°C for 20 minutes. In-vitro stent crimping and expansion tests found that the application of such substrate surface modification procedure has remarkably improved the adhesion between the ECD coating and the stent substrate, while maintaining the desired coating microstructure and phase composition.

7. X-Ray diffraction studies have confirmed that the as-deposited ECD mixed-phase calcium phosphate coating can be subsequently transformed into pure HA without

detrimental effect on the coating microstructure. The post-treatment process involved a 0.1N $NaOH_{(aq)}$ phase conversion at 75°C for 12 hours and a 500°C heat treatment for 20 minutes.

8. The process parameters for optimized ECD-HA coatings on stents include:

• Electrolyte Ca/P ratio	1.95
Calcium Nitrate [$Ca(NO_3)_2$ $4H_2O$]	0.02329 M
Ammonium phosphate [$NH_4H_2PO_4$]	0.04347M
• Current Density	1.0 mA/cm^2
• Deposition Time	1 minute
• Electrolyte pH	4.5
• Electrolyte Temperature	45°C

9. The standard 40 million cycles fatigue test validated the safety and reliability of the optimized ECD-HA coatings with the incorporation of the substrate surface treatment and the phase conversion processes. SEM and EDX analyses of the stent specimens retrieved from fatigue test have shown no sign of cracking or delamination. Filter analysis have further verified that there were no ECD-HA coating debris >0.4μm detached from the stent substrate.

7 RECOMMENDATIONS FOR FUTURE WORK

Based on the previous studies done on electrochemical deposition and this current research, the recommendation for future work can be listed as follows:

- Study of electrochemical deposition on various substrates. The difference in substrate material and geometry strongly influence the process of deposition, and certainly poses multiple challenges. Application of ECD on other implantable biomedical devices should be highlighted, such as Co-Cr alloys for stents or Ti alloys for implants.

- Quantification of the mechanical properties of ECD coating to allow a more complete understanding of the coating mechanical behavior under the influence of varies ECD parameters.

- There are indications that ECD in diluted electrolyte at particularly higher current densities (>10mA/cm^2) may yield nanostructure coatings. These conditions should be explored further.

- Drug encapsulation in combination with electrochemical deposition technology. Competition to bring to markets polymer-free drug elution stent is vigorous. Investigation of drug encapsulation or impregnation into ECD-HA should focus on maximizing the drug content in the coatings, and optimization of the drug release profile.

- Electrochemical co-deposition of organo-ceramic coatings. The co-deposition studies should emphasize feasibility of co-depositing pharmaceutical agents for drug eluting purpose and co-depositing reinforcing agents, such as polymer, for coating mechanical properties improvement (Appendix A), such that thicker (several microns thick) coatings with higher capacity for drug encapsulation can be processed.

REFERENCES

1. American Heart Association, "Cardiovascular Disease Statistics," **2006,** 1 (2005).

2. F. Faccioni, P. Franceschetti, M. Cerpelloni and M.E. Fracasso. "In vivo study on metal release from fixed orthodontic appliances and DNA damage in oral mucosa cells," American Journal of Orthodontics and Dentofacial Orthopedics, **124,** 687-93 (2003).

3. J.J. Popma and M. Tulli. "Drug-eluting stents," Cardiol. Clin., **24,** 217, (2006).

4. C.M. Gibson, D. Karmpaliotis and L. Kosmidou, et al. "Comparison of effects of bare metal versus drug-eluting stent implantation on biomarker levels following percutaneous coronary intervention for non-ST-elevation acute coronary syndrome," Am. J. Cardiol., **97,** 1473-7 (2006).

5. R. Wessely, A. Kastrati and A. Schomig. "Late restenosis in patients receiving a polymer-coated sirolimus-eluting stent," Ann. Intern. Med., **143,** 392-4 (2005).

6. Joon B. Park and Joseph D. Bronzino. "Biomaterials: Principles and Applications," 264 (August 29, 2002).

7. K.A. Hing, S.M. Best, K.E. Tanner, W. Bonfield and P.A. Revell. "Biomechanical assessment of bone ingrowth in porous hydroxyapatite," Journal of Materials Science-Materials in Medicine, **8,** 731-6 (1997).

8. G. Willmann, "Coating of implants with hydroxyapatite material connections between bone and metal," Advanced Engineering Materials, **1,** 95-105 (1999).

9. W. Suchanek and M. Yoshimura. "Processing and properties of hydroxyapatite-based biomaterials for use as hard tissue replacement implants," J. Mater. Res., **13,** 94-117 (1998).

10. L.L. Hench, "Bioceramics - from Concept to Clinic," American Ceramic Society Bulletin, **72,** 93-8 (1993).

11. X. Lu and Y. Leng. "Theoretical analysis of calcium phosphate precipitation in simulated body fluid," Biomaterials, **26,** 1097-108 (2005).

12. W. Suchanek and M. Yoshimura. "Processing and properties of hydroxyapatite-based biomaterials for use as hard tissue replacement implants," J. Mater. Res., **13,** 94-117 (1998).

13. S.L. Shi, W. Pan, M.H. Fang and Z.Y. Fang. "Reinforcement of hydroxyapatite bioceramic by addition of Ti3SiC2," J Am Ceram Soc, **89,** 743-5 (2006).

14. S. Pezzatini, R. Solito and L. Morbidelli, et al. "The effect of hydroxyapatite nanocrystals on microvascular endothelial cell viability and functions," Journal of Biomedical Materials Research Part a, **76A,** 656-63 (2006).

15. K. Degroot, R. Geesink, C.P.A.T. Klein and P. Serekian. "Plasma Sprayed Coatings of Hydroxylapatite," J. Biomed. Mater. Res., **21,** 1375-81 (1987).

16. J. Weng, Q. Liu, J.G.C. Wolke, X.D. Zhang and K. deGroot. "Formation and characteristics of the apatite layer on plasma-sprayed hydroxyapatite coatings in simulated body fluid," Biomaterials, **18,** 1027-35 (1997).

17. H. Liang, B. Shi, A. Fairchild and T. Cale. "Applications of plasma coatings in artificial joints: an overview," Vacuum, **73,** 317-26 (2004).

18. C.M. Lopatin, V. Pizziconi, T.L. Alford and T. Laursen. "Hydroxyapatite powders and thin films prepared by a sol-gel technique," Thin Solid Films, **326,** 227-32 (1998).

19. C.K. Wang, J.H.C. Lin, C.P. Ju, H.C. Ong and R.P.H. Chang. "Structural characterization of pulsed laser-deposited hydroxyapatite film on titanium substrate," Biomaterials, **18,** 1331-8 (1997).

20. T. Seno, Y. Izumisawa and I. Nishimura, et al. "The interfacial strength in sputtering-hydroxyapatite-coating implants with Arc-deposited surface," Journal of Veterinary Medical Science, **65,** 419-22 (2003).

21. I. Zhitomirsky, "Electrophoretic hydroxyapatite coatings and fibers," Mater Lett, **42,** 262-71 (2000).

22. H.B. Hu, C.J. Lin, P.P.Y. Lui and Y. Leng. "Electrochemical deposition of hydroxyapatite with vinyl acetate on titanium implants," Journal of Biomedical Materials Research Part a, **65A,** 24-9 (2003).

23. S.K. Yen and C.M. Lin. "Cathodic reactions of electrolytic hydroxyapatite coating on pure titanium," Mater. Chem. Phys., **77,** 70-6 (2003).

24. I. Zhitomirsky, "New developments in electrolytic deposition of ceramic films," American Ceramic Society Bulletin, **79,** 57-63 (2000).

25. I. Zhitomirsky, "Cathodic electrodeposition of ceramic and organoceramic materials. Fundamental aspects," Adv. Colloid Interface Sci., **97,** 279-317 (2002).

26. M.C. Kuo and S.K. Yen. "The process of electrochemical deposited hydroxyapatite coatings on biomedical titanium at room temperature," Materials Science & Engineering C-Biomimetic and Supramolecular Systems, **20,** 153-60 (2002).

27. MIVI Technologies Inc., "Structural Analysis of MIVI Technologies Coronary Stent Model C8-6: Finite Element Analysis Report," **1,** 17-80 (2000).

28. K.A. Gross, W. Walsh and E. Swarts. "Analysis of retrieved hydroxyapatite-coated hip prostheses," J. Therm. Spray Technol., **13,** 190-9 (2004).

29. H. Gierse and K. Donath. "Reactions and complications after the implantation of Endobon including morphological examination of explants," Arch. Orthop. Trauma Surg., **119,** 349-55 (1999).

30. L.M. Sun, C.C. Berndt, K.A. Khor, H.N. Cheang and K.A. Gross. "Surface characteristics and dissolution behavior of plasma-sprayed hydroxyapatite coating," J. Biomed. Mater. Res., **62,** 228-36 (2002).

31. American Heart Association, "Heart Attack," **2006,** 1 (2006).

32. Heart & Stoke Foundation, "Heart Disease," **2006,** 1 (2006).

33. A.H. Gershlick, "Coronary disease - Role of stenting in coronary revascularisation," Heart, **86,** 104-12 (2001).

34. M.M. Gandhi and K.D. Dawkins. "Intracoronary stents," Br. Med. J., **318,** 650-3 (1999).

35. P.W. Serruys and D. Keane. "Randomized Trials of Coronary Stenting - Introduction," J. Interv. Cardiol., **7,** 331- (1994).

36. C.L. Zollikofer, F. Antonucci, G. Stuckmann, P. Mattias and E.K. Salomonowitz. "Historical Overview on the Development and Characteristics of Stents and Future Outlooks," Cardiovasc. Intervent. Radiol., **15,** 272-8 (1992).

37. Kutyk MJ.B. and Serruys PW. *"Historical Overview,"* pp. 1-16 in *CORONARY STENT Current Perspectives.* Edited by Kutyk MJ.B. and Serruys PW. Martin Dunitz, United Kingdom, 1999.

38. P.W. Serruys, P. Dejaegere and F. Kiemeneij, et al. "A Comparison of Balloon-Expandable-Stent Implantation with Balloon Angioplasty in Patients with Coronary-Artery Disease," N. Engl. J. Med., **331,** 489-95 (1994).

39. D.L. Fishman, M.B. Leon and D.S. Baim, et al. "A Randomized Comparison of Coronary-Stent Placement and Balloon Angioplasty in the Treatment of Coronary-Artery Disease," N. Engl. J. Med., **331,** 496-501 (1994).

40. Ioannis K. Stefanidis, Vasilios A. Tolis, Dimitrios G. Sionis and Lambros K. Michals. "Development in Intracoronary Stents," HJC, **43,** 63-7 (2002).

41. V. Rajagopal and S.G. Rockson. "Coronary restenosis: A review of mechanisms and management," Am. J. Med., **115,** 547-53 (2003).

42. F. Airoldi, A. Colombo and D. Tavano, et al. "Comparison of diamond-like carbon-coated stents versus uncoated stainless steel stents in coronary artery disease," Am. J. Cardiol., **93,** 474-7 (2004).

43. K. Gutensohn, C. Beythien and J. Bau, et al. "In vitro analyses of diamond-like carbon coated stents: Reduction of metal ion release, platelet activation, and thrombogenicity," Thromb. Res., **99,** 577-85 (2000).

44. B. Heublein, C. Ozbek and K. Pethig. "Silicon carbide-coated stents: Clinical experience in coronary lesions with increased thrombotic risk," Journal of Endovascular Surgery, **5,** 32-6 (1998).

45. M. Unverdorben, M. Schywalsky and D. Labahn, et al. "Stents coated with hypothrombogenic amorphous silicon carbide - preliminary results in the New Zealand White Rabbit," Perfusion, **13,** 124,+ (2000).

46. N. Huang, P. Yang and X. Cheng, et al. "Blood compatibility of amorphous titanium oxide films synthesized by ion beam enhanced deposition," Biomaterials, **19,** 771-6 (1998).

47. A. Kastrati, A. Schomig and J. Dirschinger, et al. "Increased risk of restenosis after placement of gold-coated stents - Results of a randomized trial comparing gold-coated with uncoated steel stents in patients with coronary artery disease," Circulation, **101,** 2478-83 (2000).

48. Thomson Healthcare, "MedlinePlus Drug Information: Heparin," 1 (2006).

49. E.J. Topol and P.W. Serruys. "Frontiers in interventional cardiology," Circulation, **98,** 1802-20 (1998).

50. A. Colombo and E. Karvouni. "Biodegradable stents - "Fulfilling the mission and stepping away"," Circulation, **102,** 371-3 (2000).

51. H. Tamai, K. Igaki and E. Kyo, et al. "Initial and 6-month results of biodegradable poly-l-lactic acid coronary stents in humans," Circulation, **102,** 399-404 (2000).

52. R. Albiero and A. Colombo. "European high-activity P-32 radioactive stent experience," J. Invasive Cardiol., **12,** 416-21 (2000).

53. R.N. Saunders, M.S. Metcalfe and M.L. Nicholson. "Rapamycin in transplantation: A review of the evidence," Kidney Int., **59,** 3-16 (2001).

54. E.K. Rowinsky and R.C. Donehower. "Drug-Therapy - Paclitaxel (Taxol)," N. Engl. J. Med., **332,** 1004-14 (1995).

55. C.J. Creel, M.A. Lovich and E.R. Edelman. "Arterial paclitaxel distribution and deposition," Circ. Res., **86,** 879-84 (2000).

56. C21.01, "C242-01 Standard Terminology of Ceramic Whitewares and Related Products," ASTM International,

57. L.L. Hench, "Bioceramics - from Concept to Clinic," J Am Ceram Soc, **74,** 1487-510 (1991).

58. E.B. Riska, "Ceramic-on-ceramic total hip replacement," Current Orthopaedics, **13,** 320-4 (1999).

59. R.H. Dauskardt, R.O. Ritchie, J.K. Takemoto and A.M. Brendzel. "Cyclic Fatigue and Fracture in Pyrolytic Carbon-Coated Graphite Mechanical Heart-Valve Prostheses - Role of Small Cracks in Life Prediction," J. Biomed. Mater. Res., **28,** 791-804 (1994).

60. A. Lasserre and P.K. Bajpai. "Ceramic drug-delivery devices," Crit. Rev. Ther. Drug Carrier Syst., **15,** 1-56 (1998).

61. Morris L and Bajpai PK. "Development of a resorbable tricalcium phosphate (TCP) amine antibiotic composite," In Biomedical Materials and Devices, 293–300 (1989).

62. J.E. Lemons, "Ceramics: Past, present, and future," Bone, **19,** S121-8 (1996).

63. A. Tonino, C. Oosterbos, A. Rahmy, M. Therin and C. Doyle. "Hydroxyapatite-coated acetabular components - Histological and histomorphometric analysis of six cups retrieved at autopsy between three and seven years after successful implantation," Journal of Bone and Joint Surgery-American Volume, **83A,** 817-25 (2001).

64. M. Vallet-Regi and J.M. Gonzalez-Calbet. "Calcium phosphates as substitution of bone tissues," Progress in Solid State Chemistry, **32,** 1-31 (2004).

65. L.M. Sun, C.C. Berndt, K.A. Khor, H.N. Cheang and K.A. Gross. "Surface characteristics and dissolution behavior of plasma-sprayed hydroxyapatite coating," J. Biomed. Mater. Res., **62,** 228-36 (2002).

66. P. Ducheyne, S. Radin and L. King. "The Effect of Calcium-Phosphate Ceramic Composition and Structure on Invitro Behavior .1. Dissolution," J. Biomed. Mater. Res., **27,** 25-34 (1993).

67. P. Koutsoukos, Z. Amjad, M.B. Tomson and G.H. Nancollas. "Crystallization of Calcium Phosphates - Constant Composition Study," J. Am. Chem. Soc., **102,** 1553-7 (1980).

68. M. Jarcho, C.H. Bolen, M.B. Thomas, J. Bobick, J.F. Kay and R.H. Doremus. "Hydroxylapatite Synthesis and Characterization in Dense Polycrystalline Form," J. Mater. Sci., **11,** 2027-35 (1976).

69. W.R. Rao and R.F. Boehm. "Study of Sintered Apatites," J. Dent. Res., **53,** 1351-4 (1974).

70. G. Daculsi, R.Z. Legeros, E. Nery, K. Lynch and B. Kerebel. "Transformation of Biphasic Calcium-Phosphate Ceramics Invivo - Ultrastructural and Physicochemical Characterization," J. Biomed. Mater. Res., **23,** 883-94 (1989).

71. N. Rangavittal, A.R. Landa-Canovas, J.M. Gonzalez-Calbet and M. Vallet-Regi. "Structural study and stability of hydroxyapatite and beta-tricalcium phosphate: Two important bioceramics," J. Biomed. Mater. Res., **51,** 660-8 (2000).

72. M. Noor Hasimah and O. Radzali. "The effect of sintering temperature on the mechanical properties of hydroxyapatite," School of Material and Minerial Resources Engineering, Universiti Sains Malaysia.

73. G. Muralithran and S. Ramesh. "The effects of sintering temperature on the properties of hydroxyapatite," Ceram. Int., **26,** 221-30 (2000).

74. E. Grenadier, A. Roguin and I. Hertz, et al. "Stenting very small coronary narrowings (< 2 mm) using the biocompatible phosphorylcholine-coated coronary stent," Catheterization and Cardiovascular Interventions, **55,** 303-8 (2002).

75. R.J. Furlong and J.F. Osborn. "Fixation of Hip Prostheses by Hydroxyapatite Ceramic Coatings," Journal of Bone and Joint Surgery-British Volume, **73,** 741-5 (1991).

76. S.R. Sousa and M.A. Barbosa. "Effect of hydroxyapatite thickness on metal ion release from Ti6Al4V substrates," Biomaterials, **17,** 397-404 (1996).

77. S.R. Sousa and M.A. Barbosa. "The effect of hydroxyapatite thickness on metal ion release from stainless steel substrates," Journal of Materials Science-Materials in Medicine, **6,** 818-23 (1995).

78. H.X. Ji, C.B. Ponton and P.M. Marqutis. "Microstructural Characterization of Hydroxyapatite Coating on Titanium," Journal of Materials Science-Materials in Medicine, **3,** 283-7 (1992).

79. S.R. Radin and P. Ducheyne. "Plasma Spraying Induced Changes of Calcium-Phosphate Ceramic Characteristics and the Effect on Invitro Stability," Journal of Materials Science-Materials in Medicine, **3,** 33-42 (1992).

80. G.H.A. Therese and P.V. Kamath. "Electrochemical synthesis of metal oxides and hydroxides," Chemistry of Materials, **12,** 1195-204 (2000).

81. J. Redepenning, T. Schlessinger, S. Burnham, L. Lippiello and J. Miyano. "Characterization of electrolytically prepared brushite and hydroxyapatite coatings on orthopedic alloys," J. Biomed. Mater. Res., **30,** 287-94 (1996).

82. M. Shirkhanzadeh, "Bioactive Calcium-Phosphate Coatings Prepared by Electrodeposition," J. Mater. Sci. Lett., **10,** 1415-7 (1991).

83. P. Royer and C. Rey. "Calcium-Phosphate Coatings for Orthopedic Prosthesis," Surf Coat Technol, **45,** 171-7 (1991).

84. M. Manso, C. Jimenez, C. Morant, P. Herrero and J.M. Martinez-Duart. "Electrodeposition of hydroxyapatite coatings in basic conditions," Biomaterials, **21,** 1755-61 (2000).

85. M. Shirkhanzadeh, "Calcium-Phosphate Coatings Prepared by Electrocrystallization from Aqueous-Electrolytes," Journal of Materials Science-Materials in Medicine, **6,** 90-3 (1995).

86. X.L. Cheng, M. Filiaggi and S.G. Roscoe. "Electrochemically assisted co-precipitation of protein with calcium phosphate coatings on titanium alloy," Biomaterials, **25,** 5395-403 (2004).

87. X.H. Hou, X. Liu, J.M. Xu, J. Shen and X.H. Liu. "A self-optimizing electrodeposition process for fabrication of calcium phosphate coatings," Mater Lett, **50,** 103-7 (2001).

88. Y.W. Fan, K. Duan and R.Z. Wang. "A composite coating by electrolysis-induced collagen self-assembly and calcium phosphate mineralization," Biomaterials, **26,** 1623-32 (2005).

89. P. Peng, S. Kumar, N.H. Voelcker, E. Szili, R.S. Smart and H.J. Griesser. "Thin calcium phosphate coatings on titanium by electrochemical deposition in modified simulated body fluid," Journal of Biomedical Materials Research Part a, **76A,** 347-55 (2006).

90. L.Y. Huang, K.W. Xu and J. Lu. "A study of the process and kinetics of electrochemical deposition and the hydrothermal synthesis of hydroxyapatite coatings," Journal of Materials Science-Materials in Medicine, **11,** 667-73 (2000).

91. F.H. Lin, Y.S. Hsu, S.H. Lin and J.S. Sun. "The effect of Ca/P concentration and temperature of simulated body fluid on the growth of hydroxyapatite coating on alkali-treated 316L stainless steel," Biomaterials, **23,** 4029-38 (2002).

92. K. Koski, J. Holsa, J. Ernoult and A. Rouzaud. "The connection between sputter cleaning and adhesion of thin solid films," Surf Coat Technol, **80,** 195-9 (1996).

93. M. Shirkhanzadeh, "Electrochemical Preparation of Bioactive Calcium-Phosphate Coatings on Porous Substrates by the Periodic Pulse Technique," J. Mater. Sci. Lett., **12,** 16-9 (1993).

94. U.S. Food and Drug Administration, "Selected Guidance Documents Applicable to Combination Products- Draft Guidance for the Submission of Research and Marketing Applications for Interventional Cardiology Devices: PTCA Catheters, Atherectomy Catheters, Lasers, Intravascular Stents,"

95. S. Ban and S. Maruno. "Effect of Ph Buffer on Electrochemical Deposition of Calcium-Phosphate," Japanese Journal of Applied Physics Part 2-Letters, **33,** L1545-8 (1994).

96. J. Redepenning and J.P. Mcisaac. "Electrocrystallization of Brushite Coatings on Prosthetic Alloys," Chemistry of Materials, **2,** 625-7 (1990).

97. T.S. Light, S. Licht, A.C. Bevilacqua and K.R. Morash. "The fundamental conductivity and resistivity of water," Electrochemical and Solid State Letters, **8,** E16-9 (2005).

98. M.C. Kuo and S.K. Yen. "Immersion characteristics of electrolytic calcium phosphate coated Ti in simulated physiological fluid," J. Mater. Sci., **39,** 2357-63 (2004).

99. A. Strawbridge and H.E. Evans. "Mechanical Failure of Thin Brittle Coatings," Eng. Failure Anal., **2,** 85-103 (1995).

100. M. Kumar, H. Dasarathy and C. Riley. "Electrodeposition of brushite coatings and their transformation to hydroxyapatite in aqueous solutions," J. Biomed. Mater. Res., **45,** 302-10 (1999).

101. Y. Han, K.W. Xu and J.A. Lu. "Morphology and composition of hydroxyapatite coatings prepared by hydrothermal treatment on electrodeposited brushite coatings," Journal of Materials Science-Materials in Medicine, **10,** 243-8 (1999).

102. M. Leoni and P. Scardi. "Nanocrystalline domain size distributions from powder diffraction data," Journal of Applied Crystallography, **37,** 629-34 (2004).

103. M.P. Mahabole, R.C. Aiyer, C.V. Ramakrishna, B. Sreedhar and R.S. Khairnar. "Synthesis, characterization and gas sensing property of hydroxyapatite ceramic," Bull. Mater. Sci., **28,** 535-45 (2005).

104. O.E. Petrov, E. Dyulgerova, L. Petrov and R. Popova. "Characterization of calcium phosphate phases obtained during the preparation of sintered biphase Ca-P ceramics," Mater Lett, **48,** 162-7 (2001).

105. C. Richard Brundle, Charles A. Evans, Jr. and ShaunWilson. *"Surfaces, Interfaces, Thin Films,"* pp. 120-9 in *Encyclopedia of Materials Characterization.* Edited by Lee E. Fitzpatrick. Butterworth-Heinemann, Stoneham, MA, 1992.

APPENDIX A – PRELIMINARY RESULTS ON ECD CO-DEPOSITION OF ORGANO-CERAMIC COATINGS

The study of electrochemical co-deposition was not fully complete in this part of the research project, however, preliminary experimental work was performed to investigate the feasibility of such process. The objective of this study was to (i) co-deposit calcium phosphate coating with a polymer for mechanical properties enhancement; (ii) confirmation of the possibility of drug co-deposition technique. Previous study done by Fan et al has demonstrated a uniform collagen fibril/octacalcium phosphate composite coating by electrolytic deposition. Preliminary results indicated that the composite coating may have higher elastic modulus and more scratch resistance than monolithic porous calcium phosphate coating[88].

Polyvinyl alcohol (PVA) is a water-soluble polymer, it was chosen as the model reagent for co-deposition. Electrochemical co-deposition was conducted with the optimized process parameters listed in Table 5.2-1, on bare metal stents without the application of substrate surface treatment. Polyvinyl alcohol was dissolved in the standard ECD electrolyte before deposition. Two different electrolytes were prepared with 0.1wt% PVA and 0.8wt% PVA.

Figure A 1 and Figure A 3 illustrate the resulting ECD co-deposited coatings on coronary stents with 0.1wt% and 0.8wt% PVA, respectively. Both of these coatings demonstrated good uniformity and full coverage. It was obvious that the co-deposition with 0.8wt% PVA exhibits a denser structure compared to the 0.1wt% PVA. Figure A 2

and Figure A 4 illustrate the stent expansion test results of the 0.1wt% and 0.8wt% PVA, respectively. Even though both substrates have not been modified for coating adhesion enhancement, the stent expansion results revealed dramatic improvement over ECD coating of CaP alone on bare metal stent as illustrated in Figure 5.2-10. These results confirmed the possibility of ECD co-deposition with PVA for coating integrity enhancement. Although the fundamental mechanism of co-deposition was not clear at this stage, it was reasonable to believe that the dissolved PVA was encapsulated while calcium phosphate was being deposited.

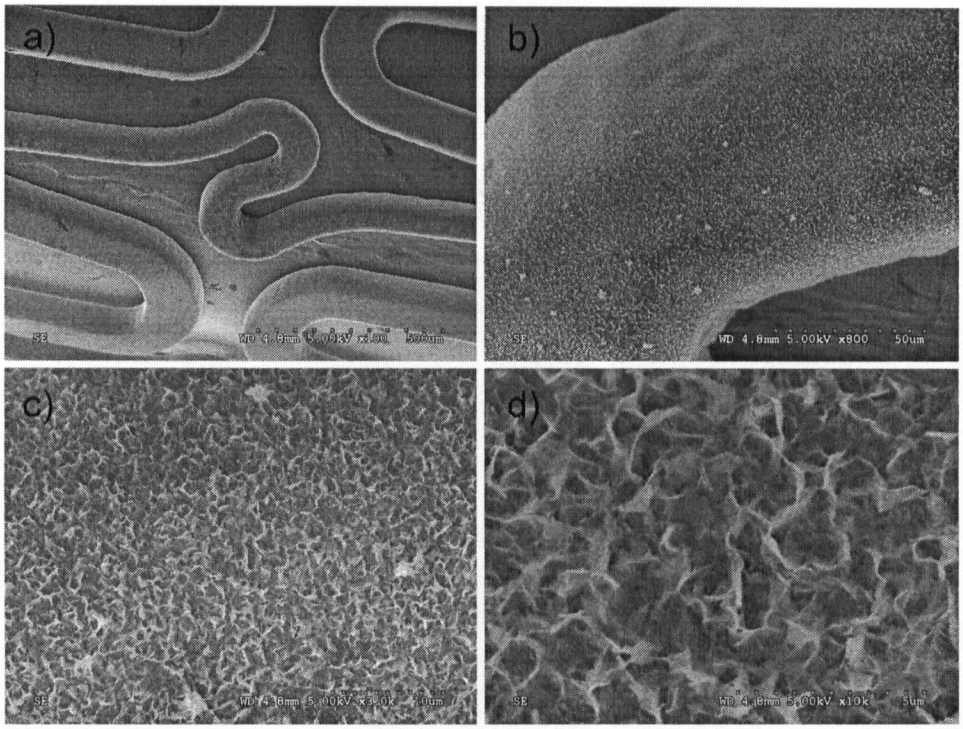

Figure A 1. SEM images of an ECD coating co-deposited with 0.1wt% of PVA on coronary stent. (a) [×100], (b) [×800], (c) [×3,000], and (d) [×10,000]

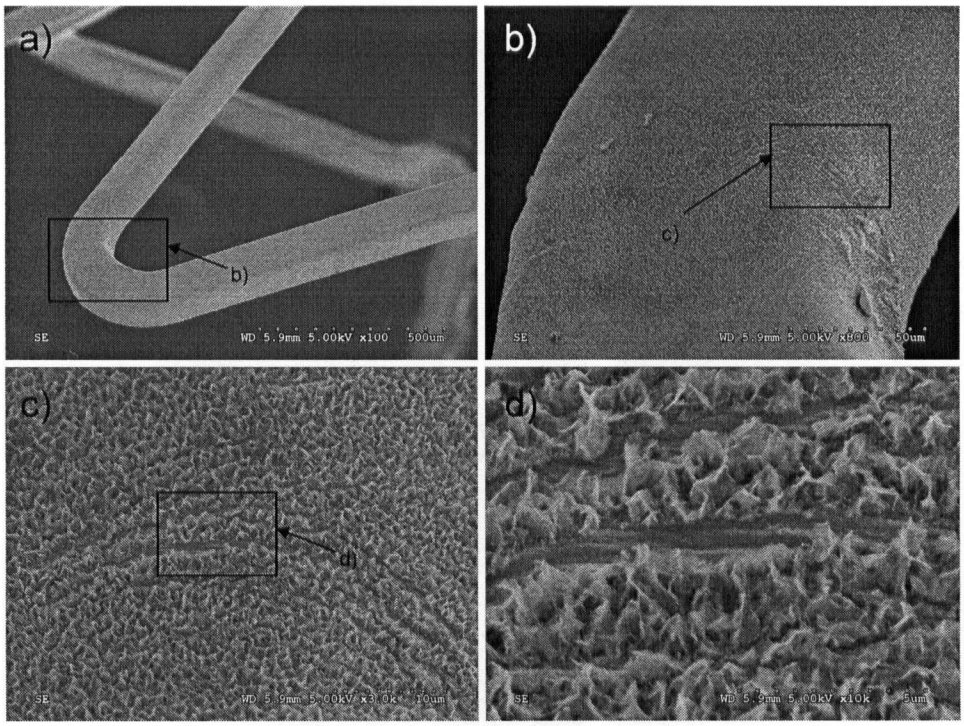

Figure A 2. SEM images of an expanded stent coated with ECD co-deposited with 0.1wt% PVA. (a) [×100], (b) [×800], (c) [×3,000], and (d) [×10,000]

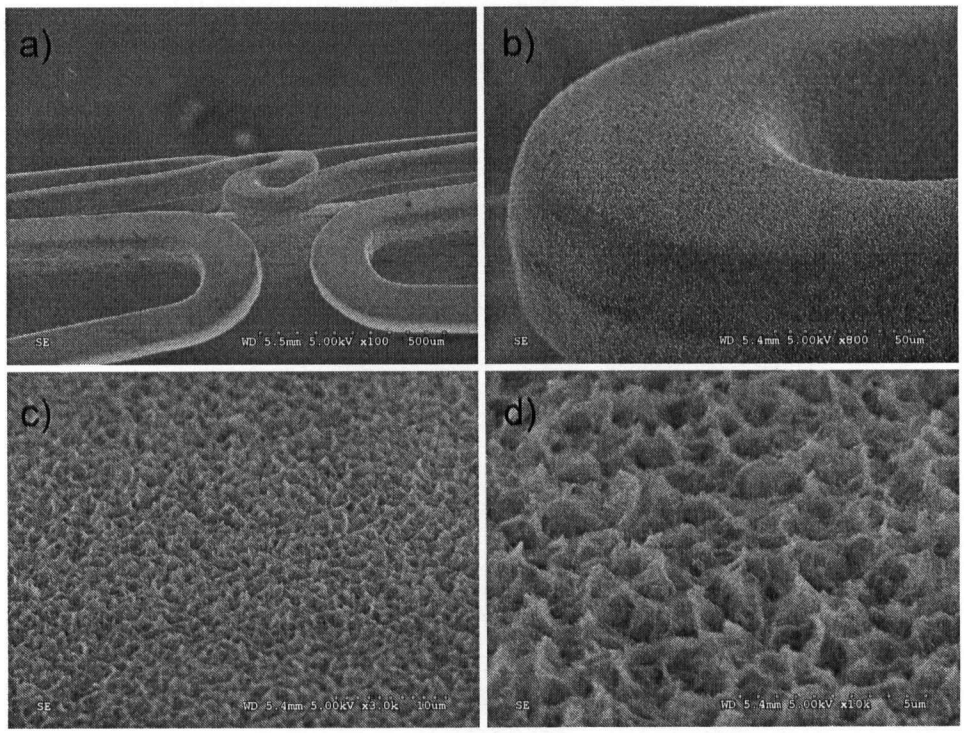

Figure A 3. SEM images of an ECD coating co-deposited with 0.8wt% PVA on coronary stent. (a) [×100], (b) [×800], (c) [×3,000], and (d) [×10,000]

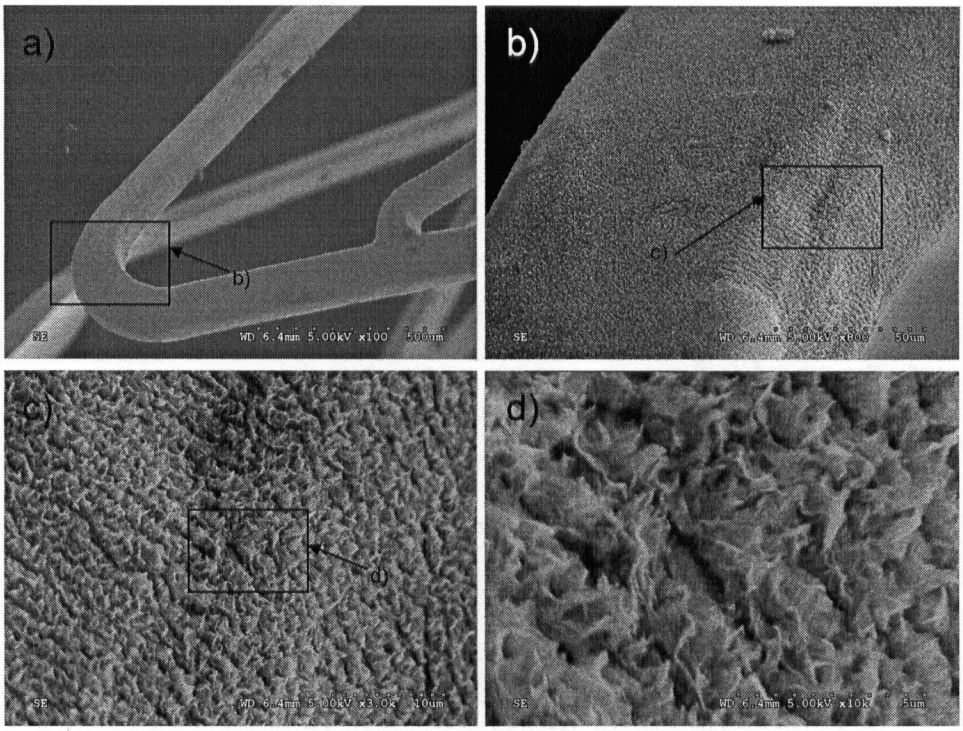

Figure A 4. SEM images of an expanded stent coated with ECD co-deposited with 0.8wt% PVA. (a) [×100], (b) [×800], (c) [×3,000], and (d) [×10,000]

APPENDIX B DETAILED RECORDS OF REPRODUCIBILITY STUDY

Table B 1. Preparation record for ECD coating batch ECD-RP-001.

Substrate

Marks & Identity:	n/a
Ref No.	n/a
Size:	14 mm
Description:	MIVI 700 Series Coronary Stent

ECD Coating

Preparation Date:	January 16, 2006
Batch Number:	ECD-RP-001
Prepared By:	MT
Electrolyte Ca:P Ratio:	1.23
Applied Current (mA):	1.0
Electrolyte Temp. (°C):	45°C ± 2 °C
Electrolyte pH:	4.5
Deposition Time (min):	1.0
Surface Treatment:	Yes
Phase Conversion:	Yes
Sintering Temp. (°C):	500 °C (20 min)

Sample Name	Bare Stent Weight (mg)	Final Stent Weight (mg)	Coating Weight (ug)	Pass/Fail
ECD-RP-001-01	15.601	15.663	62	Pass
ECD-RP-001-02	15.716	15.779	63	Pass
ECD-RP-001-03	15.745	15.811	66	Pass
ECD-RP-001-04	16.087	16.152	65	Pass
ECD-RP-001-05	16.187	16.251	64	Pass
ECD-RP-001-06	16.219	16.279	60	Pass
ECD-RP-001-07	15.789	15.850	61	Pass
ECD-RP-001-08	15.852	15.914	62	Pass
ECD-RP-001-09	16.716	16.782	66	Pass
ECD-RP-001-10	15.798	15.863	65	Pass
Average:	**15.971**	**16.034**	**63.4**	
Standard Dev.	**0.317**	**0.318**	**2.0**	

Yield Rate of ECD-RP-001 =100%

Table B 2. Preparation record for ECD coating batch ECD-RP-002.

Substrate

Marks & Identity:	n/a
Ref No.	n/a
Size:	14 mm
Description:	MIVI 700 Series Coronary Stent

ECD Coating

Preparation Date:	January 23, 2006
Batch Number:	ECD-RP-002
Prepared By:	MT
Electrolyte Ca:P Ratio:	1.23
Applied Current (mA):	1.0
Electrolyte Temp. (°C):	45°C ± 2 °C
Electrolyte pH:	4.5
Deposition Time (min):	1.0
Surface Treatment:	Yes
Phase Conversion:	Yes
Sintering Temp. (°C):	500 °C (20 min)

Sample Name	Bare Stent Weight (mg)	Final Stent Weight (mg)	Coating Weight (ug)	Pass/Fail
ECD-RP-002-01	15.768	15.828	60	Pass
ECD-RP-002-02	15.785	15.847	62	Pass
ECD-RP-002-03	15.743	15.806	63	Pass
ECD-RP-002-04	16.220	16.281	61	Pass
ECD-RP-002-05	16.735	16.795	60	Pass
ECD-RP-002-06	16.234	16.296	62	Pass
ECD-RP-002-07	15.982	16.043	61	Pass
ECD-RP-002-08	15.687	15.729	42	Fail
ECD-RP-002-09	16.889	16.954	65	Pass
ECD-RP-002-10	16.426	16.490	64	Pass
Average:	16.147	16.207	62.0	
Standard Dev.	0.408	0.411	1.6	

Yield Rate of ECD-RP-002 =90%

Table B 3. Preparation record for ECD coating batch ECD-RP-003.

Substrate

Marks & Identity:	n/a
Ref No.	n/a
Size:	14 mm
Description:	MIVI 700 Series Coronary Stent

ECD Coating

Preparation Date:	January 31, 2006
Batch Number:	ECD-RP-003
Prepared By:	MT
Electrolyte Ca:P Ratio:	1.23
Applied Current (mA):	1.0
Electrolyte Temp. (°C):	45°C ± 2 °C
Electrolyte pH:	4.5
Deposition Time (min):	1.0
Surface Treatment:	Yes
Phase Conversion:	Yes
Sintering Temp. (°C):	500 °C (20 min)

Sample Name	Bare Stent Weight (mg)	Final Stent Weight (mg)	Coating Weight (ug)	Pass/Fail
ECD-RP-003-01	16.024	16.085	61	Pass
ECD-RP-003-02	15.655	15.714	59	Pass
ECD-RP-003-03	15.979	16.040	61	Pass
ECD-RP-003-04	16.246	16.310	64	Pass
ECD-RP-003-05	16.897	16.970	73	Fail
ECD-RP-003-06	15.786	15.847	61	Pass
ECD-RP-003-07	15.243	15.303	60	Pass
ECD-RP-003-08	16.099	16.161	62	Pass
ECD-RP-003-09	16.565	16.628	63	Pass
ECD-RP-003-10	15.662	15.724	62	Pass
Average:	**16.016**	**16.078**	**61.4**	
Standard Dev.	**0.452**	**0.455**	**1.4**	

Yield Rate of ECD-RP-003 =90%

Table B 4. Preparation record for ECD coating batch ECD-RP-004.

Substrate	
Marks & Identity:	n/a
Ref No.	n/a
Size:	14 mm
Description:	MIVI 700 Series Coronary Stent

ECD Coating	
Preparation Date:	February 8, 2006
Batch Number:	ECD-RP-004
Prepared By:	MT
Electrolyte Ca:P Ratio:	1.23
Applied Current (mA):	1.0
Electrolyte Temp. (°C):	45°C ± 2 °C
Electrolyte pH:	4.5
Deposition Time (min):	1.0
Surface Treatment:	Yes
Phase Conversion:	Yes
Sintering Temp. (°C):	500 °C (20 min)

Sample Name	Bare Stent Weight (mg)	Final Stent Weight (mg)	Coating Weight (ug)	Pass/Fail
ECD-RP-004-01	15.277	15.341	64	Pass
ECD-RP-004-02	15.349	15.372	23	Fail
ECD-RP-004-03	16.021	16.084	63	Pass
ECD-RP-004-04	16.730	16.797	67	Pass
ECD-RP-004-05	15.976	16.041	65	Pass
ECD-RP-004-06	15.991	16.053	62	Pass
ECD-RP-004-07	16.767	16.828	61	Pass
ECD-RP-004-08	16.765	16.828	63	Pass
ECD-RP-004-09	15.429	15.490	61	Pass
ECD-RP-004-10	15.657	15.723	66	Pass
Average:	15.996	16.056	63.6	
Standard Dev.	0.557	0.561	2.0	

Yield Rate of ECD-RP-004 =90%

Table B 5. Preparation record for ECD coating batch ECD-RP-005.

Substrate	
Marks & Identity:	n/a
Ref No.	n/a
Size:	14 mm
Description:	MIVI 700 Series Coronary Stent

ECD Coating	
Preparation Date:	February 13, 2006
Batch Number:	ECD-RP-005
Prepared By:	MT
Electrolyte Ca:P Ratio:	1.23
Applied Current (mA):	1.0
Electrolyte Temp. (°C):	45°C ± 2 °C
Electrolyte pH:	4.5
Deposition Time (min):	1.0
Surface Treatment:	Yes
Phase Conversion:	Yes
Sintering Temp. (°C):	500 °C (20 min)

Sample Name	Bare Stent Weight (mg)	Final Stent Weight (mg)	Coating Weight (ug)	Pass/Fail
ECD-RP-005-01	15.767	15.832	65	Pass
ECD-RP-005-02	16.341	16.405	64	Pass
ECD-RP-005-03	16.792	16.856	64	Pass
ECD-RP-005-04	16.139	16.202	63	Pass
ECD-RP-005-05	15.672	15.737	65	Pass
ECD-RP-005-06	15.887	15.949	62	Pass
ECD-RP-005-07	16.099	16.158	59	Pass
ECD-RP-005-08	16.754	16.815	61	Pass
ECD-RP-005-09	15.780	15.845	65	Pass
ECD-RP-005-10	16.024	16.083	59	Pass
Average:	16.126	16.188	62.7	
Standard Dev.	0.375	0.375	2.2	

Yield Rate of ECD-RP-005 =100%